THE IDENTIFICATION OF GATA4 AND TBX5 TRANSCRIPTION NETWORK IN HUMAN MESOTHELIUM LINEAGE SPECIFICATION

by

LUOMAN CHEN

(Under the Direction of Stephen Dalton)

ABSTRACT

The mesothelium is a protective barrier on the outmost layer of coelomic organs and plays an essential role in organ development, especially during heart development. Only with the presence of mesothelium over the heart, also known as epicardium, coronary blood vessels start to form to support blood supply to the heart. Epicardium can also secrete paracrine factors to facilitate cardiomyocytes maturation and blood vessel formation. However, little is known about molecular mechanisms in the mesothelium/epicardium specification. Therefore, in this project, we aim at utilizing high throughput sequencing techniques (RNA-seq and ATAC-seq) along with CRISPR-Cas9 knockout technique on an *in vitro* human pluripotent stem cell (hPSC) based mesothelium differentiation model to identify and investigate a key transcription network involved in human mesothelium development. Our study identified that GATA4 was the essential pioneer factor in driving mesothelium specification and GATA4 cannot be replaced by GATA6 in mesothelium determination. We also discovered that the specificity of GATA4 in mesothelium depends on its interaction with TBX5 at codon 296

of human GATA4. The role of GATA4 and TBX5 in mesothelium formation is conserved in mouse and human.

INDEX WORDS: mesothelium, vascular progenitor, developmental mechanism, GATA4, TBX5, transcriptional regulation

THE IDENTIFICATION OF GATA4 AND TBX5 TRANSCRIPTION NETWORK IN HUMAN MESOTHELIUM LINEAGE SPECIFICATION

by

LUOMAN CHEN

BS, Tongji University, China, 2013

MD, Tongji University, China, 2015

A Dissertation Submitted to the Graduate Faculty of The University of Georgia in Partial Fulfillment of the Requirements for the Degree

DOCTOR OF PHILOSOPHY

ATHENS, GEORGIA

2020

THE IDENTIFICATION OF GATA4 AND TBX5 TRANSCRIPTION NETWORK IN HUMAN MESOTHELIUM LINEAGE SPECIFICATION

by

LUOMAN CHEN

Major Professor:	Stephen Dalton
Committee:	Amar Singh
	Takahiro Ito
	Pengpeng Bi
	Nadja Zeltner

Electronic Version Approved:

Ron Walcott
Dean of the Graduate School
The University of Georgia
December 2020

DEDICATION

This work is dedicated to my family, my parent and my brother. My family has taught me the kindness and perseverance, which have helped me in good and bad times. Thanks for the freedom and support they have given me to let me pursue whatever I want for my life. Without you, I wouldn't be where I am today.

ACKNOWLEDGEMENTS

It is a journey that has benefited me professionally and personally. I want to acknowledge everyone I have encountered and to give special thanks to the people below.

First, I want to thank my supervisor, Dr. Stephen Dalton, for taking me in as a graduate student in his lab, and his continuous efforts to challenge me to become better. His passion and enthusiasm in science have always inspired me. His scientific integrity and attention to detail have guided me throughout my graduate education. Thank him again for showing me what a good scientist is like.

I would like to thank all my committee members, Dr. Amar Singh, Dr. Takahiro Ito, Dr. Pengpeng Bi and Dr. Nadja Zeltner. Dr. Amar Singh has been a second mentor to me and is always happy to provide advice on my project as well as career development. Thanks to Dr. Takahiro Ito, who has always asked me thought-provoking questions and provided useful suggestions to the experiments. Thanks to Dr. Pengpeng Bi's help with the mouse experiments. Thanks to Dr. Nadja Zeltner setting an example for female scientists.

It has been a pleasure to work with my fellow Dalton lab members. Each one of you has helped me in some way.

Last but not least, I want to thank my friends, as well as previous PIs and colleagues from Shanghai Tenth People's Hospital, Tongji University. There is never enough appreciation from me to my kindest friends. Thank all of you for being there for me whenever I needed you guys. Thanks to my previous PIs and colleagues from

Shanghai Tenth People's Hospital, who guided and helped me get onto this journey and who always have believed in me and encouraged me.

I have made this because of all of you. Thank you.

TABLE OF CONTENTS

LIST OF TABLES

Page

LIST OF FIGURES

Page

CHAPTER 1

INTRODUCTION AND LITERATURE REVIEW

1. Mesothelium

1.1 What is mesothelium?

The mesothelium is a monolayer of elongated and flatten squamous-like mesothelial cells and covers coelomic organs, body walls, and the internal reproductive organs [1]. It is a conserved structure in mammalian species and is also observed in zebrafish [2]. Its name is a combination of its embryological origin from mesoderm and its morphological similarity to the epithelium. Many epithelium morphological features also show in the mesothelium, including apical/basal polarity, well-developed cell junctions, and basement membrane production. The polarity is supported by the apical side facing towards the coelomic cavity and tight junction on the lateral side of cells, which is characterized by the localization of Bves, ZO1, E-cadherin, and cytokeratin [3]. The basement membrane is formed with extracellular matrix produced by the mesothelium and separates the mesothelium from underlying connective tissues. This structure and semi-permeability of the mesothelium facilitate fluid diffusion between coelomic cavities and sub-mesothelial connective tissues [4].

According to its anatomical localization in the body, mesothelium can be subcategorized to different subtypes; pericardium and epicardium, lining the cardiac cavity and heart; visceral and parietal pleura, lining the lung and the thoracic cavity; and

visceral and parietal peritoneum, covering coelomic organs and body walls in the abdomen (Figure 1.1) [3].

However, despite different anatomical locations, mesothelial layers have similar function and share a common embryonic origin.

1.2 Basic functions of mesothelium

As an outmost layer, mesothelium serves as a protective physical barrier for coelomic organs and body walls [4, 5]. Its semi-permeability allows fluid and cell transportation across serosa [2, 6]. The mesothelium also produces glycosaminoglycans and lubricant fluid to provide a non-adhesive surface for frictionless organ movement [2, 7, 8]. Mesothelium can also participate in many biological functions that are significant in disease/injury progression such as immunomodulation, coagulation/fibrinolysis regulation, and wound healing [4].

Immunomodulation

The mesothelium is actively involved in immune modulation, mainly through three different mechanisms. As the outmost layer, the mesothelium is the first defense line to prevent pathogen invasion [4, 5, 9]. Secondly, multiple immune-related receptor proteins are expressed on the mesothelium, such as pattern recognition receptors, antigen presenting molecules and their accessory molecules so that the mesothelium can detect pathogens and present antigens to T cells [6, 10-16]. In the stimulation of circulating inflammatory factors, the mesothelium releases various chemokine and cytokines (IL-1β, TNF-α, IFN-γ, stromal cell-derived factor-1, IL-6/8 and macrophage colony stimulating factor) to signal different subsets of leukocytes to the injured site [17-22]. The mesothelium also expresses integrins (integrins a6b1 and a4b1, VLA4, and VLA5) and

adhesive molecules (ICAM, VCAM, E-Cadherin, N-Cadherin and CD49, CD29) and mediate the transmigration of leukocytes into underlying organs [2, 23-26]. The massive influx of leukocytes from the bloodstream to the injury site and the interaction between leukocytes and the mesothelium effectively initiates and propagates immune response at injured site [5, 6, 17, 27-30]. The mesothelium can also modulate the immune response by synthesis and secretion of various growth factors, extracellular matrix proteins, prostaglandins, prostacyclin and nitric oxide, as well as reactive nitrogen and oxygen species [31-45].

Coagulation and Fibrinolysis

Coagulation and fibrinolysis are two essential steps in wound healing and the mesothelium is active in both processes [6, 46]. The mesothelium's pro-coagulation relies on its secretion of tissue factor (TF), the primary inducer of the extrinsic coagulation cascade [47, 48]. Meanwhile, the mesothelium can also inhibit the coagulation reaction via its production of the TF pathway inhibitor (TFPI) [49, 50]. Protein C (PC) pathway is the other inhibitory mechanism of mesothelium in anti-coagulation. Mesothelium expresses endothelial protein C receptor (EPCR) and thrombomodulin. Thrombomodulin and EPCR form complexes with thrombin to activate PC [51, 52]. Activated PC inhibits factor Va and VIIIa in the coagulant cascade and blocks the cascade.

The fibrinolysis activity of the mesothelium is mainly regulated by its secretion of plasminogen activators and inhibitors [29]. The mesothelium produces both tissue-type plasminogen activator (tPA) and urokinase-type plasminogen [53-56]. tPA and uPA are major serine proteolytic enzymes, which convert plasminogen into plasmin [57]. Plasmin dissolves fibrin blood clots. On the other hand, this process is restricted by plasminogen

inhibitors (PAI-1 and -2), which can be also synthesized by the mesothelium [55, 58]. PAI-1 and PAI-2 bind to both PAs to block enzymatic activity of plasminogen activators. Inactivated plasminogen activators are degraded and can no longer initiate fibrinolysis [59].

The functions of the mesothelium in coagulation and fibrinolysis are essential in fibrin turnover within serosa cavities. Their fine balance can prevent coelomic organs and cavities from adhesion and fibrosis.

1.3 The roles of mesothelium in organogenesis

During embryonic development, the mesothelium functions as a multipotent progenitor. Upon reaching the coelomic organs, it loses epithelial features but gains mesenchymal characteristics via an epithelial to mesenchymal transition (EMT) process. The mesenchymal form of mesothelium can further differentiate into different cell types depending on its location and involved in organogenesis [60-62].

Mesothelium in the heart

The mesothelium covering the heart is called the epicardium and has been studied in significant detail. At the early stage of heart development, before E8.5 in mouse, the heart is deprived of coronary vessels and connective tissues and only has two layers, the endocardium and myocardium. The epicardium gradually migrates to cover the heart, which forms a three-layer heart structure [63-65]. Immediately after it attaches to the surface, the epicardium invades into the heart and undergoes an EMT to become epicardium-derived cells (EPDCs) [66, 67]. EPDCs are mesenchymal cells, and they can continue differentiating into fibroblasts, smooth muscle cells (SMCs) and pericytes to construct connective tissues and coronary vessels (Figure 1.2) [68-73]. EPDCs can also

generate endothelial cells (ECs) but to a lesser extent [74, 75]. However, it is disputable if EPDCs are capable of deriving cardiomyocytes (CMs) [76]. Lineage tracing studies in mouse embryos have shown the epicardial origin of CM [77-79]. However, a controversy arose in the discovery that the lineage tracing markers used in these studies are also expressed by CMs endogenously [80]. Very recently, epicardium was also discovered to have the potency to generate adipocytes [81-83].

In addition to the direct cellular contribution to cardiogenesis, epicardium also acts as a signaling center for heart maturation [84-86] and coronary vessel growth [87-89] (Figure 1.3). The retinoic acid (RA) pathway is the key signaling pathway from epicardium to promote cardiac growth [62]. RA is generated from retinol by retinal hydrogenase (RDH) and three retinal dehydrogenases (RALDH1/2/3). It activates target gene expression by binding to retinoic acid receptors (RARα/β/γ) and retinoid X receptors (RXRα/β/γ) [90]. The heart is one of the most sensitive organs to RA [91]. Both RALDH2$^{-/-}$ and RXRα$^{-/-}$ mutants were embryonic lethal and had server cardiac malformation with abnormal ventricular septation and thin-walled, underdeveloped ventricles [92-95]. However, the heart defects found in RALDH2$^{-/-}$ and RXRα$^{-/-}$ embryos were not cell-autonomous of CMs, but due to defected RA signaling from epicardium [93, 94]. Conditional knockout of RXRα in epicardium resulted in the detached epicardium and heart malformation, rather than ventricle RXRα$^{-/-}$ [94, 95]. Epicardial RXRα$^{-/-}$ also had defective coronary vessel development, including tortilla and abnormal branching of vascular beds [94, 96].

Erythropoietin, well-known for its critical role in erythropoiesis, is also an important mesothelium signaling molecule [97, 98]. EPO$^{-/-}$ and EPO receptor [97]$^{-/-}$

mouse embryos were embryonic lethal at E13.5-14.5 [97]. Apart from defects in erythropoietic and fetal liver development, $EPO^{-/-}$ and $EPOR^{-/-}$ embryos also exhibited severe cardiac hyperplasia, similar to the defects found in embryos with epicardial RA signaling deficiency [99]. In *in vitro* organ culture, the heart developed well in the presence of epicardium, but the heart growth was prohibited when epicardial EPO or RA production was blocked. The inhibitory effect of EPO and RA deprivation on cardiac growth was rescued by either exogenous RA or EPO administration, suggesting that EPO in epicardium functions either downstream or coordinately with RA signaling [100]. However, RA and EPO do not act on CMs directly but are mediated via their downstream signaling induced in the epicardium, including insulin-like growth factor (IGF) [101], fibroblast growth factor (FGF) [94, 102] and Wnt [94, 103].

IGF, especially IGF2, is the primary cardiomyocyte mitogen produced by the epicardium where it is expressed from E10.5-E14.5 in mouse embryos [104, 105]. It acts through the binding of IGF1/2 to the insulin receptor (INS) and IGF receptors1 (IGF1) and induces ERK or PI3K signaling [104, 106-108]. Global and cardiac $IGF2^{-/-}$ resulted in a ventricular hyperplasia wall in mouse embryos [104, 109]. The source of IGFs supporting CM proliferation comes from epicardium, considering the epicardial IGF2 knockouts recapitulated the heart defects in $IGF2^{-/-}$ mouse embryos [108].

Mammals have 18 FGF types and 4 FGF receptors (FGFRs) [110]. FGF1, FGF2, FGF4, FGF6, FGF9, and FGF20 are FGF ligands expressed in the epicardium. FGFR-1 and -2 are two main and redundant FGF receptors expressed on CMs [86, 102]. Conditional depletion of FGF signaling in epicardium displayed decreased CM proliferation and led to the thinning of ventricular walls [102, 111]. FGF signaling also

acts autonomously and regulates the epicardium proliferation, EMT, and vascular lineage differentiation [111-113].

Mesothelium in other organs

Compared to the comprehensive understanding of epicardium, mesothelium over other coelomic organs is less studied. In mouse embryonic development, the lung bud is deprived of the mesothelium until E10.5 [114]. The mesothelium is vital for normal lung morphogenesis [115]. In the lung, Wt1 is exclusively expressed in the mesothelium, so the Wt1 lineage tracing is a good tool to explore mesothelium contributions in developing lung. The conclusions vary on genetic labeling protocols developed in different labs [114-118]. Non-inducible Wt1 lineage tracing results showed that lung mesothelial cells differentiated into SMCs in the blood vessel walls associated with bronchioles and larger bronchi, bronchial SMCs as well as mesenchymal cells within the alveoli and the interstitial tissue [114, 116, 118]. Another group discovered a broader role of the mesothelium in lung development. Their results supported the mesothelium origin of SMCs and fibroblasts. Additionally, they found that ~25% of all the ECs in the lung were mesothelium derivatives and a subpopulation of pulmonary cartilage and chondrocytes in trachea bronchi was also mesothelium descendants at E16.5 [115]. However, when Wt1 labeling was induced at E10.5 or E11.5, the mesothelium only had a minor contribution to mesenchymal cells in the lung [117].

How mesothelium involves in liver development has been investigated in both chick and mouse embryos [119-124]. Fetal liver mesothelium is critical for hepatocyte proliferation [125] and generates various cell types in the liver. By tracing liver mesothelium *in ovo* and using chick-quail chimeric culture, mesothelium has shown to

given rise to endothelial and stellate cells and form sinusoid-like vessels in the liver [119]. Hepatic stellate cells (HSCs) are mesenchyme cells residing between sinusoids and hepatocytes. They are responsible for vitamin A storage in the liver and myofibroblasts regeneration during liver fibrosis after injury [126]. In mouse embryos, liver mesothelium can derive a subset of HSCs and perivascular mesenchymal cells, including fibroblasts and SMCs [121, 122]. But no evidence supports that mesothelium is a source of ECs in the liver [122].

The functions of the mesothelium in the pancreas are similar to their role in the liver. It generates pancreatic satellite cells, SMCs, pericytes, fibroblasts, and affects pancreas growth and morphology. The mesothelium can also contribute to a small portion of ECs in fetal pancreas [127-129]. Wt1 positive mesothelium becomes detectable on the gut at E10.5, and by E11.5 the entire gut is enclosed by a mesothelium layer [130]. SMCs of all major blood vessels in the mesentery and gut are derived from the mesothelium [130, 131].

Studies about the mesothelium derivatives heavily depend on mesothelium lineage markers, such as Wt1, Tbx18, Tcf21. However, those markers are not exclusively expressed in the mesothelium during development. In addition to mesothelium expression, Wt1 is also expressed in the metanephros, the gonads, the skeletal muscular system, coronary EC and the nervous system [132]. Tbx18 is present in CM and presomitic mesoderm, where it is actively involved in different stages of somite development [84, 133]. Tcf21 can be found in the mesenchyme of the lung and the metanephros as well as surrounding the adrenals, gonads and ureter [134].

To summarize, the mesothelium origin of SMC and fibroblasts is conserved in different organs. Mesothelium can generate EC in the heart, possibly in the lung and pancreas, even though it may not be the only and primary source. However, if CMs and other mesenchyme cells can be derived from mesothelium requires more specific mesothelium lineage markers or a better-defined labeling time point to draw a solid conclusion.

1.4 Embryology of mesothelium

Mesothelium is one of splanchnic mesoderm (SplM) derivatives [135, 136]. Only the developmental program of epicardium has been well characterized. After gastrulation, a three-germ layer structure of ectoderm, mesoderm, and endoderm is established [137]. Mesoderm contains three components: paraxial mesoderm, intermediate mesoderm, and lateral mesoderm. The lateral mesoderm is further separated into somatic mesoderm and SplM [138]. The parietal somatic mesoderm is close to the ectoderm and develops into connective tissues of the body wall and limbs, and SplM on the visceral side is adjacent to the endoderm and splits into the first heart field (FHF) and the second heart field (SHF) which generates the majority cells in the heart [139, 140]. Cardiac progenitors from FHF first differentiate into CMs at the atria and left ventricle region forming a primary tubular heart. As the linear heart looping, SHF starts differentiating and actively expanding the primary heart tube at the right ventricle and outflow tract regions [141, 142]. Progenitors in SHF also make non-myocardial cells, pro/epicardium [135, 143, 144]. Proepicardium (PE) is an intermediate stage from SplM to epicardium. It first presents between the sinus venous and liver at E8.5 in mouse and becomes evident as a cauliflower or grape-shaped organ at E9.5 [67, 145]. The size of PE keeps diminishing as

it migrates towards the heart as free-floating cellular vesicles (in mammals) [145-147]. Upon reaching the heart, PE first attaches to the atrioventricular groove at its dorsal side and becomes epicardium [144, 147, 148]. The epicardium proliferates and migrates, and eventually covers both the ventricle and atrium surface by E11.5 [65, 144, 149] (Figure 1.4).

The mesothelium formation in other coelomic organs is less explored. It was proposed that the pleural and peritoneal mesothelium were differentiated from the SplM resident in developing organs of the respiratory and digestive system, unlike the epicardium migrated from the PE, which is an exogenous tissue to the heart [130, 136, 150].

1.5 Heterogeneity of mesothelium

Using the light and electron microscopy, at least three morphologically distinct PE populations was first identified in chick [151]. Wt1, Tbx18 and Tcf21 are classic mesothelium markers used for the mesothelium lineage tracing. By including Scleraxis (Scx) and Semaphorin3D (Sema3D) along with Wt1 and Tbx18 to trace mesothelium lineage, different sub-compartments of pro/epicardium were identified in mouse embryos. They were not only divergent at molecular level but also had different functionalities; Wt1+/Tbx18+ pro/epicardium made vascular SMCs, whereas Scx+/Sema3D+ mainly generated coronary ECs [75]. However, later this conclusion was disputed by another study. They failed to identify discrete pro/epicardium sub-compartments but discovered that pro/epicardium co-express Wt1, Tbx18, Tcf21, Sema3, and Scx transcripts until E13.5 [149].

With the development of a single-cell sequencing, multiple single-cell sequencing studies have been conducted in the zebrafish heart, human developing heart and hPSC derived epicardium [152-155]. Three subpopulations of *tcf21*+ epicardium was identified in uninjured adult zebrafish. Group I *tcf21*+ epicardium populated the outmost epithelial layer and had high expression of the classic epicardial marker, *raldh2*. Group II *tcf21*+ epicardium resided within the ventricular wall, possibly perivascular cells and had the specific expression of *nrg1*. Group III epicardium were EPDCs in the innermost layer, and they exclusively expressed *cxcl12a*. They also discovered pan- and subset specific injury-induced genes, including pan-expression of *igf2b* and *tms*, *bmp4* and *tfa* for group I, *col18a1* and *ltbp1* for group II, and *loxl2a*, *loxl2b* and *timp2b* for group II and III [152]. However, this study only investigated *tcf21*+ epicardium, so it might neglect *tcf21* negative epicardium. Another zebrafish single-cell sequencing study utilized a different cell sorting strategy, and they collected all *wt1*, *tbx18*, and *tcf21* positive cells for single-cell sequencing. In this study, three distinct epicardial subpopulations, Epi1, Epi2, and Epi3, were identified. Epi1 subpopulation represented the main epicardial sheet and was critical to maintaining the epicardium integrity. Epi1 cells concurrently expressed classic epicardial markers, *wt1*, *tbx18*, *tcf21*, and *aldh1a2* and also had high *tgm2b* expression. Epi2 cells were *sema3fb*+*tbx18*+*wt1*-*tcf21*- and genes highly expressed in Epi2 were enriched for the biological processes of cell migration in heart development and vasoconstriction. Epi3 cells only had *tcf21* expression and were actively involved in the recruitment of leukocytes to the developing heart [153]. The transcriptome of human developing heart has been studied at three different developmental stages, and the result showed that epicardial markers,

TBX18, TCF21, and WT1, were not evenly distributed on the heart surface, indicating human epicardium contains different cell populations [154]. The single-cell sequencing study in human epicardium differentiated from hPSCs also discovered two epicardium subsets, BNC1 high compartment and TCF21 high compartment. BNC1 high epicardium were associated with the cell-to-cell interactions and cell migration, while TCF21 high epicardium were potentially more involved in blood vessel development [155].

1.6 Molecular mechanisms in mesothelium development

In contrary to its well-established functions during development, molecular mechanisms in mesothelium development are less known. insulin gene enhancer LIM homeobox protein Islet1 (Isl1) and NK2 transcription factor related, locus 5 (Nkx2-5) are two main markers of SplM, and their deletion in mouse embryos led to developmental delay and severe cardiac dysfunction. Pro/epicardium was barely detectable in Nkx2-5$^{-/-}$ mutants, and the pro/epicardial Wt1 expression was significantly downregulated. However, the depletion of Isl1 did not show significant effects on pro/epicardium specification [135]. Epicardium formation and integrity are not affected by the level of Wt1, Tbx18, and Tcf21 but their depletion impairs the epicardium functions, including EMT and vascular vessel development [71, 156-165]. When Wt1 was conditionally mutated in mouse epicardium, epicardium was intact but with an immature cuboidal morphology [157, 160]. The immature epicardium failed to undergo EMT properly, which led to abnormal coronary plexus formation [156, 158, 164]. Wt1 also effects epicardium paracrine functions via its downstream targets, including RA, BMP, and Wnt pathways [157, 158, 160]. Tcf21 is essential for epicardium maturation and attachment to the heart surface [163, 165]. Loss of Tcf21 resulted in epicardial blisters and defective

epicardial EMT, which led to failed differentiation of SMCs and cardiac fibroblast [71, 163]. Tbx18 is dispensable for epicardium development but it is vital for proper SMCs differentiation from epicardium [161, 162, 166].

GATA factors are a family of zinc finger proteins. They can bind to GATA- or GATA-like DNA binding motifs and regulate tissue-specific gene programs [167]. Gata1, 2, and 3 are predominantly expressed in hematopoietic lineages and determine hematopoietic stem cell fate. Gata4, 5, and 6 are expressed in endoderm, and mesoderm derived tissues [168]. Gata4 and Gata6 can compensate for each other in the most cases during development [169-172]. However, Gata6 is believed to be more specific for endoderm lineages [170, 173]. Gata4 compensates for Gata6 at early endoderm differentiation, but Gata6 becomes non-redundant in a subset of hepatic cells, which are important for liver bud expansion after E9.5. No cardiovascular defects were detected in Gata6 null mice [170]. The unique role of Gata4 is displayed in heart development. Gata4 depletion disrupted the heart looping and septation process, and defected hearts had thin ventricular myocardium [174]. However, both *in vivo* and *in vitro*, Gata4$^{-/-}$ CMs maintained normal expression of CM markers including Acta1,2 and Myh6,7, but were less proliferative [171, 175, 176]. These results suggest that Gata4 and Gata6 are redundant in cardiomyocytes differentiation, and the effect of Gata4 depletion on the heart is non-cell autonomous. Besides abnormal cardiac morphogenesis, Gata4$^{-/-}$ hearts were deprived of the epicardium [174, 177]. Considering the paracrine impact of epicardium on myocardium growth, the absence of epicardium might explain the heart defects seen in Gata4 mutants. This hypothesis was first supported by Gata4$^{-/-}$ mouse studies. Gata4$^{-/-}$ embryos were deprived of pro/epicardium and had a significant reduction

in cardiomyocytes proliferation, which led to the thinning of the myocardial wall [174, 177]. However, the epicardial conditional double knockout of Gata4 and Gata6 study had different conclusions. Epicardial loss of both Gata4 and Gata6 resulted in deficient cardiomyocyte proliferation and a significant reduction in the number of sub-epicardial endothelial cells (SSECs), which resulted in a thin myocardial wall and failed coronary vasculature. But no change in epicardium number was observed by E13.5, and only a small percentage (~30%) of SSEC loss was from epicardium [178]. They concluded that Gata factors play a more important role in the paracrine function of the epicardium, rather than the epicardium cell fate determination.

Hand2, a basic helix-loop-helix DNA binding protein, has also been suggested to be important for epicardium development. Hand2 shares some expression patterns and functions with Hand1 in the developing heart [179, 180]. While Hand1has a specific role in FHF development, Hand2 is more associated with SHF differentiation [181, 182]. A series of conditional knockouts have shown that Hand2 regulates multiple stages and aspects of SHF development [180, 183-186]. Hand2 is expressed starting at the onset of heart development, and its early deletion in SplM led to embryonic lethality around E10.5 with severe ventricle hypoplasia and shortened outflow tract [183]. Conditional deletion of Hand2 in epicardium resulted in decreased Wt1 positive epicardium at E13.5. The mutants failed to form a compact layer over the heart and had disruptive coronary plexus by E14.5 [184]. In addition, Hand2 is also irreplaceable for CMs [185, 186] and neural crest [187, 188] functionalities in the developing heart, which is critical for cardiac valve and outflow tract development.

Tbx5 is another transcription factor that has been reported to regulate pro/epicardium development. Tbx5 is a T-box transcription factor and plays an important role in multiple stages of the heart development, including epicardium [189]. But its role in pro/epicardium specification is less conserved [190-192]. Zebrafish studies showed that in the absence of tbx5, PE was undetectable in the heart region, indicating that tbx5 is essential for PE specification [191]. But in mouse and chick embryos, pro/epicardium had the regular expression of epicardium markers at E9.5. Mutated pro/epicardium only presented migration defects, as shown by its delayed epicardium attachment to the heart and decreased number of EDPCs in sub-epicardium space and resulted in defective coronary vessel formation. Therefore, murine and avian Tbx5 is only required for proper epicardium migration [190, 192].

Besides these well-known transcription factors, a few other factors have been investigated in epicardium development, such as C/EBP [193, 194], YAP-TAZ/TEAD complex [195], Sox9 [196], Est1/2 [197], Lhx9 [198] and Myh10 [199]. Embryos carrying disrupted expressions of these factors shared similar phenotypic defects, including defective coronary vasculature and thin myocardium [193-197, 199]. Sox9 deletion led to complete absence of pro/epicardium in zebrafish [196] and C/EBP recruits Brg1 to activate the transcription of epicardium markers [194]; the depletion of other factors only hampered the epicardium functions, due to either its decreased proliferation or its defected EMT [193, 195-199]. Some extracellular matrix factors, such as Cx43 [200] and Lmnb1 [201], have also been shown to be crucial for epicardium migration.

The conclusions about how each of these reported TFs is involved in epicardium development are inconsistent. This controversy may be related to the species differences

and different knockout strategies. Current studies only focused on one single TF at a time. However, it has become more evident that lineage specification depends on a specific regulatory network within multiple TFs, rather than a single cell-type-specific TF [202]. The question also remains if the molecular mechanism identified in epicardium specification also applies to mesothelium formation in other coelomic organs. Therefore, more research is needed to explore the regulatory mechanisms in mesothelium development and to address the question if the developmental mechanism in mesothelium formation is conserved in various organs.

2. *in vitro* human epicardium/mesothelium differentiation method

The isolation and generation of pluripotent stem cells (PSCs) have advanced researches in various areas [203, 204]. With the understanding of developmental mechanisms in both mouse embryo and other organism models, mimicking the tissue-specific microenvironment in Petri dishes has made it possible to recapitulate *in vivo* developmental process and derive numerous cell types from PSCs *in vitro* [205, 206]. The establishment of these protocols has provided a powerful tool to study human embryonic development, as well as for disease modeling and regenerative medicine [203].

2.1 Human pluripotent stem cells (hPSCs)

PSCs are characterized by their self-renewal capacity and pluripotency. Under maintenance conditions, PSCs divide indefinitely, and their daughter cells carry identical properties to the parental cells. With the stimulation of specific signaling, PSCs can develop into three germ layer cells of early embryos and then differentiate into all cell

types in the adult body [207]. The first human embryonic stem cells (hESCs) were isolated from inner cell mass (ICM) at the blastocyte stage via in vitro fertilization in 1998 [208]. hESC culture protocol was first adopted from mouse ESCs culture, which utilized mitotically inactivated mouse embryo fibroblasts (MEFs) as a feeder layer and required serum to maintain hESC identity [209]. But hESCs present heterogeneity from spontaneous differentiation and contain cell contaminations from feeder cells under this culture condition [210, 211]. The animal source of MEFs and serum, and their lot variances have brought contaminations and instability of hESCs, which limited their reproducibility and therapeutic applications [209]. Therefore, numerous efforts have been made to find substitutes for MEFs and serum in order to generate a feeder-free and xeno-free hESC culture system. Human cells (human skin fibroblasts, fetal muscle cells, bone marrow and amniotic epithelium), the extracellular matrix and synthesized substrates have all been shown to be good substitutions for MEFs [211-216]. In the absence of feeders, basic FGF (bFGF) is required to maintain hESCs pluripotency [216, 217]. A few other factors, TGF-β, Activin A/Nodal, LIF and stem cell factor, in various media formulations, have been shown to support hESCs identity in serum-free medium [216].

In 2006, mouse induced PSCs (iPSCs) were first generated from fibroblasts in Japan with four Yamanaka factors (Oct4, Nanog, Sox2, and c-Myc) [218]. A year later, the same group successfully reprogrammed human dermal fibroblasts into iPSCs using the same cocktail [219]. The same year, another group also succeeded in reprogramming human somatic cells using a different cocktail of *OCT4*, *NANOG*, *SOX2,* and *LIN28* [220]. However, these reprogramming methods were not efficient, and the usage of either retrovirus or lentivirus systems to introduce reprogramming factors brought the risk of

new insertional mutagenesis in iPSCs [221]. Thereafter, different strategies, including applying new gene-editing techniques, replacing transcription factors with their drug-like molecules or small RNA molecules, and reprogramming other somatic cells (peripheral blood, cord blood endothelium/stem cells, etc.), have been widely explored to increase reprogramming efficiency and safety [222]. The iPSC technology has broadened the applications of PSC by avoiding ethical and legal issues with hESC, preventing immunological issues with allogeneic cell transplants generated from hESCs and personalizing medicine using patients derived cells [223].

2.2 Splanchnic mesoderm cells (SplM)

Lineage tracing studies have demonstrated that Nkx2-5 and Isl1 are conservative markers for SplM, and their dynamic expression pattern marks different stages of heart development [224]. Nkx2-5 is a universal cardiac progenitor marker. It first is expressed in the FHF, then in SHF and CMs, but Isl1 is only transiently expressed in the SHF [225-227]. Therefore, their concurrent expression marks progenitors from the SHF [227, 228].

Wnt signaling is a critical pathway in regulating SplM specification, which regulates heart development in a time and space-dependent manner [229, 230]. At the early stage of SplM induction, Wnt signaling is essential, especially for SHF development [97, 231]. But its high and sustaining activity, on the other hand, prohibits the downstream differentiation of SplM, leading to SHF expansion [232]. Wnt pathway activates a signaling cascade for SHF gene program activation [97, 229, 232, 233].

Both FGF and BMP pathways are the downstream signaling of the Wnt pathway [97, 232, 233]. BMP signaling is crucial for FHF development [232]. Conditional

knockout of BMP signaling in the Isl1+ lineage resulted in the malformation of SHF generated heart structures, including the outflow tract and right ventricle, in mouse embryo [234]. FGF pathway is another downstream signaling of the Wnt pathway [97]. When FGF signaling was conditionally depleted in cardiac progenitors, the primary heart tube formation was not affected, but heart looping and SHF differentiation were severely disrupted [235-238]. FGF signaling also regulates SHF cell proliferation and acts directly on Isl1 gene activation [236].

Based on these understandings, several *in vitro* SplM differentiation protocols have been established from hPSC, by induction of Wnt signaling alone or a combination of FGF and BMP signaling [239-242].

2.3 Mesothelium

The mesothelium is characterized by its expression of WT1, TBX18, TCF21, CDH1, and a few other makers, such as ALDH1A2 and BNC1. Gene mutation and chick-quail chimera studies have demonstrated that RA and FGF pathways are both essential for epicardium development [96, 243-248]. Additionally, the fine balance between FGF and BMP pathways determines the cell fate choice between CMs and epicardium from SplM [247, 248]. At this stage, FGF signaling specifies epicardium from SplM and BMP pathway mainly drives CM lineage [247, 248]. However, BMP pathway can also induce the expression of some epicardium gene and affects pro/epicardium migration [191, 249-251]. Wnt signaling has also been shown to enhance the epicardium cell fate [252], and TGFβ pathway is critical for epicardium/mesothelium migration [253, 254].

A few reports have described mesothelium induction protocols from ISL1+NKX2-5+ mesoderm cells via the manipulation of the BMP pathway, RA

signaling, and Wnt pathway [255-260]. Based on the differences in the SplM induction methods, the signaling dependency varies. When SplM is mainly induced by BMP4, the continuous presence of BMP4 and the addition of RA are required to specify SplM into mesothelium [255, 256, 260]. If the induction of SplM depends on the modulation of Wnt signaling, the default downstream cell fate is CM. The activation of mesothelium cell fate requires the strong activation of Wnt signaling with or without RA treatment [257-259].

3. Potential utility of mesothelial cells in tissue engineering and regenerative medicine

As an epithelium in nature, a frictionless and lubricant surface and its functions during development, the mesothelium has shown broad potential clinical applications.

Post-operation adhesion is one of the major and severe complications after abdominal and pelvic surgeries, which can cause chronic abdominal pain, postoperative small bowel obstruction, and female infertility [261]. Mesothelium has been shown to be an effective anti-adhesive strategy in animal models [8, 262-264]. The application of mesothelium reduced the grade and area of postoperative adhesion without significant inflammatory reactions and also prevented fibrin deposition, angiogenesis and macrophage infiltration around adhesion sites [262, 264].

Primary endothelium has been widely used to seed tissue engineered constructs for clinical usage. But it is labor intensive to harvest and expand endothelium from autologous tissues [265, 266]. The mesothelium has shown great potential as good biomimetic substitutes for cornea and vascular endothelium. Decellularized anterior lens capsules showed sustainable monolayer coverage and structure integrity after being lined

with mesothelium, which provides an idea of the mesothelium-based cornea bio-substitute as a good alternative for cornea replacement [267]. Pre-endothelization of nude grafts with ECs has significant improvement in small-diameter (<6mm) vascular prosthesis patency [268]. The mesothelium had comparable adherence to synthesized vessel grafts (Dacron, ePTFE, and Silastic tubes) to ECs and the short-term patency (> 4 months) has significantly increased with mesothelium lining in rat and rabbit models [269-272]. Vascular progenitors from mesothelium lineage (MesoT), derived from hPSC, have also been explored as a cell source for seeding vessel grafts. MesoT-lining grafts formed a physiological vessel structure with ECs on the luminal side and SMCs on the abluminal side. The transplanted grafts maintained morphological integrity and no occlusion or leakage were observed after being connected to rat circulation [273].

The mesothelium is very active during embryonic development and contributed both cellular components and signaling molecules to organogenesis. It is rational to hypothesize that the mesothelium might contribute to heart regeneration post-natal. However, it is not always the case. Zebrafish epicardium is essential for heart regeneration. It repopulated the massive cell loss, generated neo-vasculature and constitutively secreted various paracrine factors to accelerate myocardium regeneration after ablation [273-278]. But its role is unclear in mammals. Early studies showed that mesothelium treatment to mice with myocardial infarction (MI) significantly improved their post-injury heart function via angiogenesis and the direct contribution to cardiomyocytes around injured sites [279-283]. However, later studies showed that the neo-vasculature observed around injured sites was derived from pre-existing vessels, and the multipotency of epicardium was very limited after birth [284]. It is more likely that

the beneficial effects of mesothelium treatment in myocardial infarction (MI) mice were due the paracrine factors [281].

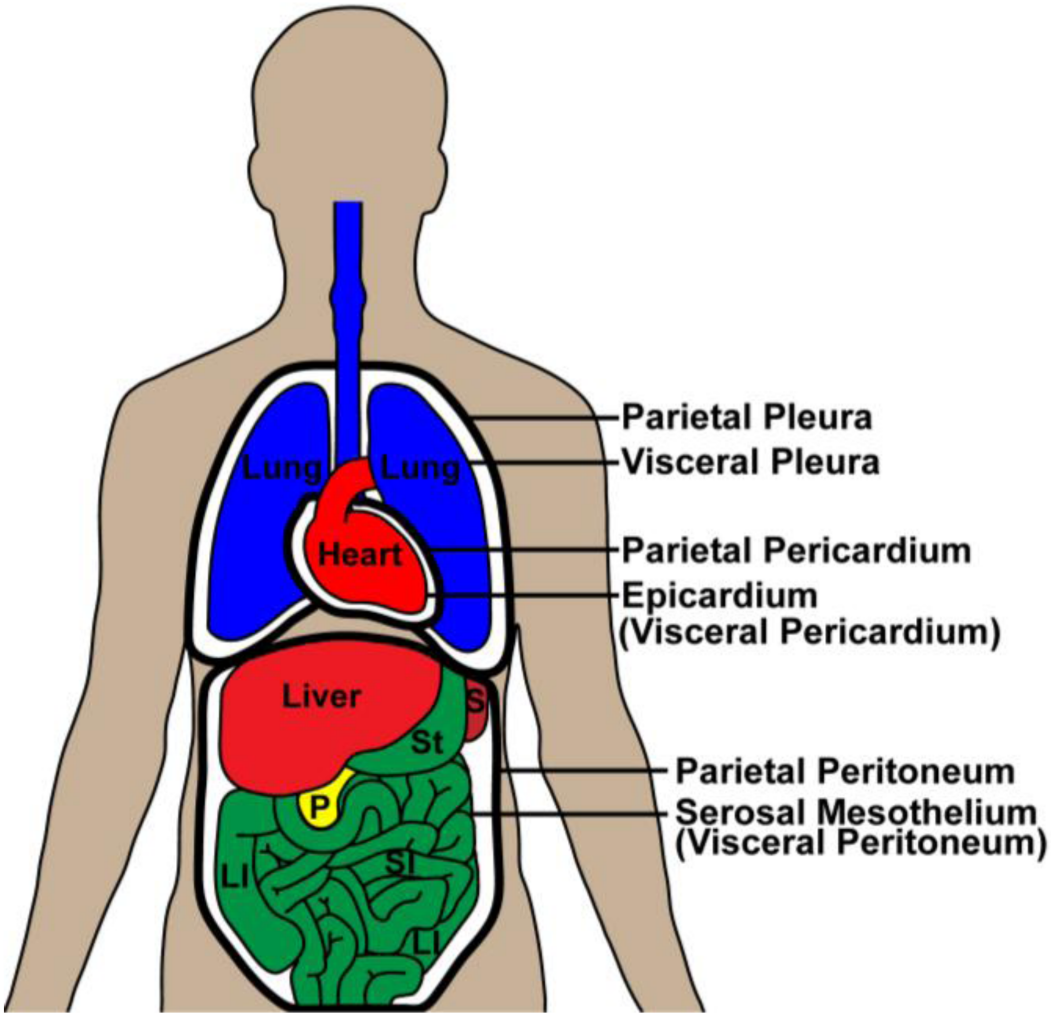

Figure 1.1. Mesothelium covers coelomic wall and organs in human body. It divides into pleura in thoracic cavity, pericardium in cardiac cavity and peritoneum in abdomen. They can be further categorized into parietal versus visceral. Adopted from Nichelle I. Winters et al. 2013.

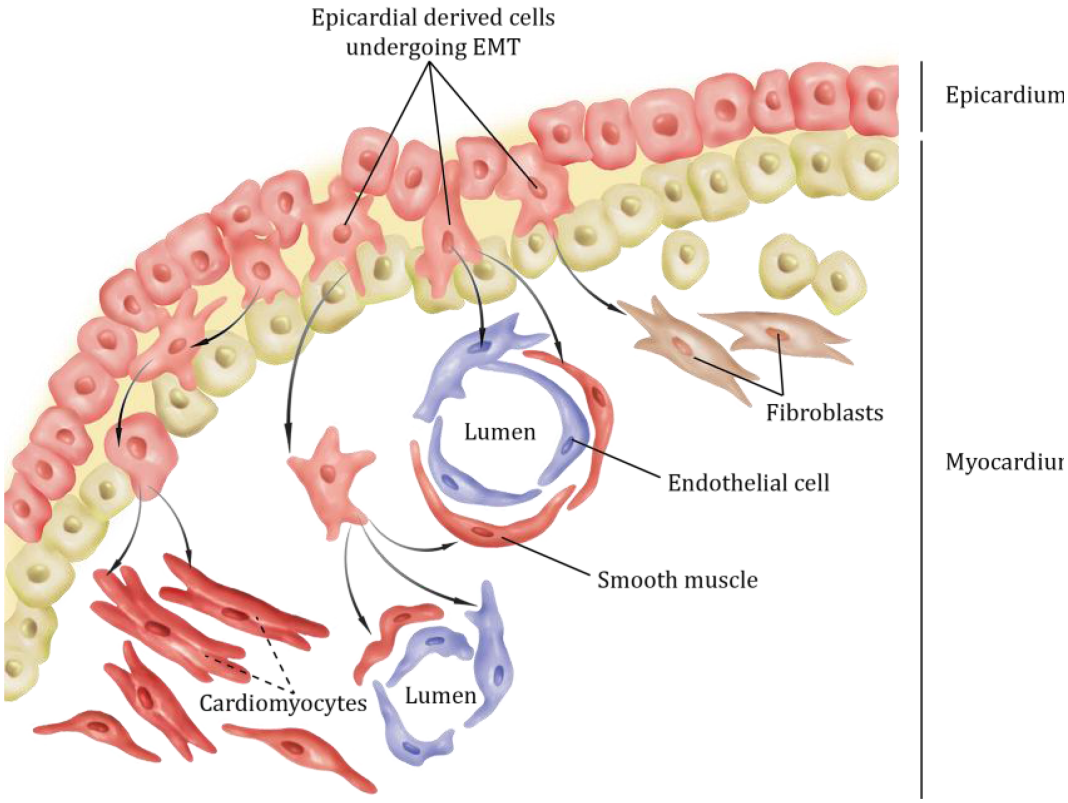

Figure 1.2. Epicardium invades into sub epicardium space and undergoes EMT. It differentiates into cardiomyocytes, fibroblasts, smooth muscle, endothelial cells and forms blood vessels. Adapted from Manvendra K. Singh et al.

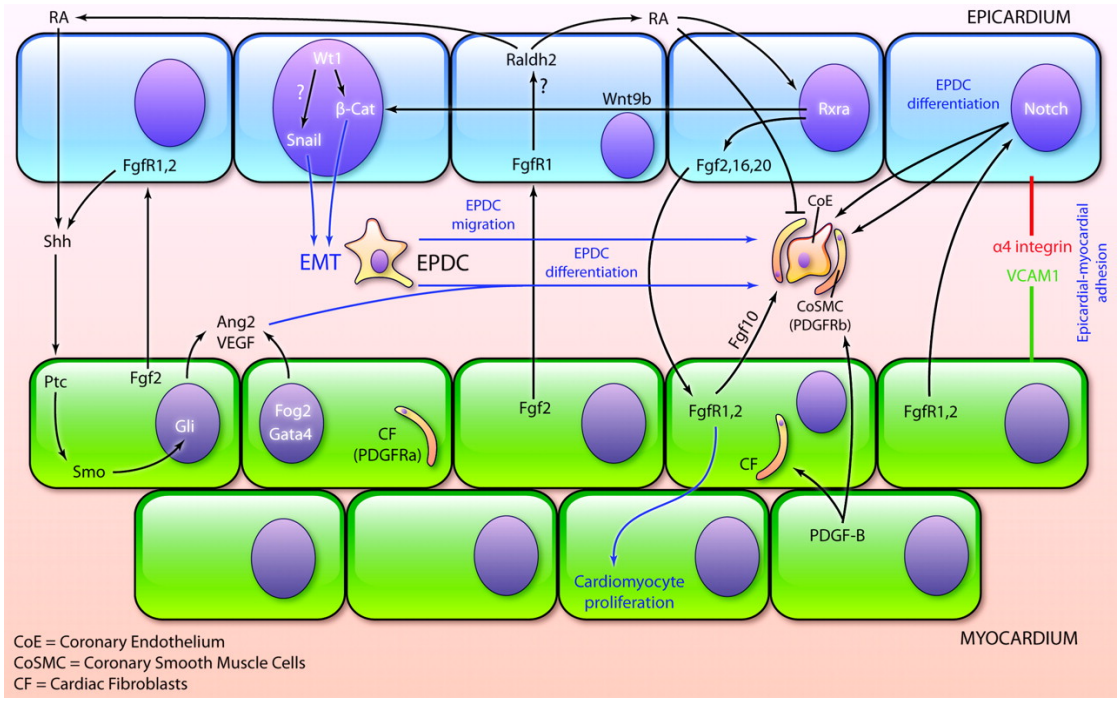

Figure 1.3. The signaling crosstalk between epicardium and myocardium.

Epicardial cells in blue and cardiomyocytes in green. Adopted from Olivey, H.E., et

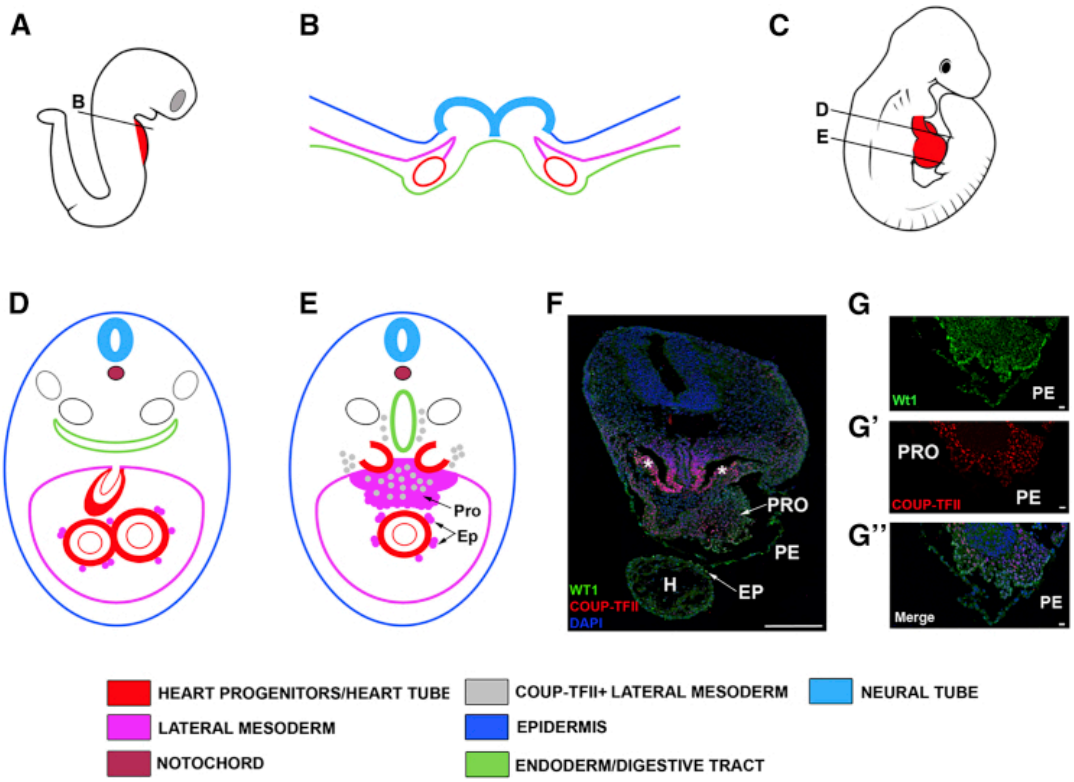

Figure 1.4. The development of epicardium in mouse embryo. A-B. The blastoderm develops into three germ layers, ectoderm (blue), mesoderm (pink) and endoderm (green), and the heart forms a linear structure at E8.5. C-E. From E9.5 to E10.5, as the heart starts looping, the splanchnic mesoderm from the lateral mesoderm migrates towards the heart and forms an outer layer of epicardium (EPI), via an intermediate stage of pro-epicardium (PRO). F-G'' WT1 (green) stains the majority of splanchnic mesoderm derivatives, PRO and EP, and COUP-TF II (red) stains cardiac inflow myocardial progenitors (asterisks) and PRO. Adopted from Juan Antonio Guadix, et al. 2017.

REFERENCES

1. Ksiazek, K., Mesothelial cell: a multifaceted model of aging. Ageing Res Rev, 2013. 12(2): p. 595-604.

2. Mutsaers, S.E., Mesothelial cells: their structure, function and role in serosal repair. Respirology, 2002. 7(3): p. 171-91.

3. Bader, N.I.W.a.D.M., Development of the Serosal Mesothelium. Journal of Development Biology, 2013. 1: p. 64-81.

4. Mutsaers, S.E. and S. Wilkosz, Structure and function of mesothelial cells. Cancer Treat Res, 2007. 134: p. 1-19.

5. Chan, S.Y.a.T.M., INTRINSIC CELLS: MESOTHELIAL CELLS — CENTRAL PLAYERS IN REGULATING INFLAMMATION AND RESOLUTION. Peritoneal Dialysis International, 2009. 29.

6. Mutsaers, S.E., et al., Mesothelial cells and peritoneal homeostasis. Fertil Steril, 2016. 106(5): p. 1018-1024.

7. Kawanishi, K., Diverse properties of the mesothelial cells in health and disease. Pleura Peritoneum, 2016. 1(2): p. 79-89.

8. Kawanishi, K., Mesothelial cell transplantation: history, challenges and future directions. Pleura Peritoneum, 2016. 1(3): p. 135-143.

9. Falk, P., et al., Studies of TGF-beta(1-3) in serosal fluid during abdominal surgery and their effect on in vitro human mesothelial cell proliferation. J Surg Res, 2009. 154(2): p. 312-6.

10. Jantz, M.A. and V.B. Antony, Pathophysiology of the pleura. Respiration, 2008. 75(2): p. 121-33.

11. Shaw, T.J., et al., Human Peritoneal Mesothelial Cells Display Phagocytic and Antigen-Presenting Functions to Contribute to Intraperitoneal Immunity. Int J Gynecol Cancer, 2016. 26(5): p. 833-8.

12. Glik, A. and A. Douvdevani, T lymphocytes: the "cellular" arm of acquired immunity in the peritoneum. Perit Dial Int, 2006. 26(4): p. 438-48.

13. Valle, M.T., et al., Antigen-presenting function of human peritoneum mesothelial cells. Clin Exp Immunol, 1995. 101(1): p. 172-6.

14. Hausmann, M.J., et al., Accessory role of human peritoneal mesothelial cells in antigen presentation and T-cell growth. Kidney Int, 2000. 57(2): p. 476-86.

15. Basok, A., et al., CD40 is expressed on human peritoneal mesothelial cells and upregulates the production of interleukin-15 and RANTES. J Am Soc Nephrol, 2001. 12(4): p. 695-702.

16. Mazar, J., et al., CD40 ligand (CD154) takes part in regulation of the transition to mononuclear cell dominance during peritonitis. Kidney Int, 2005. 67(4): p. 1340-9.

17. Park, J.H., et al., Nod1/RICK and TLR signaling regulate chemokine and antimicrobial innate immune responses in mesothelial cells. J Immunol, 2007. 179(1): p. 514-21.

18. Antony, V.B., et al., Pleural mesothelial cell expression of C-C (monocyte chemotactic peptide) and C-X-C (interleukin 8) chemokines. Am J Respir Cell Mol Biol, 1995. 12(6): p. 581-8.

19. Betjes, M.G., et al., Interleukin-8 production by human peritoneal mesothelial cells in response to tumor necrosis factor-alpha, interleukin-1, and medium *conditioned* by

macrophages cocultured with Staphylococcus epidermidis. J Infect Dis, 1993. 168(5): p. 1202-10.

20. Visser, C.E., et al., Chemokines produced by mesothelial cells: huGRO-alpha, IP-10, MCP-1 and RANTES. Clin Exp Immunol, 1998. 112(2): p. 270-5.

21. Balabanian, K., et al., Interleukin-10 modulates the sensitivity of peritoneal B lymphocytes to chemokines with opposite effects on stromal cell-derived factor-1 and B-lymphocyte chemoattractant. Blood, 2002. 99(2): p. 427-36.

22. Lanfrancone, L., et al., Human peritoneal mesothelial cells produce many cytokines (granulocyte colony-stimulating factor [CSF], granulocyte-monocyte-CSF, macrophage-CSF, interleukin-1 [IL-1], and IL-6) and are activated and stimulated to grow by IL-1. Blood, 1992. 80(11): p. 2835-42.

23. van Grevenstein, W.M., et al., Inflammatory cytokines stimulate the adhesion of colon carcinoma cells to mesothelial monolayers. Dig Dis Sci, 2007. 52(10): p. 2775-83.

24. Cannistra, S.A., et al., Vascular cell adhesion molecule-1 expressed by peritoneal mesothelium partly mediates the binding of activated human T lymphocytes. Exp Hematol, 1994. 22(10): p. 996-1002.

25. Liberek, T., et al., Adherence of neutrophils to human peritoneal mesothelial cells: role of intercellular adhesion molecule-1. J Am Soc Nephrol, 1996. 7(2): p. 208-17.

26. Bellingan, G.J., et al., Adhesion molecule-dependent mechanisms regulate the rate of macrophage clearance during the resolution of peritoneal inflammation. J Exp Med, 2002. 196(11): p. 1515-21.

27. Guazzone, V.A., et al., Expression of cell adhesion molecules, chemokines and chemokine receptors involved in leukocyte traffic in rats undergoing autoimmune orchitis. Reproduction, 2012. 143(5): p. 651-62.

28. Yung, S. and T.M. Chan, Pathophysiological changes to the peritoneal membrane during PD-related peritonitis: the role of mesothelial cells. Mediators Inflamm, 2012. 2012: p. 484167.

29. Mutsaers, S.E., et al., Mesothelial cells in tissue repair and fibrosis. Front Pharmacol, 2015. 6: p. 113.

30. Li, F.K., et al., Leukocyte migration across human peritoneal mesothelial cells is dependent on directed chemokine secretion and ICAM-1 expression. Kidney Int, 1998. 54(6): p. 2170-83.

31. Abendstein, B., et al., Regulation of transforming growth factor-beta secretion by human peritoneal mesothelial and ovarian carcinoma cells. Cytokine, 2000. 12(7): p. 1115-9.

32. Bird, S.D., et al., Platelet derived growth factor-BB induced calcium transients in cultured human peritoneal mesothelial cells. ASAIO J, 1998. 44(6): p. 835-40.

33. Jayne, D.G., et al., Activated mesothelial cells produce heparin-binding growth factors: implications for tumour metastases. Br J Cancer, 2000. 82(6): p. 1233-8.

34. Faull, R.J., et al., HB-EGF is produced in the peritoneal cavity and enhances mesothelial cell adhesion and migration. Kidney Int, 2001. 59(2): p. 614-24.

35. Kimura, I., et al., Release of endothelins and platelet-activating factor by a rat pleural mesothelial cell line. Eur Respir J, 2000. 15(1): p. 170-6.

36. Warn, R., et al., HGF/SF induces mesothelial cell migration and proliferation by autocrine and paracrine pathways. Exp Cell Res, 2001. 267(2): p. 258-66.

37. Yung, S., G.J. Thomas, and M. Davies, Induction of hyaluronan metabolism after mechanical injury of human peritoneal mesothelial cells in vitro. Kidney Int, 2000. 58(5): p. 1953-62.

38. Saed, G.M., et al., Alteration of type I and III collagen expression in human peritoneal mesothelial cells in response to hypoxia and transforming growth factor-beta1. Wound Repair Regen, 1999. 7(6): p. 504-10.

39. Yang, W.S., et al., Interleukin-1beta stimulates the production of extracellular matrix in cultured human peritoneal mesothelial cells. Perit Dial Int, 1999. 19(3): p. 211-20.

40. Yung, S., et al., Source of peritoneal proteoglycans. Human peritoneal mesothelial cells synthesize and secrete mainly small dermatan sulfate proteoglycans. Am J Pathol, 1995. 146(2): p. 520-9.

41. Ma, C., R.W. Tarnuzzer, and N. Chegini, Expression of matrix metalloproteinases and tissue inhibitor of matrix metalloproteinases in mesothelial cells and their regulation by transforming growth factor-beta1. Wound Repair Regen, 1999. 7(6): p. 477-85.

42. Lopez-Cotarelo, C., et al., Expression of heat shock proteins 72/73 in human peritoneal mesothelial cells in vivo and in vitro. Nephron, 2000. 85(2): p. 148-55.

43. Sitter, T., et al., High glucose increases prostaglandin E2 synthesis in human peritoneal mesothelial cells: role of hyperosmolarity. J Am Soc Nephrol, 1998. 9(11): p. 2005-12.

44. Chen, J.Y., et al., Human peritoneal mesothelial cells produce nitric oxide: induction by cytokines. Perit Dial Int, 2000. 20(6): p. 772-7.

45. Benedetti, S., et al., Reactive oxygen species a double-edged sword for mesothelioma. Oncotarget, 2015. 6(19): p. 16848-65.

46. Chapin, J.C. and K.A. Hajjar, Fibrinolysis and the control of blood coagulation. Blood Rev, 2015. 29(1): p. 17-24.

47. Bottles, K.D., et al., Tissue factor expression in mesothelial cells: induction both in vivo and in vitro. Am J Respir Cell Mol Biol, 1997. 17(2): p. 164-72.

48. Jeffers, A., et al., Thrombin down-regulates tissue factor pathway inhibitor expression in a PI3K/nuclear factor-kappaB-dependent manner in human pleural mesothelial cells. Am J Respir Cell Mol Biol, 2015. 52(6): p. 674-82.

49. Bajaj, M.S., et al., Tissue factor pathway inhibitor expression by human pleural mesothelial and mesothelioma cells. Eur Respir J, 2000. 15(6): p. 1069-78.

50. Wood, J.P., et al., Biology of tissue factor pathway inhibitor. Blood, 2014. 123(19): p. 2934-43.

51. Esmon, C.T., Inflammation and the activated protein C anticoagulant pathway. Semin Thromb Hemost, 2006. 32 Suppl 1: p. 49-60.

52. Iakhiaev, A.V., A.R. Rezaie, and S. Idell, Thrombomodulin-mediated catabolism of protein C by pleural mesothelial and vascular endothelial cells. Thromb Haemost, 2007. 98(3): p. 627-34.

53. Schwarz, F., et al., Myocardial CT perfusion imaging in a large animal model: comparison of dynamic versus single-phase acquisitions. JACC Cardiovasc Imaging, 2013. 6(12): p. 1229-38.

54. Sikkink, C.J., et al., Influence of monocyte-like cells on the fibrinolytic activity of peritoneal mesothelial cells and the effect of sodium hyaluronate. Fertil Steril, 2005. 84 Suppl 2: p. 1072-7.

55. Falk, P., et al., Differential regulation of mesothelial cell fibrinolysis by transforming growth factor beta 1. Scand J Clin Lab Invest, 2000. 60(6): p. 439-47.

56. Tucker, T.A., et al., The urokinase receptor supports tumorigenesis of human malignant pleural mesothelioma cells. Am J Respir Cell Mol Biol, 2010. 42(6): p. 685-96.

57. Cortina, M.E., et al., Multiparity upregulates placental plasminogen and urokinase-type plasminogen activator. Am J Reprod Immunol, 2017. 77(4).

58. Mutsaers, S.E., et al., Pathogenesis of pleural fibrosis. Respirology, 2004. 9(4): p. 428-40.

59. Cesari, M., M. Pahor, and R.A. Incalzi, Plasminogen activator inhibitor-1 (PAI-1): a key factor linking fibrinolysis and age-related subclinical and clinical conditions. Cardiovasc Ther, 2010. 28(5): p. e72-91.

60. Carmona, R., et al., Mesothelial-mesenchymal transitions in embryogenesis. Semin Cell Dev Biol, 2019. 92: p. 37-44.

61. Ariza, L., et al., Coelomic epithelium-derived cells in visceral morphogenesis. Dev Dyn, 2016. 245(3): p. 307-22.

62. Riley, P.R., An epicardial floor plan for building and rebuilding the mammalian heart. Curr Top Dev Biol, 2012. 100: p. 233-51.

63. Smits, A.M., E. Dronkers, and M.J. Goumans, The epicardium as a source of multipotent adult cardiac progenitor cells: Their origin, role and fate. Pharmacol Res, 2018. 127: p. 129-140.

64. Niderla-BieliNska, J., et al., Proepicardium: Current Understanding of its Structure, Induction, and Fate. Anat Rec (Hoboken), 2019. 302(6): p. 893-903.

65. Brade, T., et al., Embryonic heart progenitors and cardiogenesis. Cold Spring Harb Perspect Med, 2013. 3(10): p. a013847.

66. von Gise, A. and W.T. Pu, Endocardial and epicardial epithelial to mesenchymal transitions in heart development and disease. Circ Res, 2012. 110(12): p. 1628-45.

67. Simoes, F.C. and P.R. Riley, The ontogeny, activation and function of the epicardium during heart development and regeneration. Development, 2018. 145(7).

68. Manner, J., Does the subepicardial mesenchyme contribute myocardioblasts to the myocardium of the chick embryo heart? A quail-chick chimera study tracing the fate of the epicardial primordium. Anat Rec, 1999. 255(2): p. 212-26.

69. Mikawa, T. and R.G. Gourdie, Pericardial mesoderm generates a population of coronary smooth muscle cells migrating into the heart along with ingrowth of the epicardial organ. Dev Biol, 1996. 174(2): p. 221-32.

70. Gittenberger-de Groot, A.C., et al., Epicardial outgrowth inhibition leads to compensatory mesothelial outflow tract collar and abnormal cardiac septation and coronary formation. Circ Res, 2000. 87(11): p. 969-71.

71. Acharya, A., et al., The bHLH transcription factor Tcf21 is required for lineage-specific EMT of cardiac fibroblast progenitors. Development, 2012. 139(12): p. 2139-49.

72. Duenas, A., A.E. Aranega, and D. Franco, More than Just a Simple Cardiac Envelope; Cellular Contributions of the Epicardium. Front Cell Dev Biol, 2017. 5: p. 44.

73. Vincent, S.D. and M.E. Buckingham, How to make a heart: the origin and regulation of cardiac progenitor cells. Curr Top Dev Biol, 2010. 90: p. 1-41.

74. Poelmann, R.E., et al., Development of the cardiac coronary vascular endothelium, studied with antiendothelial antibodies, in chicken-quail chimeras. Circ Res, 1993. 73(3): p. 559-68.

75. Katz, T.C., et al., Distinct compartments of the proepicardial organ give rise to coronary vascular endothelial cells. Dev Cell, 2012. 22(3): p. 639-50.

76. Rudat, C. and A. Kispert, Wt1 and epicardial fate mapping. Circ Res, 2012. 111(2): p. 165-9.

77. Zhou, B., et al., Epicardial progenitors contribute to the cardiomyocyte lineage in the developing heart. Nature, 2008. 454(7200): p. 109-13.

78. Cai, C.L., et al., A myocardial lineage derives from Tbx18 epicardial cells. Nature, 2008. 454(7200): p. 104-8.

79. Gittenberger-de Groot, A.C., et al., Epicardium-derived cells contribute a novel population to the myocardial wall and the atrioventricular cushions. Circ Res, 1998. 82(10): p. 1043-52.

80. Christoffels, V.M., et al., Tbx18 and the fate of epicardial progenitors. Nature, 2009. 458(7240): p. E8-9; discussion E9-10.

81. Liu, Q., et al., Epicardium-to-fat transition in injured heart. Cell Res, 2014. 24(11): p. 1367-9.

82. Yamaguchi, Y., et al., Adipogenesis and epicardial adipose tissue: a novel fate of the epicardium induced by mesenchymal transformation and PPARgamma activation. Proc Natl Acad Sci U S A, 2015. 112(7): p. 2070-5.

83. Lansley, S.M., et al., Mesothelial cell differentiation into osteoblast- and adipocyte-like cells. J Cell Mol Med, 2011. 15(10): p. 2095-105.

84. Weeke-Klimp, A., et al., Epicardium-derived cells enhance proliferation, cellular maturation and alignment of cardiomyocytes. J Mol Cell Cardiol, 2010. 49(4): p. 606-16.

85. Kelder, T.P., et al., The epicardium as modulator of the cardiac autonomic response during early development. J Mol Cell Cardiol, 2015. 89(Pt B): p. 251-9.

86. Olivey, H.E. and E.C. Svensson, Epicardial-myocardial signaling directing coronary vasculogenesis. Circ Res, 2010. 106(5): p. 818-32.

87. Eralp, I., et al., Coronary artery and orifice development is associated with proper timing of epicardial outgrowth and correlated Fas-ligand-associated apoptosis patterns. Circ Res, 2005. 96(5): p. 526-34.

88. Cano, E., et al., Extracardiac septum transversum/proepicardial endothelial cells pattern embryonic coronary arterio-venous connections. Proc Natl Acad Sci U S A, 2016. 113(3): p. 656-61.

89. Perez-Pomares, J.M. and J.L. de la Pompa, Signaling during epicardium and coronary vessel development. Circ Res, 2011. 109(12): p. 1429-42.

90. Kam, R.K., et al., Retinoic acid synthesis and functions in early embryonic development. Cell Biosci, 2012. 2(1): p. 11.

91. Xavier-Neto, J., et al., Signaling through retinoic acid receptors in cardiac development: Doing the right things at the right times. Biochim Biophys Acta, 2015. 1849(2): p. 94-111.

92. Sucov, H.M., et al., RXR alpha mutant mice establish a genetic basis for vitamin A signaling in heart morphogenesis. Genes Dev, 1994. 8(9): p. 1007-18.

93. Chen, J., S.W. Kubalak, and K.R. Chien, Ventricular muscle-restricted targeting of the RXRalpha gene reveals a non-cell-autonomous requirement in cardiac chamber morphogenesis. Development, 1998. 125(10): p. 1943-9.

94. Merki, E., et al., Epicardial retinoid X receptor alpha is required for myocardial growth and coronary artery formation. Proc Natl Acad Sci U S A, 2005. 102(51): p. 18455-60.

95. Kikuchi, K., et al., Retinoic acid production by endocardium and epicardium is an injury response essential for zebrafish heart regeneration. Dev Cell, 2011. 20(3): p. 397-404.

96. Wang, S., et al., Alterations in retinoic acid signaling affect the development of the mouse coronary vasculature. Dev Dyn, 2018. 247(8): p. 976-991.

97. Cohen, E.D., et al., Wnt/beta-catenin signaling promotes expansion of Isl-1-positive cardiac progenitor cells through regulation of FGF signaling. J Clin Invest, 2007. 117(7): p. 1794-804.

98. Zeigler, B.M., et al., A mouse model for an erythropoietin-deficiency anemia. Dis Model Mech, 2010. 3(11-12): p. 763-72.

99. Wu, H., et al., Inactivation of erythropoietin leads to defects in cardiac morphogenesis. Development, 1999. 126(16): p. 3597-605.

100. Stuckmann, I., S. Evans, and A.B. Lassar, Erythropoietin and retinoic acid, secreted from the epicardium, are required for cardiac myocyte proliferation. Dev Biol, 2003. 255(2): p. 334-49.

101. Brade, T., et al., Retinoic acid stimulates myocardial expansion by induction of hepatic erythropoietin which activates epicardial Igf2. Development, 2011. 138(1): p. 139-48.

102. Lavine, K.J., et al., Endocardial and epicardial derived FGF signals regulate myocardial proliferation and differentiation in vivo. Dev Cell, 2005. 8(1): p. 85-95.

103. Klopsch, C., et al., Intramyocardial angiogenetic stem cells and epicardial erythropoietin save the acute ischemic heart. Dis Model Mech, 2018. 11(6).

104. Li, P., et al., IGF signaling directs ventricular cardiomyocyte proliferation during embryonic heart development. Development, 2011. 138(9): p. 1795-805.

105. Wang, K., et al., Differential roles of insulin like growth factor 1 receptor and insulin receptor during embryonic heart development. BMC Dev Biol, 2019. 19(1): p. 5.

106. Troncoso, R., et al., New insights into IGF-1 signaling in the heart. Trends Endocrinol Metab, 2014. 25(3): p. 128-37.

107. Ma, D.K., et al., SnapShot: Insulin/IGF1 Signaling. Cell, 2015. 161(4): p. 948-948 e1.

108. Shen, H., et al., Extracardiac control of embryonic cardiomyocyte proliferation and ventricular wall expansion. Cardiovasc Res, 2015. 105(3): p. 271-8.

109. Agah, R., et al., Gene recombination in postmitotic cells. Targeted expression of Cre recombinase provokes cardiac-restricted, site-specific rearrangement in adult ventricular muscle in vivo. J Clin Invest, 1997. 100(1): p. 169-79.

110. Teven, C.M., et al., Fibroblast growth factor (FGF) signaling in development and skeletal diseases. Genes Dis, 2014. 1(2): p. 199-213.

111. Vega-Hernandez, M., et al., FGF10/FGFR2b signaling is essential for cardiac fibroblast development and growth of the myocardium. Development, 2011. 138(15): p. 3331-40.

112. Pennisi, D.J. and T. Mikawa, FGFR-1 is required by epicardium-derived cells for myocardial invasion and correct coronary vascular lineage differentiation. Dev Biol, 2009. 328(1): p. 148-59.

113. Lavine, K.J., et al., Fibroblast growth factor signals regulate a wave of Hedgehog activation that is essential for coronary vascular development. Genes Dev, 2006. 20(12): p. 1651-66.

114. Que, J., et al., Mesothelium contributes to vascular smooth muscle and mesenchyme during lung development. Proc Natl Acad Sci U S A, 2008. 105(43): p. 16626-30.

115. Cano, E., R. Carmona, and R. Munoz-Chapuli, Wt1-expressing progenitors contribute to multiple tissues in the developing lung. Am J Physiol Lung Cell Mol Physiol, 2013. 305(4): p. L322-32.

116. von Gise, A., et al., Contribution of Fetal, but Not Adult, Pulmonary Mesothelium to Mesenchymal Lineages in Lung Homeostasis and Fibrosis. Am J Respir Cell Mol Biol, 2016. 54(2): p. 222-30.

117. Ludtke, T.H., et al., Mesothelial mobilization in the developing lung and heart differs in timing, quantity, and pathway dependency. Am J Physiol Lung Cell Mol Physiol, 2019. 316(5): p. L767-L783.

118. Dixit, R., X. Ai, and A. Fine, Derivation of lung mesenchymal lineages from the fetal mesothelium requires hedgehog signaling for mesothelial cell entry. Development, 2013. 140(21): p. 4398-406.

119. Perez-Pomares, J.M., et al., Contribution of mesothelium-derived cells to liver sinusoids in avian embryos. Dev Dyn, 2004. 229(3): p. 465-74.

120. Ijpenberg, A., et al., Wt1 and retinoic acid signaling are essential for stellate cell development and liver morphogenesis. Dev Biol, 2007. 312(1): p. 157-70.

121. Asahina, K., et al., Mesenchymal origin of hepatic stellate cells, submesothelial cells, and perivascular mesenchymal cells during mouse liver development. Hepatology, 2009. 49(3): p. 998-1011.

122. Asahina, K., et al., Septum transversum-derived mesothelium gives rise to hepatic stellate cells and perivascular mesenchymal cells in developing mouse liver. Hepatology, 2011. 53(3): p. 983-95.

123. Lua, I. and K. Asahina, The Role of Mesothelial Cells in Liver Development, Injury, and Regeneration. Gut Liver, 2016. 10(2): p. 166-76.

124. Yang, L., et al., The contributions of mesoderm-derived cells in liver development. Semin Cell Dev Biol, 2019. 92: p. 63-76.

125. Onitsuka, I., M. Tanaka, and A. Miyajima, Characterization and functional analyses of hepatic mesothelial cells in mouse liver development. Gastroenterology, 2010. 138(4): p. 1525-35, 1535 e1-6.

126. Senoo, H., Y. Mezaki, and M. Fujiwara, The stellate cell system (vitamin A-storing cell system). Anat Sci Int, 2017. 92(4): p. 387-455.

127. Ariza, L., et al., Role of the Wilms' tumor suppressor gene Wt1 in pancreatic development. Dev Dyn, 2018. 247(7): p. 924-933.

128. Angelo, J.R. and K.D. Tremblay, Identification and fate mapping of the pancreatic mesenchyme. Dev Biol, 2018. 435(1): p. 15-25.

129. Byrnes, L.E., et al., Lineage dynamics of murine pancreatic development at single-cell resolution. Nat Commun, 2018. 9(1): p. 3922.

130. Wilm, B., et al., The serosal mesothelium is a major source of smooth muscle cells of the gut vasculature. Development, 2005. 132(23): p. 5317-28.

131. Rinkevich, Y., et al., Identification and prospective isolation of a mesothelial precursor lineage giving rise to smooth muscle cells and fibroblasts for mammalian internal organs, and their vasculature. Nat Cell Biol, 2012. 14(12): p. 1251-60.

132. Parenti, R., et al., Wilms' tumor 1 (WT1) protein expression in human developing tissues. Acta Histochem, 2015. 117(4-5): p. 386-96.

133. Bussen, M., et al., The T-box transcription factor Tbx18 maintains the separation of anterior and posterior somite compartments. Genes Dev, 2004. 18(10): p. 1209-21.

134. Lu, J., J.A. Richardson, and E.N. Olson, Capsulin: a novel bHLH transcription factor expressed in epicardial progenitors and mesenchyme of visceral organs. Mech Dev, 1998. 73(1): p. 23-32.

135. Zhou, B., et al., Nkx2-5- and Isl1-expressing cardiac progenitors contribute to proepicardium. Biochem Biophys Res Commun, 2008. 375(3): p. 450-3.

136. Winters, N.I., A.M. Williams, and D.M. Bader, Resident progenitors, not exogenous migratory cells, generate the majority of visceral mesothelium in organogenesis. Dev Biol, 2014. 391(2): p. 125-32.

137. Ferretti, E. and A.K. Hadjantonakis, Mesoderm specification and diversification: from single cells to emergent tissues. Curr Opin Cell Biol, 2019. 61: p. 110-116.

138. Psychoyos, D. and C.D. Stern, Fates and migratory routes of primitive streak cells in the chick embryo. Development, 1996. 122(5): p. 1523-34.

139. Buckingham, M., S. Meilhac, and S. Zaffran, Building the mammalian heart from two sources of myocardial cells. Nat Rev Genet, 2005. 6(11): p. 826-35.

140. SF, G., Developmental Biology. 6th edition. Sinauer Associates, 2000.

141. Camp, E., S. Dietrich, and A. Munsterberg, Fate mapping identifies the origin of SHF/AHF progenitors in the chick primitive streak. PLoS One, 2012. 7(12): p. e51948.

142. Ivanovitch, K., S. Temino, and M. Torres, Live imaging of heart tube development in mouse reveals alternating phases of cardiac differentiation and morphogenesis. Elife, 2017. 6.

143. Manner, J., et al., The origin, formation and developmental significance of the epicardium: a review. Cells Tissues Organs, 2001. 169(2): p. 89-103.

144. van Wijk, B. and M. van den Hoff, Epicardium and myocardium originate from a common cardiogenic precursor pool. Trends Cardiovasc Med, 2010. 20(1): p. 1-7.

145. Viragh, S., et al., Early development of quail heart epicardium and associated vascular and glandular structures. Anat Embryol (Berl), 1993. 188(4): p. 381-93.

146. Van den Eijnde, S.M., A.C. Wenink, and C. Vermeij-Keers, Origin of subepicardial cells in rat embryos. Anat Rec, 1995. 242(1): p. 96-102.

147. Ratajska, A., E. Czarnowska, and B. Ciszek, Embryonic development of the proepicardium and coronary vessels. Int J Dev Biol, 2008. 52(2-3): p. 229-36.

148. Muñoz-Chápuli, R., Epicaridal development. Eur J Anat, 2011. 1(15): p. 10-16.

149. Lupu, I.E., A.N. Redpath, and N. Smart, Spatiotemporal Analysis Reveals Overlap of Key Proepicardial Markers in the Developing Murine Heart. Stem Cell Reports, 2020. 14(5): p. 770-787.

150. Winters, N.I., R.T. Thomason, and D.M. Bader, Identification of a novel developmental mechanism in the generation of mesothelia. Development, 2012. 139(16): p. 2926-34.

151. Nahirney, P.C., T. Mikawa, and D.A. Fischman, Evidence for an extracellular matrix bridge guiding proepicardial cell migration to the myocardium of chick embryos. Dev Dyn, 2003. 227(4): p. 511-23.

152. Cao, J., et al., Single epicardial cell transcriptome sequencing identifies Caveolin 1 as an essential factor in zebrafish heart regeneration. Development, 2016. 143(2): p. 232-43.

153. Weinberger, M., et al., Functional Heterogeneity within the Developing Zebrafish Epicardium. Dev Cell, 2020. 52(5): p. 574-590 e6.

154. Asp, M., et al., A Spatiotemporal Organ-Wide Gene Expression and Cell Atlas of the Developing Human Heart. Cell, 2019. 179(7): p. 1647-1660 e19.

155. Gambardella, L., et al., BNC1 regulates cell heterogeneity in human pluripotent stem cell-derived epicardium. Development, 2019. 146(24).

156. Martinez-Estrada, O.M., et al., Wt1 is required for cardiovascular progenitor cell formation through transcriptional control of Snail and E-cadherin. Nat Genet, 2010. 42(1): p. 89-93.

157. Guadix, J.A., et al., Wt1 controls retinoic acid signalling in embryonic epicardium through transcriptional activation of Raldh2. Development, 2011. 138(6): p. 1093-7.

158. von Gise, A., et al., WT1 regulates epicardial epithelial to mesenchymal transition through beta-catenin and retinoic acid signaling pathways. Dev Biol, 2011. 356(2): p. 421-31.

159. Velecela, V., J. Fazal-Salom, and O.M. Martinez-Estrada, Biological Systems and Methods for Studying WT1 in the Epicardium. Methods Mol Biol, 2016. 1467: p. 61-71.

160. Velecela, V., et al., Epicardial cell shape and maturation are regulated by Wt1 via transcriptional control of Bmp4. Development, 2019. 146(20).

161. Greulich, F., et al., Tbx18 function in epicardial development. Cardiovasc Res, 2012. 96(3): p. 476-83.

162. Wu, S.P., et al., Tbx18 regulates development of the epicardium and coronary vessels. Dev Biol, 2013. 383(2): p. 307-20.

163. Braitsch, C.M., et al., Pod1/Tcf21 is regulated by retinoic acid signaling and inhibits differentiation of epicardium-derived cells into smooth muscle in the developing heart. Dev Biol, 2012. 368(2): p. 345-57.

164. Takeichi, M., et al., The transcription factors Tbx18 and Wt1 control the epicardial epithelial-mesenchymal transition through bi-directional regulation of Slug in murine primary epicardial cells. PLoS One, 2013. 8(2): p. e57829.

165. Tandon, P., et al., Tcf21 regulates the specification and maturation of proepicardial cells. Development, 2013. 140(11): p. 2409-21.

166. Greulich, F., et al., Lack of Genetic Interaction between Tbx18 and Tbx2/Tbx20 in Mouse Epicardial Development. PLoS One, 2016. 11(6): p. e0156787.

167. Lentjes, M.H., et al., The emerging role of GATA transcription factors in development and disease. Expert Rev Mol Med, 2016. 18: p. e3.

168. Tremblay, M., O. Sanchez-Ferras, and M. Bouchard, GATA transcription factors in development and disease. Development, 2018. 145(20).

169. Rodriguez-Segui, S., I. Akerman, and J. Ferrer, GATA believe it: new essential regulators of pancreas development. J Clin Invest, 2012. 122(10): p. 3469-71.

170. Zhao, R., et al., GATA6 is essential for embryonic development of the liver but dispensable for early heart formation. Mol Cell Biol, 2005. 25(7): p. 2622-31.

171. Narita, N., M. Bielinska, and D.B. Wilson, Cardiomyocyte differentiation by GATA-4-deficient embryonic stem cells. Development, 1997. 124(19): p. 3755-64.

172. Zhao, R., et al., Loss of both GATA4 and GATA6 blocks cardiac myocyte differentiation and results in acardia in mice. Dev Biol, 2008. 317(2): p. 614-9.

173. Morrisey, E.E., et al., GATA6 regulates HNF4 and is required for differentiation of visceral endoderm in the mouse embryo. Genes Dev, 1998. 12(22): p. 3579-90.

174. Watt, A.J., et al., GATA4 is essential for formation of the proepicardium and regulates cardiogenesis. Proc Natl Acad Sci U S A, 2004. 101(34): p. 12573-8.

175. Ang, Y.S., et al., Disease Model of GATA4 Mutation Reveals Transcription Factor Cooperativity in Human Cardiogenesis. Cell, 2016. 167(7): p. 1734-1749 e22.

176. Misra, C., et al., Disruption of myocardial Gata4 and Tbx5 results in defects in cardiomyocyte proliferation and atrioventricular septation. Hum Mol Genet, 2014. 23(19): p. 5025-35.

177. Borok, M.J., V.E. Papaioannou, and L. Sussel, Unique functions of Gata4 in mouse liver induction and heart development. Dev Biol, 2016. 410(2): p. 213-222.

178. Kolander, K.D., et al., Epicardial GATA factors regulate early coronary vascular plexus formation. Dev Biol, 2014. 386(1): p. 204-15.

179. Srivastava, D., P. Cserjesi, and E.N. Olson, A subclass of bHLH proteins required for cardiac morphogenesis. Science, 1995. 270(5244): p. 1995-9.

180. McFadden, D.G., et al., The Hand1 and Hand2 transcription factors regulate expansion of the embryonic cardiac ventricles in a gene dosage-dependent manner. Development, 2005. 132(1): p. 189-201.

181. Thomas, T., et al., The bHLH factors, dHAND and eHAND, specify pulmonary and systemic cardiac ventricles independent of left-right sidedness. Dev Biol, 1998. 196(2): p. 228-36.

182. Laforest, B. and M. Nemer, A hand for the epicardium. Circ Res, 2011. 108(8): p. 900-2.

183. Tsuchihashi, T., et al., Hand2 function in second heart field progenitors is essential for cardiogenesis. Dev Biol, 2011. 351(1): p. 62-9.

184. Barnes, R.M., et al., Hand2 loss-of-function in Hand1-expressing cells reveals distinct roles in epicardial and coronary vessel development. Circ Res, 2011. 108(8): p. 940-9.

185. VanDusen, N.J., et al., Hand2 is an essential regulator for two Notch-dependent functions within the embryonic endocardium. Cell Rep, 2014. 9(6): p. 2071-83.

186. Laurent, F., et al., HAND2 Target Gene Regulatory Networks Control Atrioventricular Canal and Cardiac Valve Development. Cell Rep, 2017. 19(8): p. 1602-1613.

187. Morikawa, Y. and P. Cserjesi, Cardiac neural crest expression of Hand2 regulates outflow and second heart field development. Circ Res, 2008. 103(12): p. 1422-9.

188. Holler, K.L., et al., Targeted deletion of Hand2 in cardiac neural crest-derived cells influences cardiac gene expression and outflow tract development. Dev Biol, 2010. 341(1): p. 291-304.

189. Steimle, J.D. and I.P. Moskowitz, TBX5: A Key Regulator of Heart Development. Curr Top Dev Biol, 2017. 122: p. 195-221.

190. Hatcher, C.J., et al., A role for Tbx5 in proepicardial cell migration during cardiogenesis. Physiol Genomics, 2004. 18(2): p. 129-40.

191. Liu, J. and D.Y. Stainier, Tbx5 and Bmp signaling are essential for proepicardium specification in zebrafish. Circ Res, 2010. 106(12): p. 1818-28.

192. Diman, N.Y., et al., Tbx5 is required for avian and Mammalian epicardial formation and coronary vasculogenesis. Circ Res, 2014. 115(10): p. 834-44.

193. Huang, G.N., et al., C/EBP transcription factors mediate epicardial activation during heart development and injury. Science, 2012. 338(6114): p. 1599-603.

194. Vieira, J.M., et al., BRG1-SWI/SNF-dependent regulation of the Wt1 transcriptional landscape mediates epicardial activity during heart development and disease. Nat Commun, 2017. 8: p. 16034.

195. Singh, A., et al., Hippo Signaling Mediators Yap and Taz Are Required in the Epicardium for Coronary Vasculature Development. Cell Rep, 2016. 15(7): p. 1384-1393.

196. Hofsteen, P., et al., Sox9b is required for epicardium formation and plays a role in TCDD-induced heart malformation in zebrafish. Mol Pharmacol, 2013. 84(3): p. 353-60.

197. Lie-Venema, H., et al., Ets-1 and Ets-2 transcription factors are essential for normal coronary and myocardial development in chicken embryos. Circ Res, 2003. 92(7): p. 749-56.

198. Tandon, P., et al., The Lhx9-integrin pathway is essential for positioning of the proepicardial organ. Development, 2016. 143(5): p. 831-40.

199. Ridge, L.A., et al., Non-muscle myosin IIB (Myh10) is required for epicardial function and coronary vessel formation during mammalian development. PLoS Genet, 2017. 13(10): p. e1007068.

200. Rhee, D.Y., et al., Connexin 43 regulates epicardial cell polarity and migration in coronary vascular development. Development, 2009. 136(18): p. 3185-93.

201. Tran, J.R., X. Zheng, and Y. Zheng, Lamin-B1 contributes to the proper timing of epicardial cell migration and function during embryonic heart development. Mol Biol Cell, 2016. 27(25): p. 3956-3963.

202. Niwa, H., The principles that govern transcription factor network functions in stem cells. Development, 2018. 145(6).

203. Radtke, S. and P.A. Horn, Pluripotent and somatic stem cells: from basic science to utilization in disease modeling and therapeutic application. Meeting report on the 7th International Meeting of the Stem Cell Network North Rhine Westphalia. Cell Reprogram, 2013. 15(5): p. 394-6.

204. Miranda, C.C., et al., Human Pluripotent Stem Cells: Applications and Challenges for Regenerative Medicine and Disease Modeling. Adv Biochem Eng Biotechnol, 2020. 171: p. 189-224.

205. Murry, C.E. and G. Keller, Differentiation of embryonic stem cells to clinically relevant populations: lessons from embryonic development. Cell, 2008. 132(4): p. 661-80.

206. Li, K., et al., Differentiation of pluripotent stem cells for regenerative medicine. Biochem Biophys Res Commun, 2016. 471(1): p. 1-4.

207. Vazin, T. and W.J. Freed, Human embryonic stem cells: derivation, culture, and differentiation: a review. Restor Neurol Neurosci, 2010. 28(4): p. 589-603.

208. Thomson, J.A., et al., Embryonic stem cell lines derived from human blastocysts. Science, 1998. 282(5391): p. 1145-7.

209. Moon, S.Y., et al., Generation, culture, and differentiation of human embryonic stem cells for therapeutic applications. Mol Ther, 2006. 13(1): p. 5-14.

210. Reubinoff, B.E., et al., Embryonic stem cell lines from human blastocysts: somatic differentiation in vitro. Nat Biotechnol, 2000. 18(4): p. 399-404.

211. McElroy, S.L. and R.A. Reijo Pera, Culturing human embryonic stem cells in feeder-free conditions. CSH Protoc, 2008. 2008: p. pdb prot5044.

212. Inzunza, J., et al., Derivation of human embryonic stem cell lines in serum replacement medium using postnatal human fibroblasts as feeder cells. Stem Cells, 2005. 23(4): p. 544-9.

213. Amit, M. and J. Itskovitz-Eldor, Derivation and spontaneous differentiation of human embryonic stem cells. J Anat, 2002. 200(Pt 3): p. 225-32.

214. Cheng, L., et al., Human adult marrow cells support prolonged expansion of human embryonic stem cells in culture. Stem Cells, 2003. 21(2): p. 131-42.

215. Miyamoto, K., et al., Human placenta feeder layers support undifferentiated growth of primate embryonic stem cells. Stem Cells, 2004. 22(4): p. 433-40.

216. Desai, N., P. Rambhia, and A. Gishto, Human embryonic stem cell cultivation: historical perspective and evolution of xeno-free culture systems. Reprod Biol Endocrinol, 2015. 13: p. 9.

217. Xu, C., et al., Basic fibroblast growth factor supports undifferentiated human embryonic stem cell growth without conditioned medium. Stem Cells, 2005. 23(3): p. 315-23.

218. Takahashi, K. and S. Yamanaka, Induction of pluripotent stem cells from mouse embryonic and adult fibroblast cultures by defined factors. Cell, 2006. 126(4): p. 663-76.

219. Takahashi, K., et al., Induction of pluripotent stem cells from adult human fibroblasts by defined factors. Cell, 2007. 131(5): p. 861-72.

220. Yu, J., et al., Induced pluripotent stem cell lines derived from human somatic cells. Science, 2007. 318(5858): p. 1917-20.

221. Omole, A.E. and A.O.J. Fakoya, Ten years of progress and promise of induced pluripotent stem cells: historical origins, characteristics, mechanisms, limitations, and potential applications. PeerJ, 2018. 6: p. e4370.

222. Singh, V.K., et al., Induced pluripotent stem cells: applications in regenerative medicine, disease modeling, and drug discovery. Front Cell Dev Biol, 2015. 3: p. 2.

223. Moradi, S., et al., Research and therapy with induced pluripotent stem cells (iPSCs): social, legal, and ethical considerations. Stem Cell Res Ther, 2019. 10(1): p. 341.

224. Dorn, T., et al., Direct nkx2-5 transcriptional repression of isl1 controls cardiomyocyte subtype identity. Stem Cells, 2015. 33(4): p. 1113-29.

225. George, V., S. Colombo, and K.L. Targoff, An early requirement for nkx2.5 ensures the first and second heart field ventricular identity and cardiac function into adulthood. Dev Biol, 2015. 400(1): p. 10-22.

226. Cai, C.L., et al., Isl1 identifies a cardiac progenitor population that proliferates prior to differentiation and contributes a majority of cells to the heart. Dev Cell, 2003. 5(6): p. 877-89.

227. Moretti, A., et al., Multipotent embryonic isl1+ progenitor cells lead to cardiac, smooth muscle, and endothelial cell diversification. Cell, 2006. 127(6): p. 1151-65.

228. Colombo, S., et al., Nkx genes establish second heart field cardiomyocyte progenitors at the arterial pole and pattern the venous pole through Isl1 repression. Development, 2018. 145(3).

229. Kwon, C., K.R. Cordes, and D. Srivastava, Wnt/beta-catenin signaling acts at multiple developmental stages to promote mammalian cardiogenesis. Cell Cycle, 2008. 7(24): p. 3815-8.

230. Ueno, S., et al., Biphasic role for Wnt/beta-catenin signaling in cardiac specification in zebrafish and embryonic stem cells. Proc Natl Acad Sci U S A, 2007. 104(23): p. 9685-90.

231. Lin, L., et al., Beta-catenin directly regulates Islet1 expression in cardiovascular progenitors and is required for multiple aspects of cardiogenesis. Proc Natl Acad Sci U S A, 2007. 104(22): p. 9313-8.

232. Klaus, A., et al., Distinct roles of Wnt/beta-catenin and Bmp signaling during early cardiogenesis. Proc Natl Acad Sci U S A, 2007. 104(47): p. 18531-6.

233. Klaus, A., et al., Wnt/beta-catenin and Bmp signals control distinct sets of transcription factors in cardiac progenitor cells. Proc Natl Acad Sci U S A, 2012. 109(27): p. 10921-6.

234. Yang, L., et al., Isl1Cre reveals a common Bmp pathway in heart and limb development. Development, 2006. 133(8): p. 1575-85.

235. Ilagan, R., et al., Fgf8 is required for anterior heart field development. Development, 2006. 133(12): p. 2435-45.

236. Park, E.J., et al., Required, tissue-specific roles for Fgf8 in outflow tract formation and remodeling. Development, 2006. 133(12): p. 2419-33.

237. Zhang, J., et al., Frs2alpha-deficiency in cardiac progenitors disrupts a subset of FGF signals required for outflow tract morphogenesis. Development, 2008. 135(21): p. 3611-22.

238. Park, E.J., et al., An FGF autocrine loop initiated in second heart field mesoderm regulates morphogenesis at the arterial pole of the heart. Development, 2008. 135(21): p. 3599-610.

239. Kattman, S.J., et al., Stage-specific optimization of activin/nodal and BMP signaling promotes cardiac differentiation of mouse and human pluripotent stem cell lines. Cell Stem Cell, 2011. 8(2): p. 228-40.

240. Lian, X., et al., Robust cardiomyocyte differentiation from human pluripotent stem cells via temporal modulation of canonical Wnt signaling. Proc Natl Acad Sci U S A, 2012. 109(27): p. E1848-57.

241. Den Hartogh, S.C., et al., Dual reporter MESP1 mCherry/w-NKX2-5 eGFP/w hESCs enable studying early human cardiac differentiation. Stem Cells, 2015. 33(1): p. 56-67.

242. Vahdat, S., et al., Expansion of Human Pluripotent Stem Cell-derived Early Cardiovascular Progenitor Cells by a Cocktail of Signaling Factors. Sci Rep, 2019. 9(1): p. 16006.

243. Xavier-Neto, J., et al., Sequential programs of retinoic acid synthesis in the myocardial and epicardial layers of the developing avian heart. Dev Biol, 2000. 219(1): p. 129-41.

244. Jenkins, S.J., D.R. Hutson, and S.W. Kubalak, Analysis of the proepicardium-epicardium transition during the malformation of the RXRalpha-/- epicardium. Dev Dyn, 2005. 233(3): p. 1091-101.

245. Lin, S.C., et al., Endogenous retinoic acid regulates cardiac progenitor differentiation. Proc Natl Acad Sci U S A, 2010. 107(20): p. 9234-9.

246. Wang, S. and A.R. Moise, Recent insights on the role and regulation of retinoic acid signaling during epicardial development. Genesis, 2019. 57(7-8): p. e23303.

247. Kruithof, B.P., et al., BMP and FGF regulate the differentiation of multipotential pericardial mesoderm into the myocardial or epicardial lineage. Dev Biol, 2006. 295(2): p. 507-22.

248. van Wijk, B., et al., Epicardium and myocardium separate from a common precursor pool by crosstalk between bone morphogenetic protein- and fibroblast growth factor-signaling pathways. Circ Res, 2009. 105(5): p. 431-41.

249. Ishii, Y., et al., BMP signals promote proepicardial protrusion necessary for recruitment of coronary vessel and epicardial progenitors to the heart. Dev Cell, 2010. 19(2): p. 307-16.

250. Allison, P., D. Espiritu, and T.D. Camenisch, BMP2 rescues deficient cell migration in Tgfbr3(-/-) epicardial cells and requires Src kinase. Cell Adh Migr, 2016. 10(3): p. 259-68.

251. Andres-Delgado, L., et al., Actin dynamics and the Bmp pathway drive apical extrusion of proepicardial cells. Development, 2019. 146(13).

252. Phillips, M.D., et al., Dkk1 and Dkk2 regulate epicardial specification during mouse heart development. Int J Cardiol, 2011. 150(2): p. 186-92.

253. Cross, E.E., et al., Application of small organic molecules reveals cooperative TGFbeta and BMP regulation of mesothelial cell behaviors. ACS Chem Biol, 2011. 6(9): p. 952-61.

254. DeLaughter, D.M., et al., Transcriptional Profiling of Cultured, Embryonic Epicardial Cells Identifies Novel Genes and Signaling Pathways Regulated by TGFbetaR3 In Vitro. PLoS One, 2016. 11(8): p. e0159710.

255. Witty, A.D., et al., Generation of the epicardial lineage from human pluripotent stem cells. Nat Biotechnol, 2014. 32(10): p. 1026-35.

256. Iyer, D., et al., Robust derivation of epicardium and its differentiated smooth muscle cell progeny from human pluripotent stem cells. Development, 2016. 143(5): p. 904.

257. Zhao, J., et al., Efficient Differentiation of TBX18(+)/WT1(+) Epicardial-Like Cells from Human Pluripotent Stem Cells Using Small Molecular Compounds. Stem Cells Dev, 2017. 26(7): p. 528-540.

258. Bao, X., et al., Directed differentiation and long-term maintenance of epicardial cells derived from human pluripotent stem cells under fully defined conditions. Nat Protoc, 2017. 12(9): p. 1890-1900.

259. Paik, D.T. and J.C. Wu, Simply derived epicardial cells. Nat Biomed Eng, 2017. 1.

260. Guadix, J.A., et al., Human Pluripotent Stem Cell Differentiation into Functional Epicardial Progenitor Cells. Stem Cell Reports, 2017. 9(6): p. 1754-1764.

261. Vrijland, W.W., et al., Abdominal adhesions: intestinal obstruction, pain, and infertility. Surg Endosc, 2003. 17(7): p. 1017-22.

262. Kawanishi, K., et al., Peritoneal cell sheets composed of mesothelial cells and fibroblasts prevent intra-abdominal adhesion formation in a rat model. J Tissue Eng Regen Med, 2016. 10(10): p. 855-866.

263. Kuga, H., et al., Construction of a transplantable tissue-engineered artificial peritoneum. Eur Surg Res, 2004. 36(5): p. 323-30.

264. Nishioka, Y., et al., Regeneration of peritoneal mesothelium in a rat model of peritoneal fibrosis. Ren Fail, 2008. 30(1): p. 97-105.

265. Rotmans, J.I., et al., Endothelial progenitor cell-seeded grafts: rash and risky. Can J Cardiol, 2006. 22(13): p. 1113-6.

266. Mimura, T., S. Yamagami, and S. Amano, Corneal endothelial regeneration and tissue engineering. Prog Retin Eye Res, 2013. 35: p. 1-17.

267. Lachaud, C.C., et al., Mesothelial cells: a cellular surrogate for tissue engineering of corneal endothelium. Invest Ophthalmol Vis Sci, 2014. 55(9): p. 5967-78.

268. Nerem, R.M. and D. Seliktar, Vascular tissue engineering. Annu Rev Biomed Eng, 2001. 3: p. 225-43.

269. Clarke, J.M., et al., Seeding Dacron arterial prostheses with peritoneal mesothelial cells: a preliminary morphological study. Br J Surg, 1984. 71(7): p. 492-4.
270. Pronk, A., et al., Mesothelial cell adherence to vascular prostheses and their subsequent growth in vitro. Cell Transplant, 1994. 3(1): p. 41-8.
271. Sparks, S.R., et al., Small-caliber mesothelial cell-layered polytetraflouroethylene vascular grafts in New Zealand white rabbits. Ann Vasc Surg, 2002. 16(1): p. 73-6.
272. Campbell, J.H., J.L. Efendy, and G.R. Campbell, Novel vascular graft grown within recipient's own peritoneal cavity. Circ Res, 1999. 85(12): p. 1173-8.
273. Colunga, T., et al., Human Pluripotent Stem Cell-Derived Multipotent Vascular Progenitors of the Mesothelium Lineage Have Utility in Tissue Engineering and Repair. Cell Rep, 2019. 26(10): p. 2566-2579 e10.
274. Beffagna, G., Zebrafish as a Smart Model to Understand Regeneration After Heart Injury: How Fish Could Help Humans. Front Cardiovasc Med, 2019. 6: p. 107.
275. Wang, J., et al., Epicardial regeneration is guided by cardiac outflow tract and Hedgehog signalling. Nature, 2015. 522(7555): p. 226-230.
276. Lepilina, A., et al., A dynamic epicardial injury response supports progenitor cell activity during zebrafish heart regeneration. Cell, 2006. 127(3): p. 607-19.
277. Kikuchi, K., et al., tcf21+ epicardial cells adopt non-myocardial fates during zebrafish heart development and regeneration. Development, 2011. 138(14): p. 2895-902.
278. Gonzalez-Rosa, J.M., M. Peralta, and N. Mercader, Pan-epicardial lineage tracing reveals that epicardium derived cells give rise to myofibroblasts and perivascular cells during zebrafish heart regeneration. Dev Biol, 2012. 370(2): p. 173-86.

279. Elmadbouh, I., et al., Mesothelial cell transplantation in the infarct scar induces neovascularization and improves heart function. Cardiovasc Res, 2005. 68(2): p. 307-17.
280. Bourahla, B., et al., Mesothelial cells vs. skeletal myoblasts for myocardial infarction. Asian Cardiovasc Thorac Ann, 2010. 18(2): p. 153-60.
281. Zhou, B., et al., Adult mouse epicardium modulates myocardial injury by secreting paracrine factors. J Clin Invest, 2011. 121(5): p. 1894-904.
282. van Wijk, B., et al., Cardiac regeneration from activated epicardium. PLoS One, 2012. 7(9): p. e44692.
283. Saifi, O., et al., Myocardial regeneration: role of epicardium and implicated genes. Mol Biol Rep, 2019. 46(6): p. 6661-6674.
284. Cai, W., et al., Limited Regeneration Potential with Minimal Epicardial Progenitor Conversions in the Neonatal Mouse Heart after Injury. Cell Rep, 2019. 28(1): p. 190-201 e3.

CHAPTER 2

THE COOPERATION OF GATA4 AND TBX5 SPECIFIES HUMAN MESOTHELIUM CELL FATE

Chen LM, Dalton S. To be submitted to *Developmental Cell*.

SUMMARY

The mesothelium covers all the coelomic organs and is actively involved in organogenesis and injury repair by contributing to vasculature and secreting paracrine factors. During development, the mesothelium is derived from the splanchnic mesoderm, but many questions remain about its formation in different organs. By establishing an *in vitro* mesothelium differentiation model from human pluripotent stem cells (hPSCs) and applying high throughput sequencing (RNA-seq and ATAC-seq); we characterized mesothelium specification at a global level. We found that mesothelium cell fate is regulated by co-occupancy of GATA4 and TBX5 at mesothelium-specific open chromatin elements. Both $GATA4^{-/-}$ and $TBX5^{-/-}$ SplM are incapable of making MLCs and result in the same defects. The specificity of GATA4 in mesothelium formation depends on GATA4-TBX5 interaction. Gata4 and Gata4;Tbx5 compound mouse mutants support the above conclusions. A significant reduction in epicardium coverage and mesothelium coverage over the gut and lung was observed in $Gata4^{-/+}Tbx5^{-/+}$, $Gata4^{Gata6/+}$ and $Gata4^{Gata6/Gata6}$ mouse embryos. Additionally, we found that iPSCs derived from congenital cardiac septal patients carrying a heterozygous GATA4-G296S mutation fail to differentiate into MLCs and display the same phenotypic defects as $GATA4^{-/-}$ and $TBX5^{-/-}$ MLCs. GATA4 G296S mutation disrupts the interaction between GATA4 and TBX5 in MLCs, leading to significantly diminished GATA4 binding to MLC active chromatin regions and reduced transcriptional activity of GATA4. This points to a new mechanism for heart development and potentially, congenital cardiac septal diseases. In summary, this work reveals the requirement for GATA4 and TBX5 in human and mouse

mesothelium development. GATA4-TBX5 interaction at GATA4 G296 site facilitates GATA4 bind to MLC chromatin regions and determines MLC cell fate.

INTRODUCTION

The mesothelium is an epithelial-like monolayer on the coelomic organs and the reproductive system in males and females [1]. As an outer layer, the mesothelium provides a physical barrier protecting organs from infection and a frictionless surface for free organ movement. The mesothelium also functions in immunomodulation and fibrinolysis via its expression of related receptors and factors [2]. The mesothelium's role in organogenesis is most understood in the heart, where it is also known as the epicardium. The epicardium comes from the proepicardium, which resides in the septum transversum. Only when the epicardium migrates from the proepicardium and covers the heart is a three-layer heart structure constructed [3]. A subset of epicardium undergoes an epithelial to mesenchymal transition (EMT) and invades the underlying myocardium. Here, the E-cadherin+/ZO+ epithelial form of epicardium transitions into the E-Cadherin-/a-SMA+ mesenchymal form, known as epicardium derived cells (EPDCs) [4]. EPDCs differentiate into vascular smooth muscle cells (VSMCs), fibroblasts and endothelial cells (Endos), which make up the coronary vascular system [5-7]. EPDCs also accumulate in heart junctional areas, including interventricular sulcus and atrioventricular junctions, and contribute to their normal morphogenesis [8-10]. While it is well-established that the epicardium gives rise to VSMCs and fibroblasts, the epicardial origin of Endos is somewhat debated [11]. In addition to direct cellular contributions, the epicardium also affects cardiomyocytes and coronary vessel growth through its reciprocal signaling with myocardium and vascular cells [12, 13].

Developmentally, the mesothelium is derived from ISL1+/NKX2-5+ splanchnic mesoderm (SplM) [14-16]. As cells transition into the mesothelium, they lose ISL1 and

NKX2-5 expression and express WT1, TBX18 and TCF21 [11, 17]. A few transcription factors, including NKX2-5, GATA4, HAND2 and TBX5, have been reported to be essential for the epicardium formation either in mouse, avian, or zebrafish embryos. Their knockout mouse mutants shared the same phenotype defects, including defective coronary vasculogenesis and thin myocardium walls [15, 19-23]. Some of these mutants also presented malformed atrioventricular septum. However, it is unclear which process, pro/epicardium specification or migration, these factors are involved in and their importance varies in different organisms. It is unknown if the developmental mechanism in the epicardium applies to the mesothelium over other organs. More importantly, it becomes more evident that cell-type-specific gene programs are specified by a transcriptional network, rather than a single transcription factor [24]. Therefore, these studies present major limitations to reveal the developmental mechanisms in mesothelium specification. Additionally, no reports have investigated how this process is regulated in human mesothelium.

Previously, we published an *in vitro* mesothelium-like cell (MLC) differentiation protocol that makes MLC from hPSC via a SplM stage, which recapitulates the *in vivo* mesothelium developmental process [25]. Here, we utilized this *in vitro* mesothelium developmental model and integrated RNA-sequencing (RNA-seq) and the assays for transposase-accessible chromatin sequencing (ATAC-seq) to identify the essential factors in MLC cell fate determination at a global level. This study revealed a key transcriptional network within GATA4 and TBX5 in human mesothelium specification.

RESULTS

GATA4 potentially regulates mesothelium transcriptome

Our previous work established an *in vitro* mesothelium developmental model [25]. hPSCs first differentiate into SplM with the gained expression of SHF markers (*ISL1*, *NKX2-5*, *FOXF1*) and the decreased pluripotency (*NANOG*, *OCT4*, *SOX2*) (Fig. 2.1a and Supplement Fig. 2.1a). Retinoic acid (RA) treatment drives SplM transiting into MLCs (Fig. 2.1a and Supplement Fig. 2.1b, c). MLCs lose ISL1 and NKX2-5 expression but obtain mesothelium markers (WT1, TBX18, TCF21). The dual suppression of EMT by removing its activator (Activin and FGF2) and adding the inhibitor (SB431542) maintains MLCs in the epithelium form (E-cadherin+/ ZO1+/a-SMA-). To evaluate the MLC transcriptome at a global level and identify cell-type specific transcripts, we performed RNA-seq for ESC, SplM and MLC. A total of 1860 transcripts (cluster4, c4) are unique to SplM and 3290 transcripts (cluster5, c5) are MLC specific (Fig. 2.1b). In addition to *WT1*, *TBX18* and *TCF21*, a few other reported mesothelium markers, including *BNC1*, *WNT2B*, *GATA4*, *GATA6* and *TBX5*, were identified. Cell fate determination is tightly controlled by chromatin dynamics [26]. Therefore, we performed ATAC-seq for SplM and MLC to identify chromatin dynamics during the SplM to MLC cell fate switch. Considering that the cardiomyocyte lineage parallels the mesothelium from SplM, we included CM ATAC-seq data into the analysis in order to define MLC-specific accessible regions [27]. k-mean clustering analysis discovered a dynamic chromatin landscape during SplM differentiation (Fig. 2.1c). Compact chromatin in cluster D (cD) become accessible as SplM differentiates into MLC but maintain closed in CM. So, cD represents MLC-specific accessible chromatin regions. By annotating MLC

unique accessible chromatin (cD) to their nearest genes and then intersecting annotated genes to MLC specific transcripts (c5), 1450 MLC transcripts were identified to be associated with 3300 accessible chromatin regions (M regions) (Fig 2.1d). 78.8% of M regions are located > 2kb away from the promotors, and only ~21.2% of them are in the promotor or 3'/5' UTR, indicating the most M regions act as enhancers (Supplementary Fig. 2.1d). To discover transcription factors (TFs) that bind to M regions, we performed the motif discovery analysis and found that GATA family motifs (GATA1-6) are the top-6 enriched motifs, followed by HAND2, PDX1, PBX2 and TEAD1/3 (Fig. 2.1e). We then checked their transcripts in MLC. GATA1-3 are critical in hematopoietic system, and GATA4-6 are more important in heart development [28]. Therefore, we focused on GATA4, GATA5 and GATA6. *GATA4*, *GATA5, GATA6* and *PBX2* have high and upregulated expression in MLC. SplM and MLC share *TEAD1* and *TEAD3* expression, but their transcripts are downregulated in MLC. MLC shows no *PDX1* and a low level of *HAND2* (Fig. 2f). Out of 1450 MLC unique transcripts, 42.3% are potentially regulated by GATA, 25.7% by PBX2 and 33.6% by TEAD (Supplementary Fig. 2.1e). Key mesothelium markers (*WT1*, *TBX18*, *TCF21*, *BNC1* and *WNT2B*) are among the transcripts regulated by at least one of the GATA, PBX2 and TEAD motifs. Only the targets of GATA motif have high enrichment in heart development via GO analysis (Supplementary Fig. 2.1f).

Gata4 has been reported to be important in mouse epicardium formation. However, it is unclear if Gata4 affects the mesothelium specification or just its migration and if GATA4 functions the same in human mesothelium development

[18, 19, 29]. Therefore, we aimed to investigate GATA4 in MLC specification. To start, we validated the binding of GATA4 to MLC chromatin using GATA4 ChIP-sequencing (ChIP-seq). Greater than 85% of GATA4 binding sites are at least 2kb away from promoters. 51% of MLC transcripts have associated GATA4 peaks, including many mesothelium signature genes, such as *WT1*, *BNC1*, *TBX5* and *TBX18* (Fig. 2.1g - i). M regions are compact in SplM in the absence of GATA4 binding and they are accessible in MLC when GATA4 binds to those regions, suggesting that M regions only become open when GATA4 gets recruited (Fig. 2.1j).

Defective mesothelium specification in GATA4$^{-/-}$ MLC

To investigate if GATA4 is required for MLC differentiation, we utilized CRISPR-Cas9 and designed a pair of gRNAs flanking 471 bp of the *GATA4* exon2, aiming to eliminate GATA4 expression (Fig. 2.2a). Two GATA4$^{-/-}$ clones (#1 and #2) were selected and amplified from the CRISPR-Cas9 edited hESC pool; then differentiated to SplM and MLC. GATA4$^{-/-}$ SplM express ISL1 and NKX2-5 at levels comparable to wild type (WT) SplM (Supplementary Fig. 2.2a, b and c). After being replated and cultured in MLCs medium for additional 18 days, both WT and GATA4$^{-/-}$ SplM lose the SplM identity but GATA4$^{-/-}$ SplM fail to differentiate into MLCs (Fig. 2.2b, c and Supplementary Fig. 2.2d). The depletion of GATA4 significantly decreases the transcription levels of mesothelium markers, including *WT1*, *TBX18*, *TCF21* (Fig. 2.2b). A remarkable reduction of other known mesothelium genes, such as *BNC1*, *TBX5*, *MEGF6*, *LRRN4* and *UPK3B*, were identified in GATA4$^{-/-}$ MLC by RNA-seq (Fig. 2.2e). GATA4$^{-/-}$ MLCs express *GATA5* and *GATA6* to WT levels and maintains epithelium

features, shown by its regular expression of *TJP1*, *CDH1*, *CDH5* and *BVES* (Fig. 2.2b and c). At protein levels, GATA4 and TBX18 are undetectable in GATA4$^{-/-}$ MLCs and most of GATA4$^{-/-}$ MLCs lose WT1 (Fig. 2.2c and Supplementary Fig2.2e). Interestingly, there are ~10% of GATA4$^{-/-}$ MLC still expressing a low level of WT1 protein (Fig. 2.2c, d and Supplement Fig. 2.2e). We then rescued GATA4 expression with a Gata4-GR fusion protein to validate if the defects in MLC differentiation are directly due to the absence of GATA4 [30]. Only in the presence of dexamethasone (Dex), when Gata4 is expressed and translocated into nucleus, are the lost mesothelium markers in GATA4$^{-/-}$ MLC re-expressed again. Neither WT GATA6 nor Gata6 overexpression can rescue the defects in GATA4$^{-/-}$ MLC (Fig. 2.f and g). Additionally, we checked if the absence of GATA4 could have the same effects on CM differentiation. However, GATA4$^{-/-}$ hESC differentiate into CM with the same efficiency as WT hESC (Supplementary Fig. 2.2f). Collectively, we showed that GATA4 is essential in human mesothelium development. GATA6 cannot compensate for GATA4 in mesothelium cell fate determination and this non-redundancy is unique for mesothelium specification.

To validate our observations *in vivo*, we examined the role of Gata4 in mouse mesothelium development. WT, Gata4$^{Gata6/+}$, and Gata4$^{Gata6/Gata6}$ mouse embryos are kind gifts from Dr. Lori Sussel [19]. In mutant embryos, Gata4 coding region is replaced by Gata6, which not only abolishes Gata4 expression but also expresses Gata6 in tissues where Gata4 is supposed to be expressed. Gata4$^{Gata6/Gata6}$ mutants were viable to E12.5 with liver hypoplasia and pancreas agenesis [19]. We chose embryos at E11.5, when the mesothelium first covers the

coelomic organs, to study the mesothelium formation. By E11.5 and in WT embryos, a compact layer of epicardium forms on both ventricle and atria (Fig. 2.2h). In heterozygotes ($Gata4^{Gata6/+}$), the epicardium becomes discontinuous. The space between epicardial cells is even more massive in homozygous mutants ($Gata4^{Gata6/Gata6}$). The mesothelium coverage was calculated as the ratio of Wt1 positive cells to the length of covered surface (Fig. 2.2i). The epicardium coverage on the heart significantly decreases in both $Gata4^{Gata6/+}$ and $Gata4^{Gata6/Gata6}$ and the difference between homozygotes and heterozygotes is significant as well. To evaluate if this requirement of Gata4 in epicardium formation applies to other coelomic organs, we did the same quantification for other organs (Fig. 2.2i and Supplement Fig. 2.2g). A substantial decline in mesothelium coverage over the gut and the lung was also observed in $Gata4^{Gata6/+}$ and $Gata4^{Gata6/Gata6}$ but no significant change was found for the liver.

TBX5 cooperates with GATA4 in MLC development and function

GATA4, GATA5 and GATA6 are expressed in both SplM and MLC but the non-redundancy of GATA4 only applies to mesothelium specification. So the question remained in what determines the specificity of GATA4 in mesothelium development. One of the known mechanisms in GATA tissue specificity is through their co-factors [31]. We searched for GATA4 co-factors in the STRING database and attempted to identify a TF that only presents in MLC. In the top 10 candidates, only TBX5 meets such criteria (Fig. 2.3a). Our result from proximity ligation assays (PLA) and co-IP supported that GATA4 and TBX5 physically interact in MLC (Fig 2.3b and c). Next, we knocked-out TBX5 in ESC with CRISPR-Cas9 and evaluated the role of TBX5 in SplM and MLC

differentiations. TBX5$^{-/-}$ ESC makes WT SplM but fails to obtain mesothelium features (Fig. 2.3d-f and Supplement Fig. 2.3a, b). The deprivation of TBX5 leads to the same transcript changes as GATA4$^{-/-}$ MLC; the downregulation of *WT1*, *TBX18*, *TCF21*, *BNC1*, *UPK3B*, *LRRN4*, *WNT2B* and *MEGF6* (Fig. 2.3 d and e). TBX5$^{-/-}$ MLC loses TBX18 protein and has a significant reduction in WT1 protein. Similar to GATA4$^{-/-}$ MLCs, ~10% of TBX5$^{-/-}$ MLCs maintain low WT1 expression (Fig. 2.3 e and f).

To evaluate if both Gata4 and Tbx5 are required for epicardium specification *in vivo*, we examined the epicardium formation in Gata4$^{-/+}$Tbx5$^{-/+}$ compound mutants at E11.5. As described above, a compact layer of Wt1+ epicardium covers both the atria and ventricle in WT embryos at E11.5 (Fig. 2.3g). The gap between Wt1+ epicardial cells increases in both Gata4$^{+/-}$ and Tbx5$^{+/-}$ heterozygotes (Supplement Fig. 2.3e). But a significant reduction of Wt1+ epicardium coverage is only observed in Gata4$^{-/+}$Tbx5$^{-/+}$ compound mutants, resulting in even larger gaps in epicardium. Some areas display malformed epicardium (Fig. 2.3g and h).

Failed mesothelium specification and impaired recruitment of GATA4 to MLC chromatin in GATA4 G296S MLC

The GATA4 and TBX5 interaction site at codon 296 of GATA4 has been previously discovered from congenital heart defects patients [32]. These patients carry a heterozygous c.886G>A mutation in *GATA4*, resulting in a glycine to serine substitution at codon 296 (G296S). GATA4 G296S disrupts the GATA4-

TBX5 interaction. Research has been done to investigate how GATA4 G296S affects heart development with a focus on cardiomyocytes. GATA4 G296S has no effects on cardiomyocyte differentiation but its proliferation and maturation are negatively impacted [33]. Considering the epicardium's role in cardiomyocyte growth, we set to explore if the heart defects linked to GATA4 G296S are non-cell-autonomous but due to the defective mesothelium. We received the GATA4 G296S iPSC cell line generated from the CHD patients by Srivastava et al., and an isogenic WT (iWT) iPSC cell line, which has the point mutant edited back to WT *GATA4* [33]. PLA results verified that GATA4 G296S abolishes the GATA4 and TBX5 interaction in MLC (Fig. 2.4a and b) without alteration in GATA4 expression level (Fig. 2.4d, f). Both iWT and GATA4 G296S iPSC generate WT SplM (Fig. 2.4c and Supplement Fig. 2.4a, b). However, GATA4 G296S SplM fails to turn on mesothelium markers (*WT1* and *TBX18*), while iWT SplM successfully differentiates into MLC under the same condition (Fig. 2.4c). GATA4 G296S MLCs have the same phenotypic defects as MLCs derived from $GATA4^{-/-}$ and $TBX5^{-/-}$; the lost expression of TBX18 and a reduction in WT1 expression but normal expression of E-cadherin (Fig. 2.4d). Most importantly, ~10% of GATA4 G296S MLCs maintain WT1+ (Fig. 2.4d-f). We then evaluated if the binding of GATA4 to MLC specific regions relies on this interaction and if the transcriptional activity of GATA4 changes in GATA4 G296S MLC. A few positive primer pairs targeting GATA4 ChIP-seq peaks near *WT1* (region1), *TBX18*, *BNC1* and *WNT2B* genes, as well as a pair of negative primers flanking a chromatin region near *WT1* but without GATA4 ChIP signal (region2) were designed. In WT MLC, GATA4, TBX5 and H3K27ac signals are significantly more robust at the anticipated positive sites, compared to the negative *WT1* region2 (Fig. 2.4g

and h). The binding affinity of GATA4 and TBX5 to these regions was remarkably decreased in GATA4 G296S MLC (Fig. 2.4g). A significant reduction in H3K27ac signals at positive regions is also detected, suggesting that GATA4 binding to MLC chromatin relies on its interaction with TBX5 and the normal transcriptional activity of GATA4 requires the GATA4-TBX5 interaction (Fig. 2.4h).

DISCUSSION

This study here utilized an *in vitro* mesothelium development model from hPSC and paired RNA-seq and ATAC-seq to describe the transcriptome and chromatin landscape dynamics in the SplM to mesothelium cell fate transition. The analysis revealed a general mechanism in mesothelium cell fate determination at a global level. In summary, the mesothelium specification requires both GATA4 and TBX5. When cells switch from SplM to MLCs, GATA4 recruitment to MLC specific chromatin regions induces chromatin opening in these regions, which activates the MLC specific gene program. Unlike other cell types, this role of GATA4 is non-redundant with GATA6 and the recruitment of GATA4 to MLC chromatin depends on its physical interaction with TBX5 at amino acid 296 site of GATA4. A glycine-to-serine change at codon 296 (G296S) disrupts the GATA4-TBX5 interaction which diminishes both GATA4 and TBX5 affinity to MLC chromatin. Additionally, the loss of the GATA4-TBX5 interactions reduces the transcriptional activity of GATA4 in MLC. Furthermore, the concurrent requirement of GATA4 and TBX5 and the

non-redundancy of GATA4 in epicardium/mesothelium formation applies for mouse embryonic development as well.

GATA plays a central role in the transcriptional regulation of MLC specification

Previously, the developmental mechanisms in epicardium formation have been done in mouse, avian and zebrafish models, and these animal studies only focused on a single transcription factor at a time [14, 18-23]. However, cell-type-specific gene profiles are driven by chromatin dynamics determined by a regulatory network, but not a single factor [24]. Here, we studied the mesothelium specification mechanism in human by employing a hPSC-based mesothelium differentiation protocol. This mesothelium differentiation protocol makes MLCs from hPSC, via an intermediate stage of SplM, which recapitulates the mesothelium development process *in vivo*. The integration of whole transcriptome changes, identified by RNA-seq, and global chromatin landscape dynamics, identified by ATAC-seq, enables us to provide an in-depth regulatory network in mesothelium specification. Our analysis revealed that GATA binding sequences are the most abundant motifs associated with the MLC specific gene program. GATA factors potentially drive the expressions of the central MLC genes and determine MLC cell fate.

GATA4 drives the SplM-MLC chromatin landscape change and is required for mesothelium development

Some GATA factors have been reported to act as pioneer factors in tissue specification [28, 34]. While Gata1, 2, and 3 are predominantly expressed in hematopoietic lineages and determine hematopoietic stem cell fate; Gata4, 5, and 6 show

expression in endoderm and mesoderm and are important cardiac factors [34]. A 2004 study first revealed the requirement of Gata4 in mouse epicardium formation. They showed Gata4$^{-/-}$ mouse mutants were deprived of pro/epicardium and concluded that the heart defects observed in the mutants were not directly due to cardiomyocyte specification but resulted from the absence of pro/epicardium [18]. We found the same effects for GATA4 in human mesothelium formation, GATA4$^{-/-}$ ESCs fail to specify into MLCs. In addition, we determined the epigenetic dynamics driven by GATA4 as mesothelium is specified. GATA4 uniquely binds to MLC specific chromatin regions. These regions are compact at the SplM stage, maintain closed in CM and are only accessible in MLCs, indicating that GATA4 acts a pioneer factor to initiate chromatin structure changes in order to drive the MLC gene expression program.

GATA4 and GATA6 are interchangeable in various tissue developments [35-37]. Our results also supported that GATA4 can be compensated in SplM and CM differentiation since GATA4$^{-/-}$ ESC can make SplM and CM efficiently. However, GATA4$^{-/-}$ SplM fail to differentiate into MLCs with the regular expression of GATA6. The previous study showed that homozygous mouse mutants with GATA4 replaced by GATA6 (GATA4$^{GATA6/GATA6}$) had no pro/epicardium formation [19]. We expanded the analysis to mesothelium formation over other coelomic organs, including gut, liver and lung, at E11.5. Our analysis found remarkable reductions in the mesothelium coverage on the heart, gut and lung. No significant difference in the liver was identified, which might be due to liver hypoplasia in the mutants, so the reduced number of mesothelial cells

can still cover the smaller size of the liver. These results not only support the non-redundancy of GATA4 in epicardium formation but also implicates the requirement of GATA4 is universal in mesothelium formation.

TBX5 collaborates with GATA4 in mesothelium cell fate determination

GATA4 is a shared transcription factor in SplM and MLCs and is upregulated in MLCs. It is possible the unique role of GATA4 in MLCs is driven by a dosage-dependent mechanism, where the upregulated level of GATA4 passes a threshold and specifies MLC, or that its target specificity relies on its co-factors. If working through the dosage-dependent mechanism, we would expect to see that a high level of GATA6 could compensate for GATA4 in mesothelium differentiation as GATA4 and GATA6 share very similar DNA-binding sequences. However, we found that overexpression of GATA6 fails to rescue GATA4$^{-/-}$ MLC defects.

The co-factor dependent non-redundancy of GATA4 has been previously reported in the heart development, where GATA4 is irreplaceable for the heart function via its interaction with FOG2 [31]. In the top 10 GATA4 co-factors from the String database, we found the differential expression of TBX5 in SplM and MLCs, then identified the physical interaction of GATA4 and TBX5 in MLCs. TBX5 plays a vital role in multiple heart developmental stages, but its role in pro/epicardium specification is less conserved [21-23]. tbx5 is essential for pro/epicardium specification in zebrafish [23]. However, murine and avian Tbx5 only affects proper epicardium migration [21, 23]. Our data showed that TBX5 knockout disrupts the mesothelium differentiation in human origin cells and resulted in the same phenotypic defects as GATA4$^{-/-}$ MLCs. These results

highly suggest that TBX5 is the tissue-specific factor of GATA4 and their cooperation specifies human mesothelium.

GATA4 and TBX5 interaction determines the recruitment of GATA4 to MLC chromatin and specifies mesothelium

GATA4 and TBX5 interact with each other at codon 296 of human GATA4. A glycine-to-serine change at this site (G296S) was first identified in patients with cardiac septation defects and has been shown to disrupt the interaction between GATA4 and TBX5 [32]. We also observed the G296-mediated GATA4-TBX5 interaction in MLCs. iPSCs derived from GATA4 G296S patients differentiated into cardiomyocytes, but these cardiomyocytes had abnormal proliferation and functionality [33]. Mouse embryos with homozygous Gata4 G296S ($G296S^{ki/ki}$) displayed reduced myocardial wall thickness resulting from defective cardiomyocyte proliferation and maturation, but with normal cardiomyocyte differentiation [38]. Both studies suggest the heart defects in GATA4 G296S mutants are not cell-autonomous effects of cardiomyocytes. Many other Gata4 mouse mutant lines shared the same non-cell-autonomous cardiac defects [18, 19, 39]. Here, we showed that both $GATA4^{-/-}$ ESC and GATA4 G296S iPSC can make SplM but lose its potency for MLC differentiation. Since the paracrine factors from the epicardium are essential for cardiomyocyte growth, the cardiac defects observed in GATA4 G296S mutants and in other Gata4 mutants might be explained by the defective epicardium/mesothelium formation. More importantly, we revealed that the

epigenetic regulation of GATA4 in mesothelium differentiation depends on its interaction with TBX5 at codon 296. The disruption of GATA4-TBX5 interaction via the G296S mutation leads to the decreased affinity of GATA4 and TBX5 to MLC chromatin and the diminished transcription activity of GATA4 in MLCs.

In conclusion, this report describes the pioneer factor function of GATA4, and a regulatory network via GATA4-TBX5 interaction in mesothelium cell fate determination. The model we proposed is that TBX5 does not directly binds to chromatin but GATA4-TBX5 complex facilitates GATA4 binding to mesothelium chromatin and drives mesothelium cell fate determination. Our study expands the understanding of mesothelium development from mouse and zebrafish to human and reveals a broad regulatory mechanism in mesothelium specification for all coelomic organs. Common cardiac defects, including thinned myocardial wall and cardiac septation defects, have been observed in various Gata4/GATA4 mutants but the cell-autonomous mechanisms of cardiomyocytes failed to fully explain the phenotypes. Our discovery of mesothelium defects resulting from GATA4 G296S provides a possible novel mechanism in congenital cardiac septal diseases. Single-cell sequencing studies have brought us more insights into the heterogeneity of the epicardium. This may explain why there are ~10% WT1+ cells in all the mutants used in this study. Further studies can be conducted to reveal the cell identity of the remaining WT1+ cells in $GATA4^{-/-}$, $TBX5^{-/-}$ and GATA4 G296S MLCs and in mouse mutants, and to discuss the regulation mechanism in WT1+TBX18- cell specification. Gained understanding of mesothelium specification from this study and future investigations will direct a more defined mesothelium differentiation protocol,

which can better serve for any potential clinical applications of the mesothelium in the tissue engineering and regenerative medicine.

ACKNOWLEDGEMENTS

We thank Dr. Lori Sussel (University of Colorado), Dr. Vidu Garg (The Ohio State University) and Dr. Deepak Srivastava (University of California, San Francisco) for providing mouse embryos and iPSC cell lines for this study.

Figure 2.1 GATA4 binds to MLC specific chromatin regions and acts as a pioneer factor for MLC specification. a. A schematic of SplM and MLC differentiation protocol. SplM is induced with Wnt3a and BMP4 from hPSC and differentiate into MLC by removing FGF2, Activin and adding retinoic acid (RA), SB431542. **b.** k-mean clustering of hESC, SplM and MLC RNA-seq identifying 3 cell type specific transcript clusters, c2, c4 and c5. Refer to Supplement Table3.1 for raw counts of the transcripts listed. Biological replicates for each cell type. **c.** Heatmap showing the k-mean clustering analysis for average ATAC-seq signals from two biological replicates of SplM, MLC and CM. **d.** Venn diagram showing the overlap of transcripts annotated to MLC-specific peaks in cD (yellow) and MLC-specific transcripts from c5 (blue). 1450 transcripts associated with 3300 accessible chromatin regions (M regions). **e.** Top 10 motifs in M region (**d**) ranked by -log (p-value, 10). GATA includes GATA1-6. **f.** Transcription levels (in counts per million, cpm) of *GATA4*, *GATA5*, *GATA6*, *HAND2*, *PDX1*, *PBX2*, *TEAD1* and *TEAD3* in SplM and MLC (diamond for SplM and circle for MLC; solid red for replicate 1, rep1; strip red for replicate 2, rep2). **g.** Peak annotation pie chart showing that 51% of GATA4 ChIP peaks fall in intergenic regions, 34% in intron regions and 7% in promoters. **h.** Pie chart showing that 51% of upregulated MLC transcripts (fold change >2, compared to SplM) have associated GATA4 ChIP peaks. **i.** IGV signal tracks of GATA4 ChIP-seq peaks around mesothelium marker genes (*WT1*, *BNC1*, *TBX5* and *TBX18*) in SplM (blue), CM (orange) and MLC (red). **j.** Average plots and heatmaps of ATAC-seq and GATA4 ChIP-seq signals in SplM and MLC around peaks associated with a subset of MLC specific transcripts, which has both annotated GATA4 ChIP peaks and MLC specific ATAC-seq peaks.

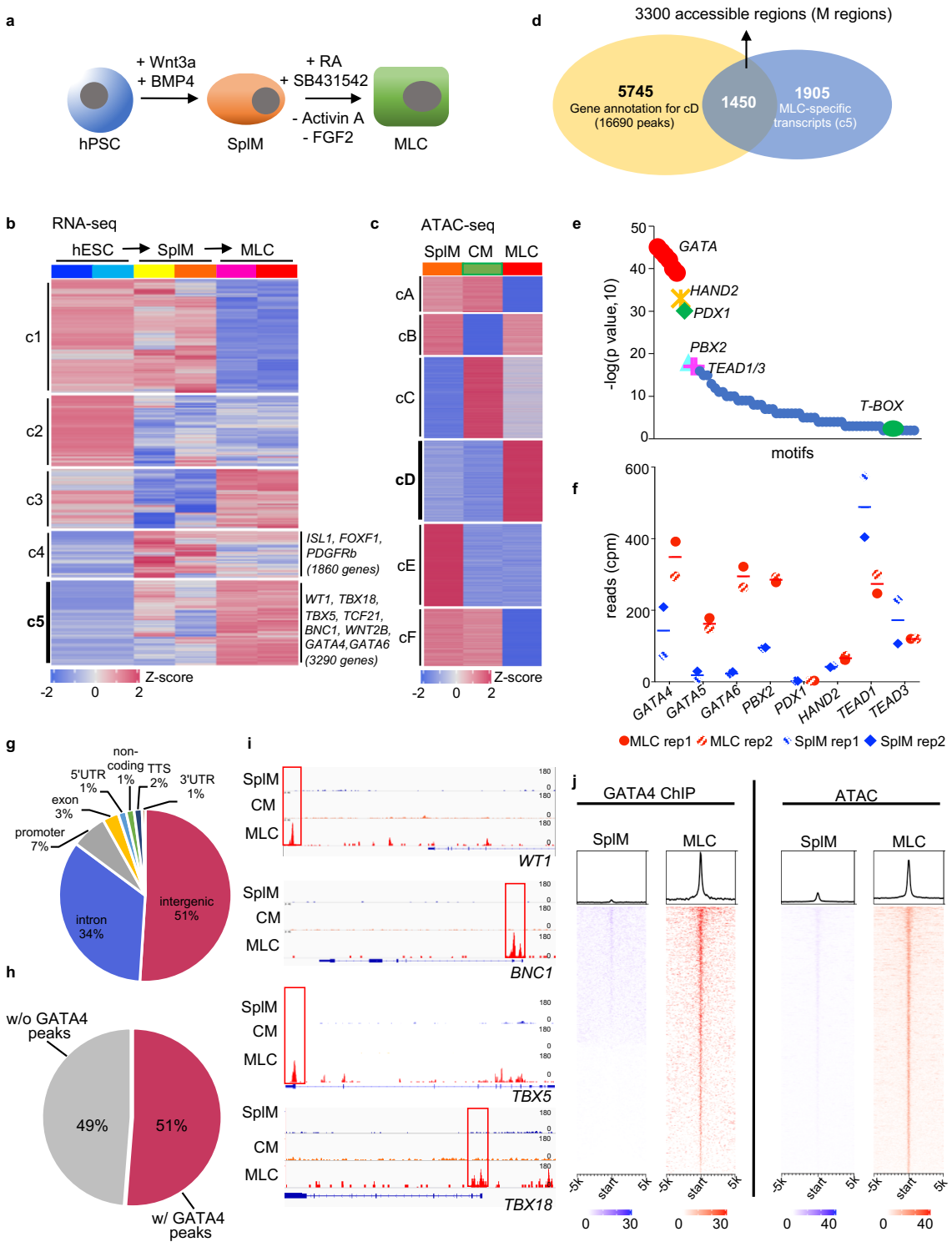
a
+ Wnt3a
+ BMP4
+ RA
+ SB431542
- Activin A
- FGF2
hPSC
SpIM
MLC
d
3300 accessible regions (M regions)
5745
Gene annotation for cD
(16690 peaks)
1450
1905
MLC-specific
transcripts (c5)
b
RNA-seq
hESC
SpIM
MLC
c1
c2
c3
c4
c5
ISL1, FOXF1,
PDGFRb
(1860 genes)
WT1, TBX18,
TBX5, TCF21,
BNC1, WNT2B,
GATA4,GATA6
(3290 genes)
Z-score
-2
0
2
c
ATAC-seq
SpIM
CM
MLC
cA
cB
cC
cD
cE
cF
Z-score
-2
0
2
e
-log(p value,10)
GATA
HAND2
PDX1
PBX2
TEAD1/3
T-BOX
motifs
f
reads (cpm)
GATA4
GATA5
GATA6
PBX2
PDX1
HAND2
TEAD1
TEAD3
MLC rep1
MLC rep2
SpIM rep1
SpIM rep2
g
non-
coding
1%
5'UTR
1%
TTS
2%
3'UTR
1%
exon
3%
promoter
7%
intron
34%
intergenic
51%
h
w/o GATA4
peaks
49%
51%
w/ GATA4
peaks
i
SpIM
CM
MLC
WT1
BNC1
TBX5
TBX18
j
GATA4 ChIP
ATAC
SpIM
MLC
-5k
start
5k
0
30
40

Figure 2.2 GATA4 is required for MLC cell fate and plays a non-redundant role in mesothelium specification. a. gRNAs design strategy for CRISPR-Cas9 mediated GATA4 knockout. **b.** Transcription levels of *GATA4*, *GATA5*, *GATA6*, *WT1*, *TBX18* and *TCF21* in WT MLC (blue) and MLC derived from two GATA4$^{-/-}$ clones (G4$^{-/-}$ #1 and G4$^{-/-}$ #2, in red and green). Values are relative to their levels in WT ESC and RNA18s. Dot represents one biological replicate and each cell type has biological triplicates. Lines represent mean +/- SEM. ***, $p<0.001$; ns, non-significant. **c.** IF assays showing ISL1, GATA4, WT1, TBX18 and E-cadherin (E-cad) in WT, G4$^{-/-}$ #1 and G4$^{-/-}$ #2 MLC. scale bar, 50 μm. **d.** Quantification of WT1+ cells in WT, G4$^{-/-}$ #1 and G4$^{-/-}$ #2 MLC. 10 different fields of view from biological triplicates were randomly selected for counting and values were calculated as WT1+ cell number / total cell number counted by DAPI. **e.** Heatmap of differentially expressed transcripts in WT vs. GATA4$^{-/-}$ MLC from RNA-seq. Experiments were done in biological replicates. Refer to Supplement Table3.2 for raw counts of the transcripts listed. **f.** Heatmap displaying the fold change of transcripts in WT MLC, GATA4$^{-/-}$ MLC, and MLC derived from GATA4$^{-/-}$ ESC rescued by Gata4-GR and Gata6-GR with or without dexamethasone (Dex). Values are relative to WT MLC and pre-normalized with their values in ESC and RNA18S level. GATA4, GATA6 and Gata4, Gata6 amplify human GATA4, GATA6 and mouse Gata4, Gata6, respectively. **g.** IF images of WT1 and TBX18 with WT GATA4 expression and in MLC derived from GATA4$^{-/-}$ ESC rescued by Gata4-GR treated with (+) or without Dex. scale bar, 50 μm. **h.** IF and bright field images of epicardium on ventricle (V) and atria (A) from cryo-sections (10 um) of E11.5 WT, GATA4$^{GATA6/+}$, and GATA4$^{GATA6/GATA6}$ embryos. Sections were probed with WT1 (red) and DAPI (blue). scale bar, 75 μm. **i.**

Quantification of mesothelium coverage on heart, gut, lung and liver by the number of WT1+ cells / length of the covering surface (mm). Lines represent mean +/- SEM. ns, non-significant.

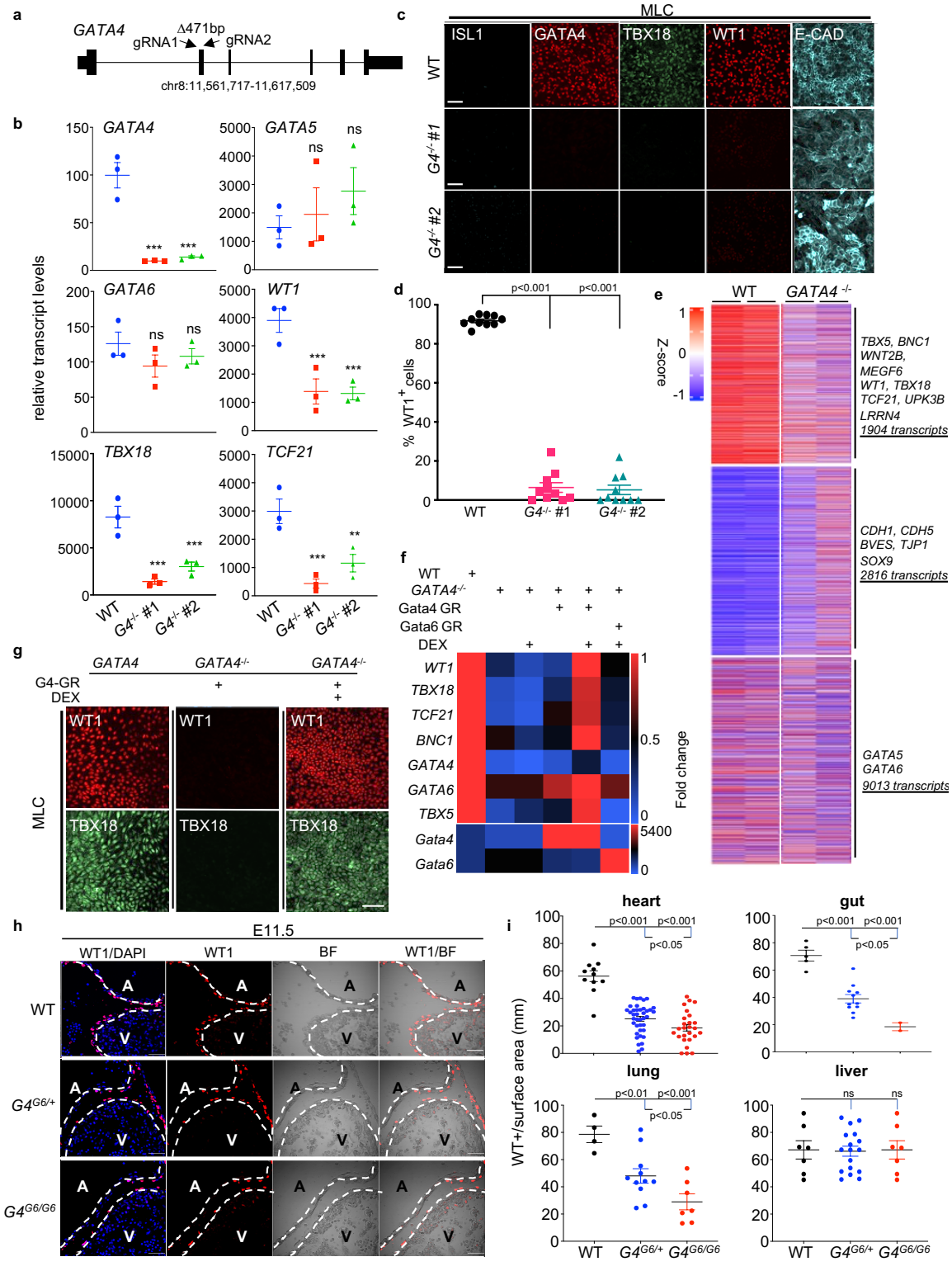
a
GATA4
Δ471bp
gRNA1
gRNA2
chr8:11,561,717-11,617,509
b
GATA4
GATA5
GATA6
WT1
TBX18
TCF21
relative transcript levels
ns
***
**
WT
G4-/- #1
G4-/- #2
c
MLC
ISL1
GATA4
TBX18
WT1
E-CAD
WT
G4-/- #1
G4-/- #2
d
p<0.001
% WT1+ cells
WT
G4-/- #1
G4-/- #2
e
WT
GATA4 -/-
Z-score
TBX5, BNC1
WNT2B,
MEGF6
WT1, TBX18
TCF21, UPK3B
LRRN4
1904 transcripts
CDH1, CDH5
BVES, TJP1
SOX9
2816 transcripts
GATA5
GATA6
9013 transcripts
f
WT
GATA4-/-
Gata4 GR
Gata6 GR
DEX
WT1
TBX18
TCF21
BNC1
GATA4
GATA6
TBX5
Gata4
Gata6
Fold change
g
GATA4
GATA4-/-
G4-GR
DEX
MLC
WT1
TBX18
h
E11.5
WT1/DAPI
WT1
BF
WT1/BF
WT
G4G6/+
G4G6/G6
A
V
i
heart
gut
lung
liver
WT+/surface area (mm)
p<0.001
p<0.05
p<0.01
ns
WT
G4G6/+
G4G6/G6

Figure 2.3 TBX5 interacts with GATA4 in MLC and the loss of TBX5 results in the same MLC defects as GATA4 knockout. a. Transcription levels (in $log2^{CPM}$) of GATA4 co-factors in SplM and MLC. Solid red for replicate 1, rep1; stripe red for replicate 2, rep2. **b.** Confocal images of proximity ligation (PLA) assays co-probed with GATA4 and TBX5 antibodies in WT, $GATA4^{-/-}$ and $TBX5^{-/-}$ MLC. Red dot indicates GATA4-TBX5 interaction site and were qualified in the bar graph as the number of red dots per cell on left y-axis (blue) and the percentage of red dots in nucleus on right y-axis (red). scale bar, 125 μm. **c.** Blot showing WB results running against GATA4 antibody with WT MLC proteins pulled down with IgG, GATA4 or TBX5 antibodies. Input, WT MLC proteins without the pull-down. **d.** Heatmap from qRT-PCR of mesothelium markers and *GATA4*, *GATA6*, *TBX5* in WT MLC and $GATA4^{-/-}$, $TBX5^{-/-}$ cells. Fold changes are relative to WT MLC after being normalized to their values in ESC and RNA18S level. **e.** IF staining of TBX5, WT1, TBX18 and E-CAD proteins in WT and $TBX5^{-/-}$ MLC. scale bar, 50 μm. **f.** Quantification of WT1+ cells in WT and $TBX5^{-/-}$ MLC in 10 different fields of view from biological triplicates. Lines represent mean +/- SEM. **g.** Confocal images showing WT1 (red), DAPI (blue) and bright field (BF) images of paraffin-embedded WT and $GATA4^{-/+}TBX5^{-/+}$ embryo sections at E11.5. scale bar, 75 μm. A, atrium; V, ventricle. **h.** Quantification of the epicardium coverage by the number of WT1+ cells / length of the covering surface (mm). Each genotype has biological triplicates. **, $p<0.05$; ns, non-significant; compared to WT.

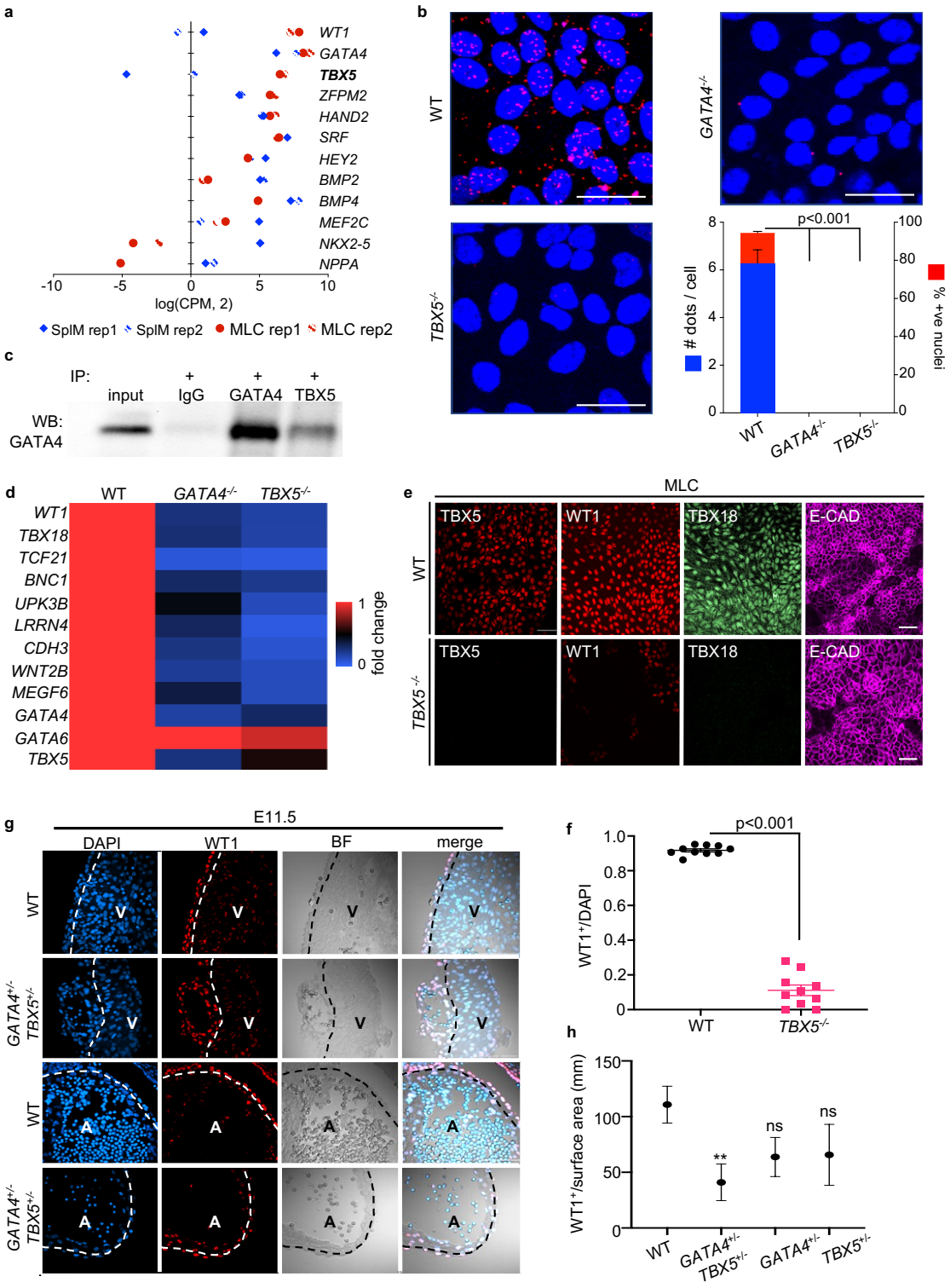
a
WT1
GATA4
TBX5
ZFPM2
HAND2
SRF
HEY2
BMP2
BMP4
MEF2C
NKX2-5
NPPA
-10
-5
0
5
10
log(CPM, 2)
SplM rep1
SplM rep2
MLC rep1
MLC rep2
b
WT
GATA4-/-
TBX5-/-
p<0.001
dots / cell
% +ve nuclei
WT
GATA4-/-
TBX5-/-
c
IP:
input
IgG
GATA4
TBX5
WB:
GATA4
d
WT
GATA4-/-
TBX5-/-
WT1
TBX18
TCF21
BNC1
UPK3B
LRRN4
CDH3
WNT2B
MEGF6
GATA4
GATA6
TBX5
1
0
fold change
e
MLC
WT
TBX5-/-
TBX5
WT1
TBX18
E-CAD
f
p<0.001
WT1+/DAPI
WT
TBX5-/-
g
E11.5
DAPI
WT1
BF
merge
WT
GATA4+/- TBX5+/-
V
A
h
WT1+/surface area (mm)
ns
**
WT
GATA4+/- TBX5+/-
GATA4+/-
TBX5+/-

Figure 2.4 G296S mutation in GATA4 leads to defective MLC differentiation due to the disrupted GATA4-TBX5 interaction. **a.** PLA assay of GATA4 and TBX5 interaction (red dot) in iWT and GATA4 G296S MLC. scale bar, 125 μm. **b.** Quantification for **a** shown as the number of red dots per cell on the left y-axis (blue) and the percentage of red dots in nucleus on the right y-axis (red). Counting was done in 5 different views for each experiment. **c.** qRT-PCR analysis for *ISL1*, *NXK2-5*, *WT1* and *TBX18* transcripts in iWT SplM (solid blue), GATA4 G296S SplM (stripe blue), iWT MLC (solid red) and GATA4 G296S MLC (stripe red). Values are normalized to the values in ESC and RNA18S. **d.** Confocal images of ISL1, NKX2-5, GATA4, WT1, TBX18 and E-CAD expression in iWT and GATA4 296S MLC. scale bar, 75 μm. **e.** The number of WT1+ cells were counted in iWT and GATA4 G296S MLC and were represented as the number of WT1+ cells divided by the total number of the cells (DAPI). 5 different views from biological replicates were randomly selected for counting. **f.** WB assay detecting WT1 and GATA4 proteins in iWT and GATA4 G296S MLC. **g.** Bar plots showing GATA4 and TBX5 qChIP assays at chromatin regions associated with *WT1 (region1)*, *TBX18*, *BNC1* and *WNT2B* in WT MLC (blue) and GATA4 G296S MLC (red). WT1 region2 serves as a negative control. Experiments were done in biological triplicates. #, $p<0.05$, t-test for values of each region vs. WT1 (region2) in WT MLC; *, $p<0.05$, t-test for values in mutant MLC vs. WT MLC at each region; n.s, non-significant. **h.** H3K27ac qChIP assays in WT MLC (blue), $GATA4^{-/-}$ MLC (green) and GATA4 G296S MLC (red) targeting the same regions in **g**. Biological triplicates for each experiment. #, $p<0.05$, t-test for values of each region vs. WT1 (region2) in WT MLC; *, $p<0.05$, t-test for values in mutant MLC vs. WT MLC at each region; n.s, non-significant.

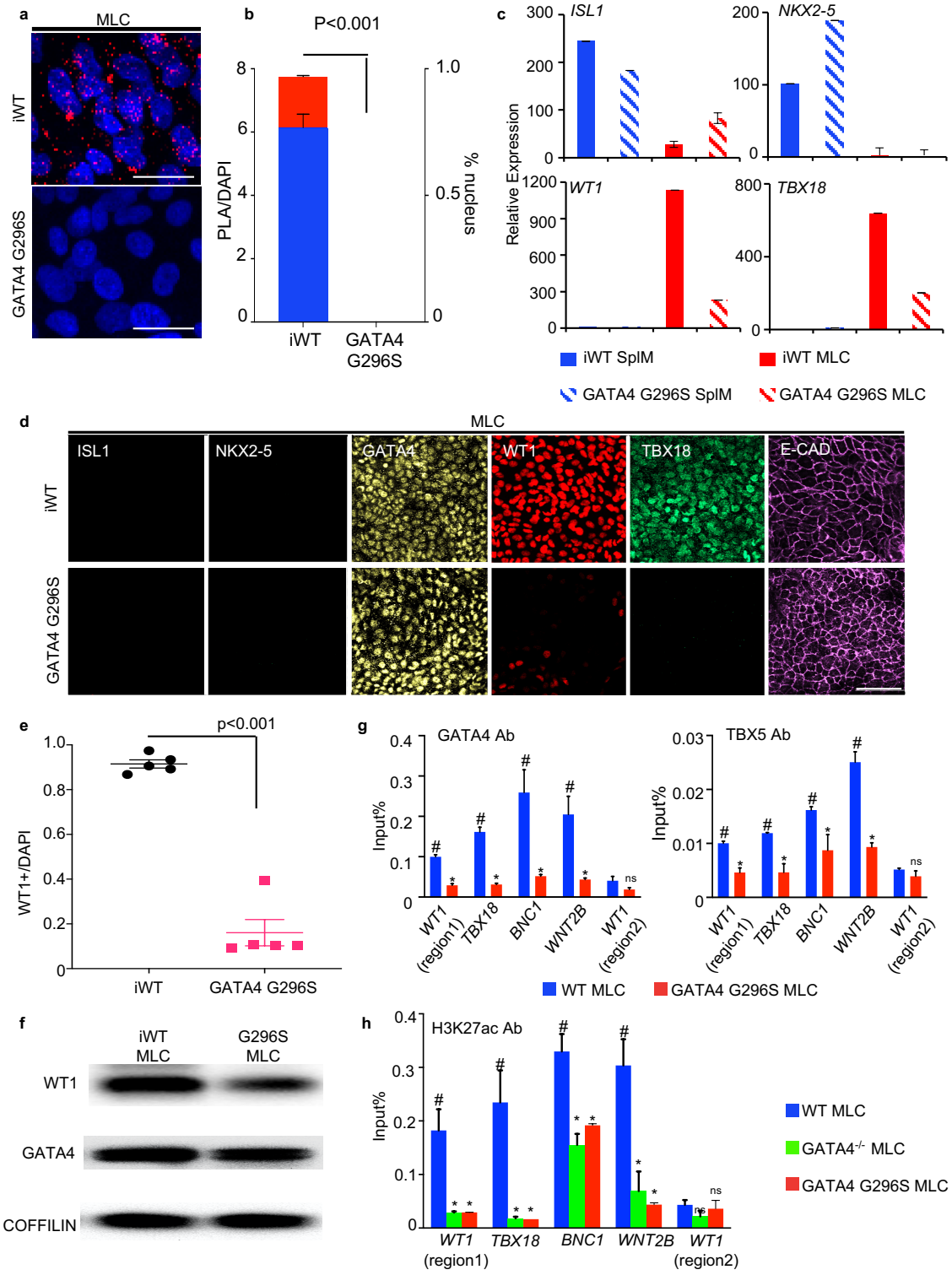
a
MLC
iWT
GATA4 G296S
b
P<0.001
PLA/DAPI
% nucleus
iWT
GATA4 G296S
c
ISL1
NKX2-5
WT1
TBX18
Relative Expression
iWT SplM
iWT MLC
GATA4 G296S SplM
GATA4 G296S MLC
d
MLC
ISL1
NKX2-5
GATA4
WT1
TBX18
E-CAD
iWT
GATA4 G296S
e
p<0.001
WT1+/DAPI
iWT
GATA4 G296S
f
iWT MLC
G296S MLC
WT1
GATA4
COFFILIN
g
GATA4 Ab
TBX5 Ab
Input%
WT1 (region1)
TBX18
BNC1
WNT2B
WT1 (region2)
WT MLC
GATA4 G296S MLC
h
H3K27ac Ab
Input%
WT1 (region1)
TBX18
BNC1
WNT2B
WT1 (region2)
WT MLC
GATA4-/- MLC
GATA4 G296S MLC

Supplement Figure 2.1 – related to Figure 2.1. **a & b.** qRT-PCR analysis showing the transcription level of pluripotency markers (*NANOG*, *OCT4*, *SOX2*), SplM markers (*ISL1*, *NKX2-5*, *FOXF1*), MLC markers (*WT1*, *TBX18*, *TCF21*) and tight junction marker (*CDH1*) in ESC, SplM and MLC. Plotted values are relative to their levels in ESC and RNA18S. **c.** IF assays of ISL1, NKX2-5, WT1, TBX18, E-Cadherin, ZO1, αSMA and DAPI in MLC. scale bar, 50 μm. **d.** Peak annotation pie chart showing peak distribution of M regions (**Fig. 2.1d**). **e.** Pie charts summarizing the percentage of 1450 MLC specific transcripts (**Fig. 2.1d**) potentially regulated by TEAD1 (green, 33.6%), PBX2 (blue, 25.7%) and GATA (red, 42.3%), respectively. The mesothelium signature genes, including *WT1*, *TBX18*, *TCF21*, *BNC1*, *WNT2B*, *GATA4*, *GATA6* and *TBX5*, are the potential targets of GATA. **f.** GO enrichment analysis for transcripts in (**e**). GO terms for transcripts associated with TEAD1 motif are shown in green, the ones for PBX2 motif are shown in blue and GATA in red. Values are in -log (p value, 10).

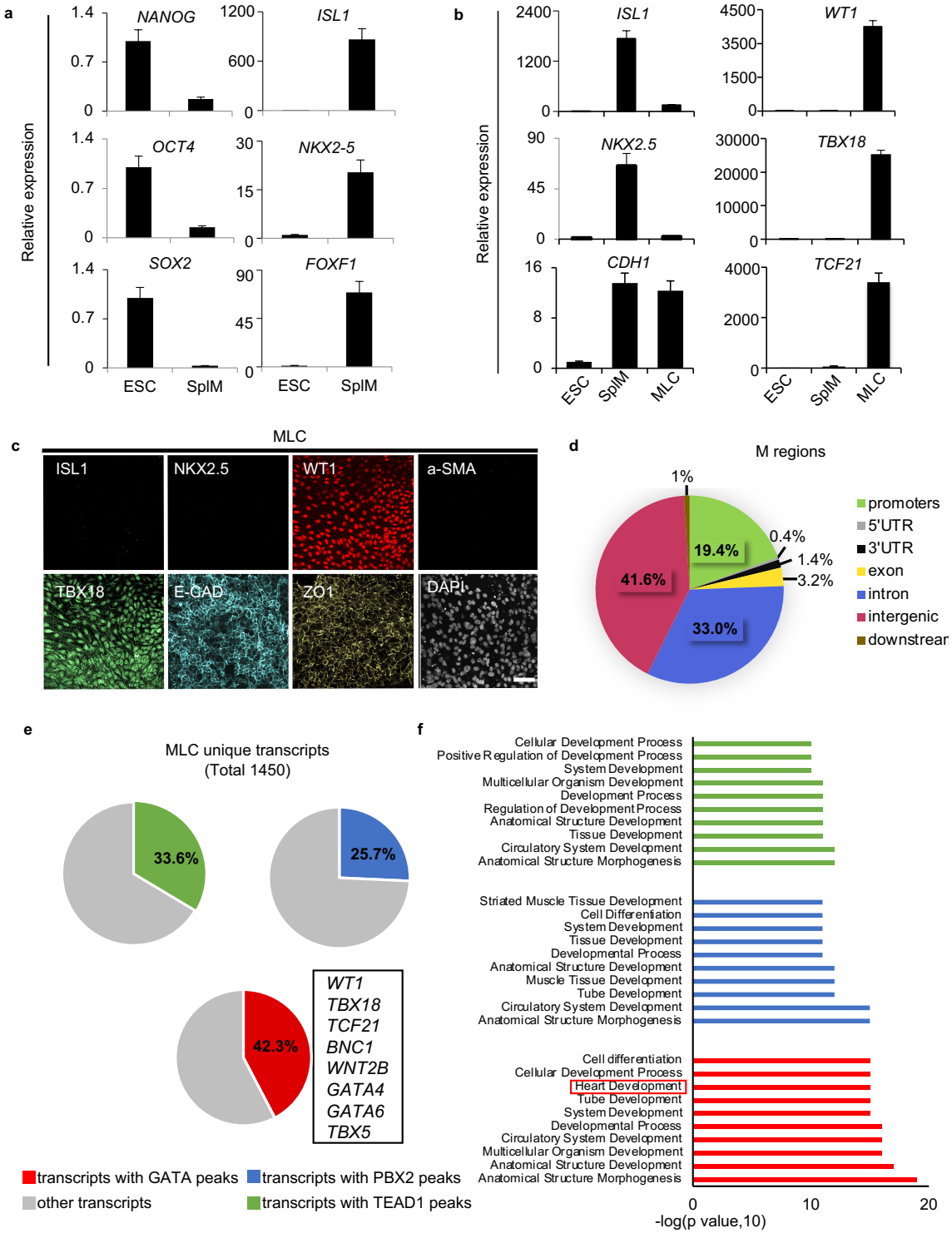
a
Relative expression
NANOG
ISL1
OCT4
NKX2-5
SOX2
FOXF1
ESC
SpIM
b
Relative expression
ISL1
WT1
NKX2.5
TBX18
CDH1
TCF21
ESC
SpIM
MLC
c
MLC
ISL1
NKX2.5
WT1
a-SMA
TBX18
E-CAD
ZO1
DAPI
d
M regions
1%
0.4%
1.4%
3.2%
19.4%
41.6%
33.0%
promoters
5'UTR
3'UTR
exon
intron
intergenic
downstrear
e
MLC unique transcripts
(Total 1450)
33.6%
25.7%
42.3%
WT1
TBX18
TCF21
BNC1
WNT2B
GATA4
GATA6
TBX5
transcripts with GATA peaks
transcripts with PBX2 peaks
other transcripts
transcripts with TEAD1 peaks
f
Cellular Development Process
Positive Regulation of Development Process
System Development
Multicellular Organism Development
Development Process
Regulation of Development Process
Anatomical Structure Development
Tissue Development
Circulatory System Development
Anatomical Structure Morphogenesis
Striated Muscle Tissue Development
Cell Differentiation
System Development
Tissue Development
Developmental Process
Anatomical Structure Development
Muscle Tissue Development
Tube Development
Circulatory System Development
Anatomical Structure Morphogenesis
Cell differentiation
Cellular Development Process
Heart Development
Tube Development
System Development
Developmental Process
Circulatory System Development
Multicellular Organism Development
Anatomical Structure Development
Anatomical Structure Morphogenesis
0
10
20
-log(p value,10)

Supplement Figure 2.2 – related to Figure 2.2. a. IF showing the expression level of ISL1, NKX2-5, GATA4 and WT1 in WT, G4$^{-/-}$ #1 and G4$^{-/-}$ #2 SplM. scale bar, 50 μm. **b.** Western blot image of ISL1 expression in WT, G4$^{-/-}$ #1 and G4$^{-/-}$ #2 SplM. COFFLIN is an internal control. **c & d.** qRT-PCR analyzing the transcription level of *GATA6* in ESC and WT, G4$^{-/-}$ #1, G4$^{-/-}$ #2 SplM (**c**); *ISL1* and *NKX2-5* transcripts in ESC, SplM and WT, G4$^{-/-}$ #1, G4$^{-/-}$ #2 MLC (**d**). Expression level shown relative to untreated ESC after normalization with RNA18S. **e.** WB analysis of GATA4 and WT1 proteins in WT, G4$^{-/-}$ #1, G4$^{-/-}$ #2 MLC. COFFLIN is an internal control. **f.** GATA4, NKX2-5 and cardiac troponin T proteins were detected by IF and assayed on day5 and day30 of cardiomyocyte differentiation. scale bar, 50 μm. **g.** IF of mesothelium formation over other coelomic organs, including gut, liver and lung, shown by WT1 positive staining cells (orange). DAPI shown in blue. scale bar, 200 μm.

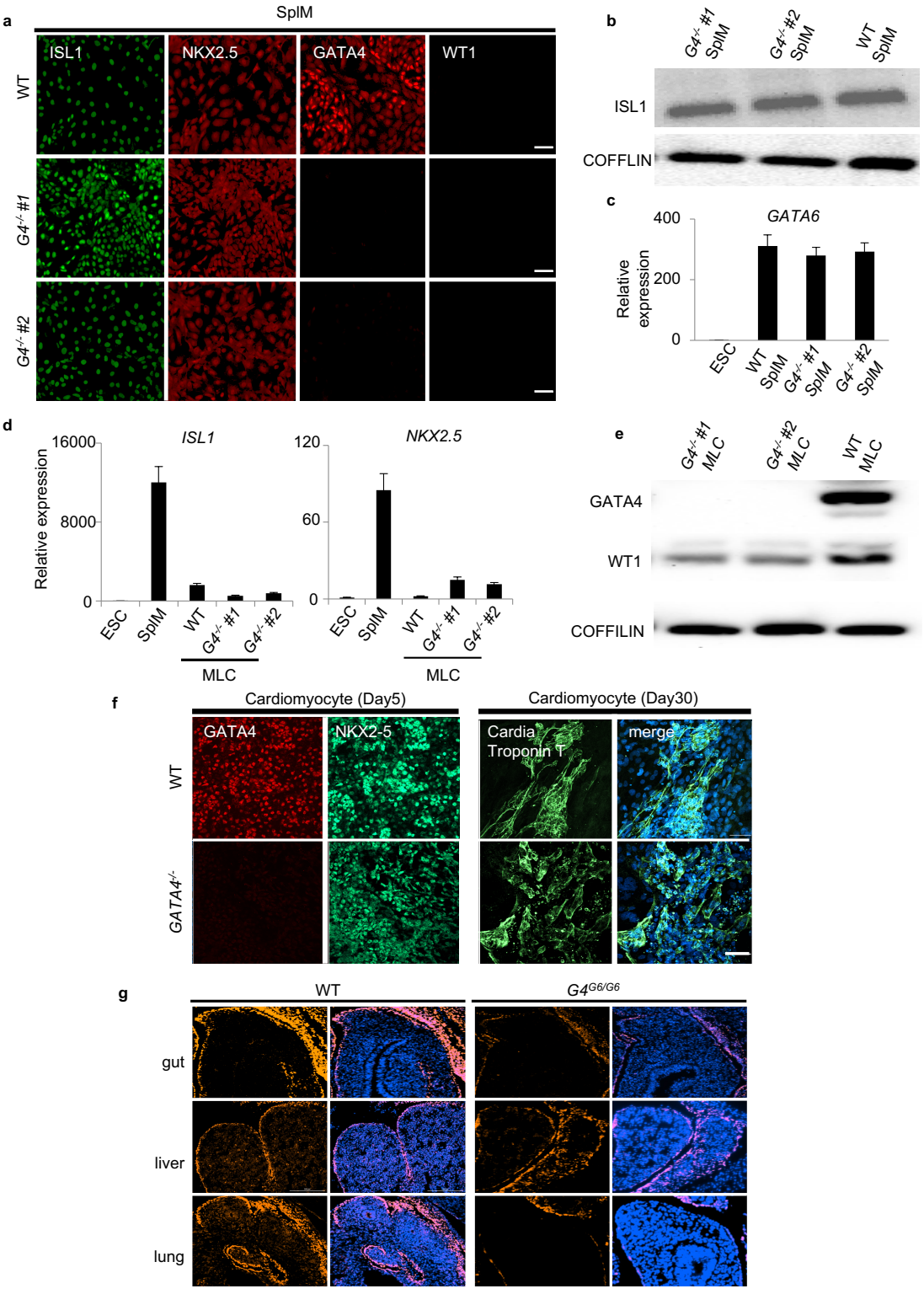
a
SplM
ISL1
NKX2.5
GATA4
WT1
WT
G4-/- #1
G4-/- #2
b
G4-/- #1 SplM
G4-/- #2 SplM
WT SplM
ISL1
COFFLIN
c
GATA6
Relative expression
400
200
0
ESC
WT SplM
G4-/- #1 SplM
G4-/- #2 SplM
d
ISL1
NKX2.5
Relative expression
16000
8000
0
120
60
0
ESC
SplM
WT
G4-/- #1
G4-/- #2
MLC
e
G4-/- #1 MLC
G4-/- #2 MLC
WT MLC
GATA4
WT1
COFFILIN
f
Cardiomyocyte (Day5)
Cardiomyocyte (Day30)
GATA4
NKX2-5
Cardia Troponin T
merge
WT
GATA4-/-
g
WT
G4G6/G6
gut
liver
lung

Supplement Figure 2.3 – related to Figure 2.3. a. qRT-PCR analysis showing *NANOG* and *NKX2-5* transcription levels in WT ESC, WT SplM and TBX5$^{-/-}$ SplM. **b.** Fixed WT and TBX5$^{-/-}$ SplM were probed with ISL1, NKX2-5 and TBX5 antibodies. scale bar, 50 μm. **c.** PLA assays with IgG antibody, GATA4 antibody and TBX5 antibody in WT MLC. scale bar, 125 μm. **d.** BF and IF images of WT1 (red) and DAPI (blue) staining for sections from E11.5 GATA4 heterozygotes (*GATA4*$^{+/-}$) and TBX5 heterozygotes (*TBX5*$^{+/-}$). scale bar, 75 μm.

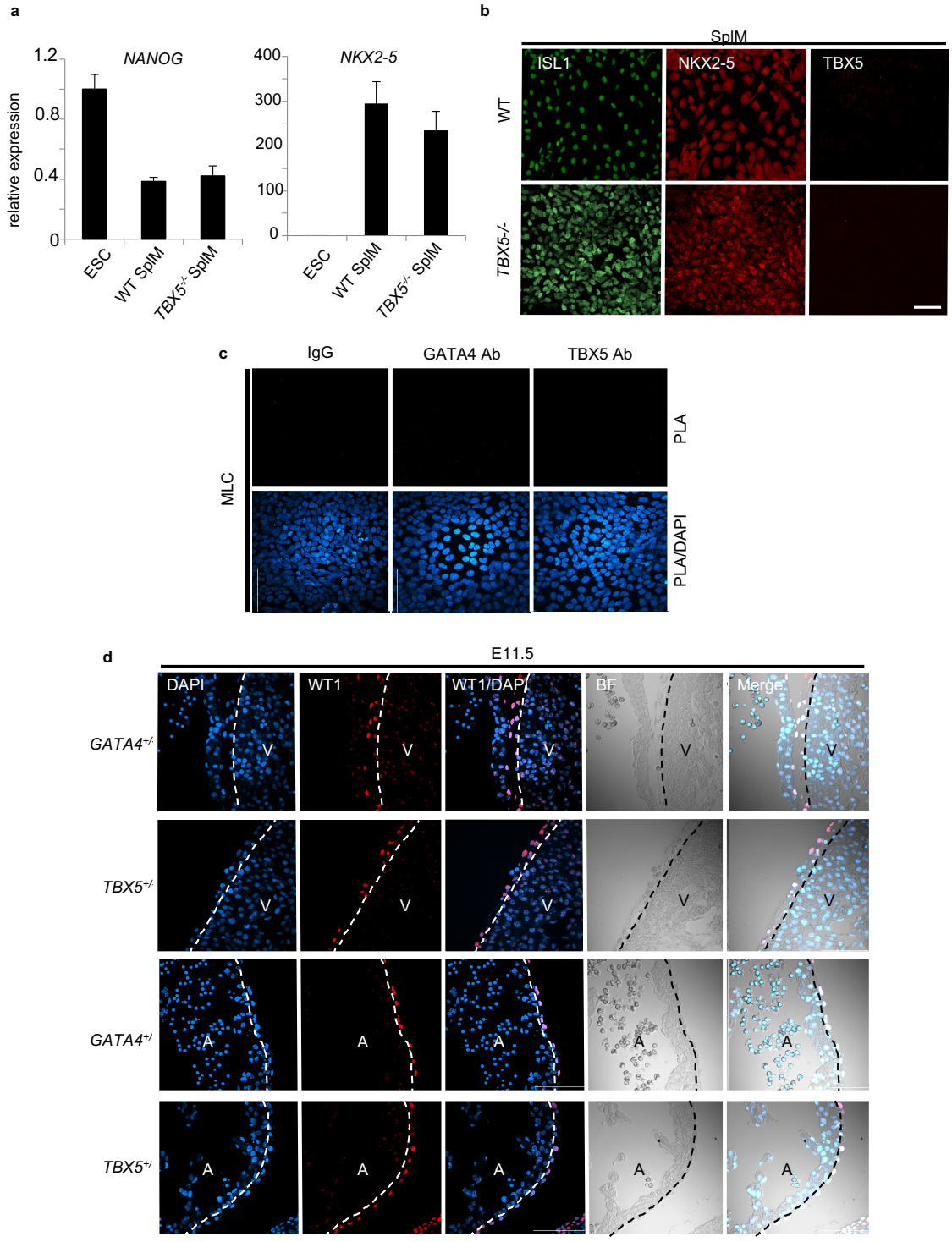
a
NANOG
NKX2-5
relative expression
1.2
0.8
0.4
0
400
300
200
100
0
ESC
WT SplM
TBX5-/- SplM
b
SplM
ISL1
NKX2-5
TBX5
WT
TBX5-/-
c
IgG
GATA4 Ab
TBX5 Ab
MLC
PLA
PLA/DAPI
d
E11.5
DAPI
WT1
WT1/DAPI
BF
Merge
GATA4+/-
TBX5+/-
GATA4+/-
TBX5+/-
V
A

Supplement Figure 2.4 – related to Figure 2.4. a. qRT-PCR analysizing relative expression of *OCT4*, *NANOG*, *SOX2*, *ISL1* and *NKX2-5* transcripts in iWT iPSC, GATA4 G296S iPSC, iWT SplM and GATA4 G296S SplM. Each sample is in technical triplicates. Values are relative to ESC and RNA18S. **b** ISL1, NKX2-5, GATA4 and WT1 IF assays for iWT and GATA4 G296S SplM. scale bar, 75 μm.

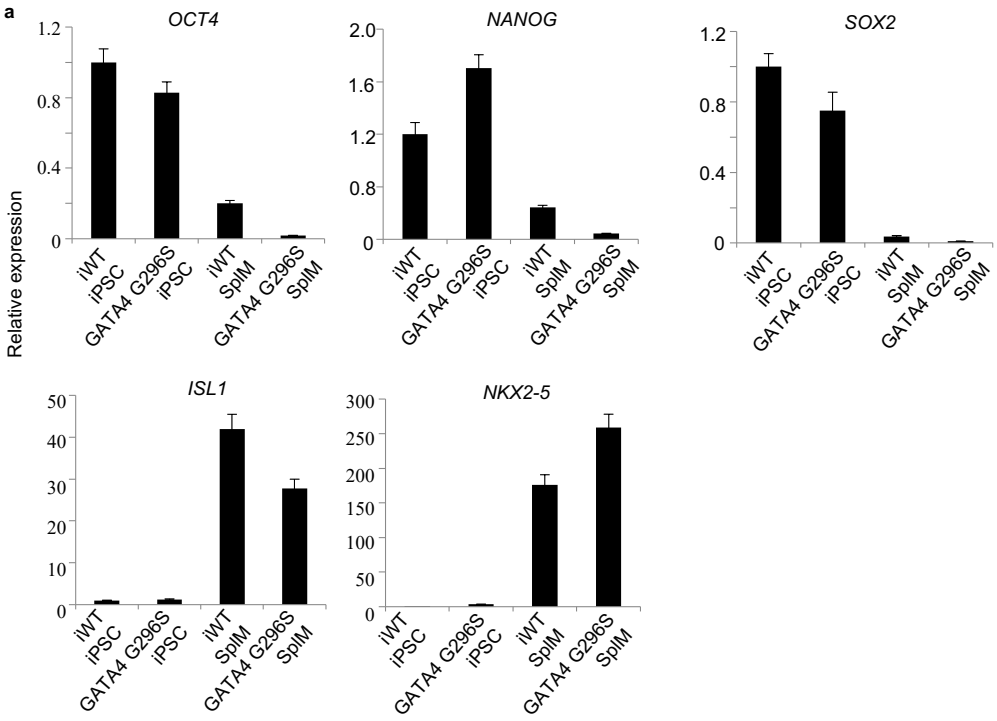
a
OCT4
NANOG
SOX2
ISL1
NKX2-5
Relative expression
iWT iPSC
GATA4 G296S iPSC
iWT SpIM
GATA4 G296S SpIM

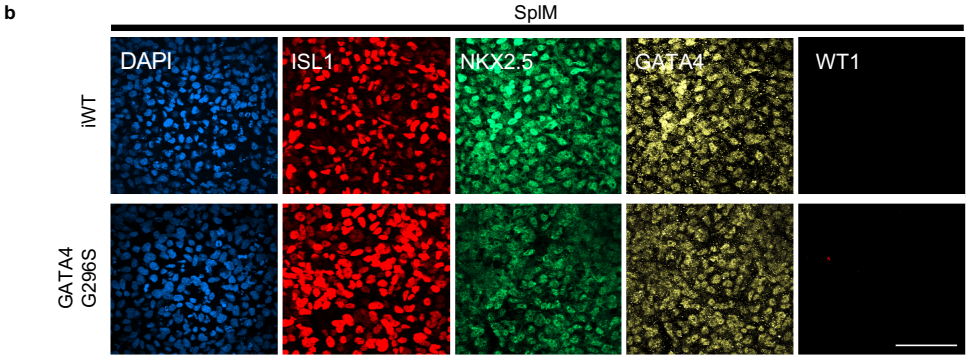
b
SpIM
DAPI
ISL1
NKX2.5
GATA4
WT1
iWT
GATA4 G296S

Supplement Table 2.1 Raw counts (in CPM) of transcripts listed in Figure 2.1b.

GENE	ESC	SplM	MLC
ISL1	0.08955717	65.3558574	12.0435729
FOXF1	0	12.6251218	3.73944964
PDGFRB	25.6581299	97.9616447	71.9630636
WT1	0.35822869	1.24919462	196.766439
TBX18	0.08955717	0.76547365	236.290439
TCF21	0.62690021	4.64240851	38.1049023
TBX5	0.08955717	0.58452634	101.542485
BNC1	0.35822869	20.2915597	259.571662
WNT2B	2.73149376	3.11731371	308.372284
GATA4	5.28387318	143.313323	351.488411
GATA6	6.26900207	24.296177	295.486428

- Mean counts from biological replicates.

Supplement Table 2.2 Raw counts (in CPM) of transcripts listed in Figure 2.2e.

GENES	WT MLC	GATA4$^{-/-}$ MLC
GATA4	326.074362	48.69760709
TBX5	94.17862931	49.11383647
BNC1	240.6935612	150.4571559
WNT2B	331.7374331	228.3571784
MEGF6	126.4937342	70.73480563
WT1	182.5727256	81.03575329
TBX18	219.0984718	92.47594584
TCF21	42.53734629	20.22416777
UPK3B	46.92839803	8.163711407
LRRN4	131.9710716	65.13068792
CDH1	197.3147956	388.3366011
CDH5	0.37764251	4.907751559
SOX9	14.30170967	38.92239135
BVES	32.15971383	42.55383544
TJP1	199.4426995	227.0148115
GATA6	274.0789579	211.9473922
GATA5	150.8341654	143.3724656

- Mean counts from biological replicates.

REFERENCES

1. Ksiazek, K., Mesothelial cell: a multifaceted model of aging. Ageing Res Rev, 2013. 12(2): p. 595-604.
2. Mutsaers, S.E. and S. Wilkosz, Structure and function of mesothelial cells. Cancer Treat Res, 2007. 134: p. 1-19.
3. Niderla-BieliNska, J., et al., Proepicardium: Current Understanding of its Structure, Induction, and Fate. Anat Rec (Hoboken), 2019. 302(6): p. 893-903.
4. von Gise, A. and W.T. Pu, Endocardial and epicardial epithelial to mesenchymal transitions in heart development and disease. Circ Res, 2012. 110(12): p. 1628-45.
5. Mikawa, T. and R.G. Gourdie, Pericardial mesoderm generates a population of coronary smooth muscle cells migrating into the heart along with ingrowth of the epicardial organ. Dev Biol, 1996. 174(2): p. 221-32.
6. Acharya, A., et al., The bHLH transcription factor Tcf21 is required for lineage-specific EMT of cardiac fibroblast progenitors. Development, 2012. 139(12): p. 2139-49.
7. Katz, T.C., et al., Distinct compartments of the proepicardial organ give rise to coronary vascular endothelial cells. Dev Cell, 2012. 22(3): p. 639-50.
8. Lockhart, M.M., et al., The Epicardium and the Development of the Atrioventricular Junction in the Murine Heart. J Dev Biol, 2014. 2(1): p. 1-17.
9. Lockhart, M.M., et al., Alk3 mediated Bmp signaling controls the contribution of epicardially derived cells to the tissues of the atrioventricular junction. Dev Biol, 2014. 396(1): p. 8-18.

10. Gittenberger-de Groot, A.C., et al., Epicardium-derived cells contribute a novel population to the myocardial wall and the atrioventricular cushions. Circ Res, 1998. 82(10): p. 1043-52.
11. Zhou, B., et al., Epicardial progenitors contribute to the cardiomyocyte lineage in the developing heart. Nature, 2008. 454(7200): p. 109-13.
12. Rudat, C. and A. Kispert, Wt1 and epicardial fate mapping. Circ Res, 2012. 111(2): p. 165-9.
13. Olivey, H.E. and E.C. Svensson, Epicardial-myocardial signaling directing coronary vasculogenesis. Circ Res, 2010. 106(5): p. 818-32.
14. Perez-Pomares, J.M. and J.L. de la Pompa, Signaling during epicardium and coronary vessel development. Circ Res, 2011. 109(12): p. 1429-42.
15. Zhou, B., et al., Nkx2-5- and Isl1-expressing cardiac progenitors contribute to proepicardium. Biochem Biophys Res Commun, 2008. 375(3): p. 450-3.
16. Winters, N.I., A.M. Williams, and D.M. Bader, Resident progenitors, not exogenous migratory cells, generate the majority of visceral mesothelium in organogenesis. Dev Biol, 2014. 391(2): p. 125-32.
17. Simoes, F.C. and P.R. Riley, The ontogeny, activation and function of the epicardium during heart development and regeneration. Development, 2018. 145(7).
18. Colombo, S., et al., Nkx genes establish second heart field cardiomyocyte progenitors at the arterial pole and pattern the venous pole through Isl1 repression. Development, 2018. 145(3).
19. Watt, A.J., et al., GATA4 is essential for formation of the proepicardium and regulates cardiogenesis. Proc Natl Acad Sci U S A, 2004. 101(34): p. 12573-8.

20. Borok, M.J., V.E. Papaioannou, and L. Sussel, Unique functions of Gata4 in mouse liver induction and heart development. Dev Biol, 2016. 410(2): p. 213-222.
21. Barnes, R.M., et al., Hand2 loss-of-function in Hand1-expressing cells reveals distinct roles in epicardial and coronary vessel development. Circ Res, 2011. 108(8): p. 940-9.
22. Hatcher, C.J., et al., A role for Tbx5 in proepicardial cell migration during cardiogenesis. Physiol Genomics, 2004. 18(2): p. 129-40.
23. Liu, J. and D.Y. Stainier, Tbx5 and Bmp signaling are essential for proepicardium specification in zebrafish. Circ Res, 2010. 106(12): p. 1818-28.
24. Diman, N.Y., et al., Tbx5 is required for avian and Mammalian epicardial formation and coronary vasculogenesis. Circ Res, 2014. 115(10): p. 834-44.
25. Niwa, H., The principles that govern transcription factor network functions in stem cells. Development, 2018. 145(6).
26. Colunga, T., et al., Human Pluripotent Stem Cell-Derived Multipotent Vascular Progenitors of the Mesothelium Lineage Have Utility in Tissue Engineering and Repair. Cell Rep, 2019. 26(10): p. 2566-2579 e10.
27. Klein, D.C. and S.J. Hainer, Chromatin regulation and dynamics in stem cells. Curr Top Dev Biol, 2020. 138: p. 1-71.
28. Kruithof, B.P., et al., BMP and FGF regulate the differentiation of multipotential pericardial mesoderm into the myocardial or epicardial lineage. Dev Biol, 2006. 295(2): p. 507-22.
29. Tremblay, M., O. Sanchez-Ferras, and M. Bouchard, GATA transcription factors in development and disease. Development, 2018. 145(20).

30. Kolander, K.D., et al., Epicardial GATA factors regulate early coronary vascular plexus formation. Dev Biol, 2014. 386(1): p. 204-15.

31. Chlon, T.M. and J.D. Crispino, Combinatorial regulation of tissue specification by GATA and FOG factors. Development, 2012. 139(21): p. 3905-16.

32. Srivastava, D., GATA4 mutations cause human congenital heart defects and reveal an interaction with TBX5. Nature, 2003. 424(24): p. 443-447.

33. Ang, Y.S., et al., Disease Model of GATA4 Mutation Reveals Transcription Factor Cooperativity in Human Cardiogenesis. Cell, 2016. 167(7): p. 1734-1749 e22.

34. Tanaka, H., et al., Interaction of the pioneer transcription factor GATA3 with nucleosomes. Nat Commun, 2020. 11(1): p. 4136.

35. Rodriguez-Segui, S., I. Akerman, and J. Ferrer, GATA believe it: new essential regulators of pancreas development. J Clin Invest, 2012. 122(10): p. 3469-71.

36. Narita, N., M. Bielinska, and D.B. Wilson, Cardiomyocyte differentiation by GATA-4-deficient embryonic stem cells. Development, 1997. 124(19): p. 3755-64.

37. Zhao, R., et al., Loss of both GATA4 and GATA6 blocks cardiac myocyte differentiation and results in acardia in mice. Dev Biol, 2008. 317(2): p. 614-9.

38. Misra, C., et al., Congenital heart disease-causing Gata4 mutation displays functional deficits in vivo. PLoS Genet, 2012. 8(5): p. e1002690.

39. Misra, C., et al., Disruption of myocardial Gata4 and Tbx5 results in defects in cardiomyocyte proliferation and atrioventricular septation. Hum Mol Genet, 2014. 23(19): p. 5025-35.

CHAPTER 3

DETAILED EXPERIMENTAL METHODS

MATERIALS AND METHODS

Cell culture and differentiation

Maintenance of hPSC was as previously described [1]. WA09 (Sex: female, WiCell, N1HhESC-10-0062), isogenic wild type (iWT) iPSC and GATA4 G296S iPSC, gifts from Dr. Deepak Srivastava [2], were cultured in chemically defined medium (CDM) and on diluted Geltrex (LDEV-Free hESC qualified reduced growth factor basement membrane matrix, ThermoFisher, A1413302) coated polystyrene culture plates. Geltrex were diluted in DMEM/F12 w/o glutamine (Fisher Sci, MT15090CM) at a ratio of 1:200. CDM base medium consisted of DMEM/F12 w/o glutamine supplemented with 2% Probumin® bovine serum albumin life science grade (EMD Millipore, 821005), 1X Antibiotic-Antimyotic (Corning, 30-004-CI), 1X MEM non-essential amino acids (Corning, 25-025-CI), 2 mM L-alanyl-L-glutamine (Corning, 25-015-CI), 1X trace element A (Corning, 25-021-CI), 1X trace element B (Corning, 25-022-CI), 1X trace element C (Corning, 25-023-CI), 50 µg/ml ascorbic acid (Sigma-Aldrich, A8960), 10 µg/ml transferrin (Athens Research and Technology, 16-16-A32001-LEL) and 0.1 mM β-mercaptoethanol (GIBCO, 21985023). Addition of 10 ng/mL human Heregulinβ-1 (Peprotech, AF-100-03), 8 ng/mL human basic-FGF (R&D Systems, 4114-TC), 200 ng/mL LONG® R3 human IGF-I (Sigma, 85580C) and 10 ng/mL Activin A (R&D

Systems, 338-AC-01M/CF) to the base medium comprised CDM. For maintenance, medium was changed daily, and cells were passaged with Accutase (Innovative Cell Technologies, AT104) upon confluency. The pluripotency of hPSC was characterized by the expression of NANOG, SOX2 and OCT4.

To induce Splanchnic Mesoderm (SplM), hPSC were passaged using Accutase and single cells were counted with a hemocytometer. hPSC were then reseeded at 5×10^4 cells/cm^2 (WA09) or 1×10^5 cells/cm^2 (iPSC) on 1:200 Geltrex coated plates and cultured in CDM supplemented with 25 ng/ml rhWNT3a (R&D Systems, 5036-WN) and 100 ng/ml rhBMP4 (R&D Systems, 314-BP) for 4 days with medium changed daily. SplM cell fate was characterized by the expression of ISL1, NKX2-5 and FOXF1.Detailed protocol has been published in [3].

To make mesothelium-like cells (MLC), SplM were passaged with 1X TrypLE select (Thermo Fisher, A1217701) diluted in a salt balanced solution composed of 1X PBS without calcium and magnesium (Corning, 21-031), 1.85 g/L sodium chloride (Fisher Scientific, S640), and 0.5 M EDTA (Thermo Fisher, AM9260G). Cells were quantified using a hemocytometer and reseeded at 1.5×10^5 cells/cm^2 on 1:200 Geltrex coated plates. MLC differentiation medium consisted of the CDM base medium supplemented with 10 ng/mL human Heregulinβ-1, 200 ng/mL LONG® R3 human IGF-I, 25 ng/ml rhWNT3a, 100 ng/ml rhBMP4, 20 μM SB431542 (Tocris, 1614) and 4 μM all-trans retinoic acid (Sigma-Aldrich, R2625). The differentiation took 18 days with medium changed daily. To identify MLC, molecular markers of WT1 (*WT1*), TBX18 (*TBX18*), TCF21 (*TCF21*), E-cadherin (*CDH1*), ZO1 (*TJP1*) and a-SMA (*ACTA2*) were used. The method has been published in [4].

qRT-PCR

mRNA was isolated from cells using E.Z.N.A.® Total RNA Kit I (Omega Bio-Tek, R6834) and quantified with a Biotek Synergy 2 plate reader. 1 μg mRNA per sample were reverse transcribed into cDNA using iSCRIPT cDNA kit (Bio-Rad, 1708841). qRT-PCR was done on a ViiA7 Real-Time PCR System (Life Technologies) with reaction mixes composed of cDNA, TaqMan Universal PCR Master Mix No AmpErase UNG (Thermo Fisher, 4324020) and TaqMan Primers. All the procedures were performed as manufacturers' manuals. TaqMan probes were listed in Table 4.1.

Immunofluorescence

Cells were fixed on the plates/dishes at the end of each differentiation using 4% paraformaldehyde (VWR, 15170) for 15 minutes. After being permeabilized with 0.2% Triton X-100 (Fisher Scientific, BP151–500) for 10 minutes, cells were blocked with a 10% donkey serum (Equitech-Bio, SD30–0500), 0.2 M Triton X-100 and 0.3 M glycine (Sigma, G8898) in DPBS solution for 1 hour at room temperature. Primary antibodies were prepared at optimized concentrations in a 10% donkey serum and 0.2 M Triton X-100 in DPBS solution and incubated overnight in 4 °C. Secondary antibodies were diluted at 1:400 in a 2.5% donkey serum and 0.2 M Triton X-100 in DPBS solution, and were incubated for 1 hour at room temperature in the dark. Nucleus were counterstained with 1 μg/mL 4,6-Diamidino-2-phenylindole dihydrochloride (Sigma, D9542) in DPBS for 5 mins. Coverslips were affixed with ProLong Diamond Antifade (Thermo Fisher, P36961). Multiple washes with DPBS were performed between each step.

To perform the immunofluorescence for mouse embryos, the whole embryos were first embedded in OCT (Fisher Scientific, 14-373-65) for sagittal sections. Sections were done at the thickness of 10 μm and stored in -80 °C. On the day of staining, slides were recovered to room temperature and then the same steps were followed as above for immunofluorescence staining but with an alteration in the blocking time for 2 hours.

Fluorescent cells/tissues were visualized on a Leica DM6000 B and BioTek Lionheart FX. Confocal images were obtained on an Olympus FV1200 laser scanning confocal microscope. Images were processed with Slidebook 6 (Intelligent Imaging Solutions) and cell counts were analyzed with Image J [5].

See Table 4.2 for a full list of antibodies.

Western Blot

Cells were harvested with cell strappers, followed by centrifugation at 1,000 rpm for 4 minutes. Cell pellets were lysed with a buffer composed of RIPA lysis buffer (Sigma, R0278), 1× protease inhibitor (Sigma, 11836170001), 1× phosphatase inhibitor (EMD Millipore, 524625) and 100 mM dithiothreitol (Sigma, D9779) on ice for 30 minutes. Supernatant were collected after lysates were centrifuged at 20,000× g for 10 minutes in 4 °C. Protein quantification was done with Bradford assay (Bio-Rad, 5000006) at 595 nm on a Biotek Synergy 2. Laemmli buffer (Bio-Rad, 1610737) supplemented with 5% 2-mercaptoethanol were mixed with proteins at 1:1. Boiled the mixes at 95 °C for 5 minutes. 30 μg proteins were loaded to Bolt Bis-Tris precast gels (Life Technologies, NW00080BOX) and separated by electrophoresis at 165 V for 35 min. Proteins were transferred to nitrocellulose membranes (Bio-Rad, 1620215) via a

Mini Blot transfer system (Life Technologies) at 10 V for 60 min. Nitrocellulose membranes were blocked with 2% non-fat blocking milk (Bio-Rad, 170–6404) in 1× TBST (0.5% Tween-20 in 25 mM TBS) for 1 hour. After blocking, membranes were incubated with primary antibodies in 4 °C overnight while rotating. Secondary antibodies were added to membranes after 3 washes with 1X TBST and incubated for 1 hour at room temperature on the rotator. Primary and secondary antibodies were diluted in the blocking buffer at the concentrations recommended in manuals. Images were captured using Amersham ECL detection kit (GE, RPN2106) on Analytik Jena UVP ChemStudio. Antibodies were listed in Table 4.2.

Co-immunoprecipitation

Cell pellets were isolated as described above and lysed on rotation in 4 °C for 30 minutes using the lysis buffer composed of 50 mM HEPES (Cellgro, 25060CI), 150 mM NaCl (Invitrogen, AM9760G), 0.1 mM EDTA (AMbion, AM9260G), 0.1 mM EGTA (BioWorld, 40520008-1), 10% glycerol (Sigma, G5516), 0.1% NP40 (Sigma, 11332473001) and 100 mM dithiothreitol in ice-cold water. Supernatant were collected after centrifugation at 12,000 rpm for 20 minutes in 4 °C. Proteins were quantified using Bradford assay at 595 nm on a Biotek Synergy 2. IgG (Abcam, ab46540), GATA4 (Bethyl Labs A303-503A) and TBX5 (FisherSci 42-6500) antibodies were conjugated to 100 ul/reation Dynabeads™ Protein G (abcam, 10004D) overnight in 4 °C with agitation. The same amount of proteins (1mg per reaction) were aliquoted into each antibody-bead reaction and the incubation was done overnight in 4 °C with agitation. The optimal volume for the reaction was 500 ul/reaction. Mixes were then mixed with Laemmli buffer

(Bio-Rad, 1610737) supplemented with 5% 2-mercaptoethanol at 1:1 and proteins were denatured at 95 °C for 5 minutes. The supernatants were collected using DynaMag-96 Side (Life technologies 12331D) and then used for the western blot against GATA4 by following the same protocol described above. 10 μg (1%) proteins were loaded as input. Beads were washed with ice-cold DPBS for 3 times between each step.

Proximity ligation assay

Cells were fixed on 8-well chamber slides at the end of differentiation using 4% paraformaldehyde for 15 minutes. After several washes with DPBS, cells were permeabilized with 0.2% Triton X-100 for 10 minutes. The interaction between GATA4 and TBX5 was detected using Duolink™ in situ proximity ligation assay (PLA®). Anti-rabbit PLUS (Sigma, DUO92002-30RXN) and anti-mouse MINUS (Sigma, DUO92004-30RXN) PLA probes were used to detect rabbit TBX5 antibody (Invitrogen, 426500) and mouse GAT4 antibody (Santa Cruz, sc-25310), respectively. The interaction signal was ligated and amplificated with Duolink™ In Situ Detection Reagents Red (Sigma, DUO92008-100RXN). The detailed protocol was followed as manufacturer's manual. For negative controls, the same steps were performed but with IgG antibody, GATA4 antibody alone and TBX5 antibody alone.

CRISPR-Cas9 knockout

GATA4 and TBX5 coding sequences were used as inputs to design gRNA pairs using Tefor CRISPOR program (http://crispor.tefor.net). gRNA pairs with high specificity and high efficiency were selected, synthesized from Integrated DNA

technology and cloned into pSpCas9(BB)-2A-GFP (Addgene, 48140). Single clones were amplified and purified for Sanger sequencing verification after transformation and plasmid with the right insertion was picked for transfection. Transfection was done on 50-60% confluency WA09 cells with Lipofectamine Stem Reagent (ThermoFisher, STEM00015) following manufacturer's protocol. Transfected WA09 cells were then FACS sorted onto the EmbryoMax® Primary Mouse Embryo Fibroblasts (EMD Millipore, PMEF-N) coated 96 well plates as single clones and cultured in DMEM-F12 supplemented with 10% Knockout Serum Replacement (FisherSci, 10828028) and 1X Antibiotic/Antimyotic. Upon confluency, clones were passed onto 1:200 Geltrex coated plates and kept in CDM. GATA4$^{-/-}$ and TBX5$^{-/-}$ clones were verified via genomic PCR. gRNA sequences and primers were listed in Table 4.3.

Rescue experiments

Gata4-GR and Gata6-GR plasmids were gifts from Dr. Hitoshi Niwa [6]. GATA4$^{-/-}$ ESC were transfected with either Gata4-GR or Gata6-GR using Lipofectamine Stem Reagent and following the manufacturers' protocol. 48 hours post-transfection, cells were selected with 5 ug/ml puromycin (Gibco, A11138-02) for a week and then maintained in CDM supplemented with 5 ug/ml puromycin. 20 uM dexamethasone (Dex, R&D Systems, 1126/100) was added into MLC differentiation media to activate Gata4 or Gata6 during SplM to MLC transition.

RNA-seq and data analysis

Total mRNAs are extracted using E.N.Z.A Total RNA kit and purified with RNase-free DNase Set I (Omega, E1091). RNA yield and quality were assayed using Qubit Fluorometer and samples with a RIN>9 were submitted to the Georgia Genomic and Bioinformatics Core (GGBC) for RNA seq (MiSeq PE75, an average of 25 million reads per sample).

Raw reads were aligned to human reference genome (hg19) using HISAT2 (version 2.1.0) with default parameters [7]. Aligned reads were converted to Bam format and sorted with Samtools (version 1.3.1) [8]. Read counts at each transcript were quantified using HTseq (version 0.6.1p1) [9]. Files generated from HTseq were imported into R studio (version 1.1.423) [10]. Data were normalized by sequencing depth and gene expression distribution with Limma edgeR and transcripts with low reads were removed [11, 12]. Gene read counts were summarized in count per million, CPM. Only transcripts with read counts over 20^{th} percentile of overall read counts were kept for k-mean clustering analysis and plotting heatmap in ComplexHeatmap [13]. All samples were in biological replicates.

ATAC-seq and data analysis

Cells were dissociated using methods described above and then counted with a hemocytometer. 50,000 cells per sample were collected in cold 1X DPBS by centrifugation at 500g in 4°C. Cell pellets were fully re-suspended in lysis buffer consist of 10mM Tris-HCl pH7.5 (Invitrogen 15567-027), 10mM NaCl, 3mM $MgCl_2$ (Invitrogen AM9530G) and 0.1% Digitonin (ThermoFisher, BN2006) in cold 1X DPBS. Lysates were spun down with centrifugation at 500g for 10 minutes in 4 °C and then incubated

with transposition reaction mix from Nextera DNA library preparation kit (Illumina, FC-121-1030) for 30 minutes at 37 °C. DNA were purified with DNA Clean & Concentrator™ (Zymo, D4014) for amplication using indexed primers and NEB Next High-Fidelity 2X PCR master mix (NEB, M0541S). The detailed steps were followed as previously published protocol [14]. The libraries were purified with magnetic beads (Omega Bio-Tek Inc, M1386-02). Fragment analysis was performed for purified products and libraries with fragment size ranging from 100 bp to 500 bp were sent for sequencing (NextSeq SE75 High Output, Illumina) at GGBC. Experiments were done in biological replicates.

Bowtie2 was used to align raw data to human genome (hg19) [15]. After removal of mitochondria DNA, aligned reads were converted into Bam files, sorted and indexed with Samtools [8]. Peaks were called using MACS2 with following parameters, -B, --keep-dup 1, --nomodel, --shift 75, --extsize 150 and -q 0.05 [16]. Peaks files were then imported into R studio [10]. Consensus regions across the samples were generated using peaks merged from all samples but subtracted with Blacklist using soGGi [17]. featureCounts was used to count reads at consensus regions in each sample [18]. Only reads presented at least in 2 samples were kept and normalized for sequencing depth using edgeR to plot heatmaps [11]. The heatmap and k-mean clustering were generated using ComplexHeatmap [13]. Peaks were annotated to hg19 using ChIPseeker with the region range for transcription start site set as +/- 2000 kb [19]. Motifs were analyzed using Homer, peak intersection was analyzed with bedtools and GO enrichment analysis were performed with Panther [20-22].

qChIP, ChIP-seq and data analysis

After dissociation and counting, 75,000 cells were collected for each ChIP reaction. Cells were fixed with 1% methanol-free formaldehyde solution (ThermoFisher, 28908) for 10 minutes at room temperature and with rotation. 0.125 M glycine were then added into the solution and the solution were incubated at room temperature for 5 minutes with rotation. Washed once with ice-cold DPBS and centrifuged at 1,000 rpm for 4 minutes to collect pellets for storing at -80 °C or performing sonication. 5 µg anti-IgG, 5 µg anti-H3K27ac (Active Motif, 39133), 10 µg anti-GATA4 (Bethyl Labs A303-503A) and 10 µg anti-TBX5 (Santa Cruz, sc-515536) were incubated with 50 µl Dynabeads™ Protein G with agitation overnight in 4 °C. Cell pellets were lysed with a solution consist of 10 mM Tris-HCl pH8.0 (Invitrogen 15568-025), 100 mM NaCl, 1 mM EDTA, 0.1% sodium deoxycholate (Sigma-Aldrich, D6750), 0.5% N-lauroylsarcosine (Research Organics, 9603L) and 1x cOmplete™, Mini, EDTA-free Protease Inhibitor Cocktail (Roche, 11836170001) in molecular grade water (Fisher Sci, MT-46-000-CM) for 10-20 minutes. Sonication was performed on Covaris S220 using the following parameters, peak power 140, duty factor 5, cycles 200. Chromatin collected from 75,000 cells was sonicated for 15 minutes. Sonicated chromatin was collected with centrifugation at max speed for 10 minutes in 4 °C and then incubated with antibody conjugated beads in 4 °C overnight with agitation. Following 2 washes with the wash buffer I (20 mM Tris-HCl pH 7.4, 150 mM NaCl, 0.1% SDS (KD Medical, RGE3235), 1 % Triton X-100 and 2 mM EDTA), reactions were washed twice with 10 mM Tris-HCl pH8.0, then resuspended in 30 µl tagmentation buffer, 1 µl of transposase (Nextera, Illumina) and incubated for 10 minutes at 37 °C. After several washes with the wash buffer I, wash

buffer II (10 mM Tris-HCl ph 7.4, 250 mM LiCl (Sigma, L4408), 1% Triton X-100, 0.7% Na-Deoxycholate and 1 mM EDTA) and TE buffer (10 mM Tris-HCl pH 8.0, 0.2 % Tween-20 (Sigma, P7949) and 1 mM EDTA), crosslinking was reversed by incubating beads in 100 μL of 10 mM Tris-HCl pH 8.0, 0.5% SDS, 300 mM NaCl, 5 mM EDTA and 3.2 units of Proteinase K (Roche, 3115828001) for 1 hr at 55 °C followed by 8 hr at 65 °C. All the washes were done on ice and in 4 °C. DNA was purified using DNA Clean & Concentrator™ and eluted in molecular grade water. 1% sonicated chromatin without beads incubation and chromatin incubated with IgG-conjugated beads were collected as controls.

qChIP was performed using purified DNA, primers (Table 4.4), 2X KAPA SYBR FAST qPCR Master Mix and KAPA SYBR FAST Rox Low on the ViiA7 Real-Time PCR System (Life Technologies). Experiments were done in triplicates. To perform ChIP-seq, a second purification with magnetic beads (Omega Bio-Tek Inc, M1386-02) was performed. Only samples with fragments ranging from 100 bp to 300 bp were sent to GGBC for sequencing (NextSeq SE75 High Output, Illumina). Biological replicates were collected for each experiment.

MLC GATA4 ChIP-seq data was from this study and SplM GATA4 ChIP-seq data were obtained from GSE61475. The same procedures were followed as ATAC-seq data analysis to align and sort reads, call and annotate peaks for ChIP-seq. Coverage tracks were generated using Deeptools and reads were normalized as reads per genomic content [23]. GATA4 ChIP-seq peaks from MLC were intersected with M regions (Fig. 2.1d) and treated as the input to generate the heatmaps using EnrichedHeatmap [24].

ATAC-seq signals and GATA4 ChIP-seq signals from SplM and MLC were then mapped to the intersected peaks in a window of -5 kb to 5 kb from peak centers.

Table 3.1 Taqman Primers for qRT-PCR

Gene	Supplier	Identifier	Chromosome Location
POU5F1/OCT4	Thermo Fisher	Hs04260367_gH	Chr.6: 31164337 - 31170693
SOX2	Thermo Fisher	Hs01053049_s1	Chr.3: 181711924 - 181714436
NANOG	Thermo Fisher	Hs02387400_g1	Chr.12: 7789396 - 7796061
ISL1	Thermo Fisher	Hs00158126_m1	Chr.5: 51383124 - 51394730
NKX2.5	Thermo Fisher	Hs00231763_m1	Chr.5: 173232104 - 173235312
FOXF1	Thermo Fisher	Hs00230962_m1	Chr.16: 86510527 - 86514464
GATA4	Thermo Fisher	Hs00171403_m1	Chr.8: 11676919 - 11760002
GATA5	Thermo Fisher	Hs00388359_m1	Chr.20: 62463497 - 62475970
GATA6	Thermo Fisher	Hs00232018_m1	Chr.18: 22169437 - 22202528
Gata4	Thermo Fisher	Mm00484689_m1	Chr.14: 63198915 - 63271714
Gata6	Thermo Fisher	Mm00802636_m1	Chr.18: 11052475 - 11085636
WT1	Thermo Fisher	Hs01103751_m1	Chr.11: 32387775 - 32435535
TBX18	Thermo Fisher	Hs01385457_m1	Chr.6: 84666834 - 84764236
TCF21	Thermo Fisher	Hs00162646_m1	Chr.6: 133889121 - 133895537
CDH1	Thermo Fisher	Hs00170423_m1	Chr.16: 68737290 - 68835542
BNC1	Thermo Fisher	Hs00231074_m1	Chr.15: 83255884 - 83284716
UPK3B	Thermo Fisher	Hs01592182_m1	-
LRRN4	Thermo Fisher	Hs00379905_m1	Chr.20: 6040546 - 6054080
CDH3	Thermo Fisher	Hs00999915_m1	Chr.16: 68644820 - 68727573
WNT2B	Thermo Fisher	Hs00921614_m1	Chr.1: 112466541 - 112521288
MEGF6	Thermo Fisher	Hs00390990_m1	Chr.1: 3487942 - 3624757

TBX5	Thermo Fisher	Hs00361155_m1	Chr.12: 114353911 - 114408708
RNA18S5	Thermo Fisher	Hs03928985_g1	Chr.Un|NT_167214: 109078 - 110946

Table 3.2 List of Antibodies

Antibody	Application	Supplier	Identifier
Goat Polyclonal anti-Islet-1	IF, WB	R&D systems	Cat#AF1837; RRID: AB_2126324
Mouse Monoclonal anti-Nkx2.5 (Clone 259416)	IF	R&D Systems	Cat#MAB2444; RRID: AB_2151378
Goat Polyclonal anti-E-cadherin	IF	R&D Systems	Cat#AF648; RRID: AB_355504
Mouse Monoclonal anti-TBX18 (Clone 635305)	IF	R&D Systems	Cat#MAB63371; RRID: AB_10892533
Mouse Monoclonal anti-ZO-1 (Clone 1)	IF	BD Biosciences	Cat#610966; RRID: AB_398279
Rabbit Monoclonal anti-Wilms Tumor Protein (Clone CAN-R9(IHC)-56-2)	IF	Abcam	Cat#ab89901; RRID: AB_2043201
Mouse Monoclonal anti-alpha Smooth Muscle Actin (Clone 1A4)	IF	Abcam	Cat#ab7817; RRID: AB_262054
Rabbit Polyclonal anti-GATA4 Antibody	WB, co-IP, ChIP	Bethyl Labs	Cat#A303-503A; RRID: AB_10951496
Rabbit Monoclonal anti-GATA4 Antibody (EPR4768)	IF	Abcam	Cat# ab134057; RRID: AB_2725747
Mouse Monoclonal anti-GATA4 Antibody (G4)	IF, PLA	Santa Cruz	Cat#sc-25310; RRID: AB_627667
Rabbit Polyclonal anti-TBX5 Antibody	IF, co-IP, PLA	Thermo Fisher	Cat#42-6500; RRID: AB_2533533
Mouse Monoclonal anti-TBX5 Antibody (A6)	ChIP	Santa Cruz	Cat#sc-515536
Rabbit Anti-Mouse IgG H&L	co-IP, ChIP	Abcam	Cat# ab46540; RRID: AB_2614925
Rabbit Polyclonal Histone H3K27ac Antibody	ChIP	Abcam	Cat#ab4729; RRID: AB_2118291
Rabbit Polyclonal Histone H3K27ac Antibody	ChIP	Active Motif	Cat#39133; RRID: AB_2722569
Rabbit Monoclonal anti-Cardiac Troponin T Antibody (EPR3695)	IF	Abcam	Cat#ab91605; RRID: AB_2050427
Mouse Monoclonal anti-Cofilin Antibody (E-8) HRP	WB	Santa Cruz	Cat#sc-376476; RRID: AB_11150468
Donkey Polyclonal anti-Mouse IgG (H+L) Alexa Fluor 488 Conjugated	IF	Thermo Fisher	Cat#A21202; RRID: AB_141607
Donkey Polyclonal anti-Rabbit IgG (H+L) Alexa Fluor 488 Conjugated	IF	Thermo Fisher	Cat#A21206; RRID: AB_141708

Donkey Polyclonal anti-Goat IgG (H+L) Alexa Fluor 555 Conjugated	IF	Thermo Fisher	Cat#A21432; RRID: AB_141788
Donkey Polyclonal anti-Mouse IgG (H+L) Alexa Fluor 555 Conjugated	IF	Thermo Fisher	Cat#A31570; RRID: AB_2536180
Donkey Polyclonal anti-Rabbit IgG (H+L) Alexa Fluor 555 Conjugated	IF	Thermo Fisher	Cat#A31572; RRID: AB_162543
Donkey Polyclonal anti-Goat IgG (H+L) Alexa Fluor 647 Conjugated	IF	Thermo Fisher	Cat#A21447; RRID: AB_141844
Donkey Polyclonal anti-Rabbit IgG (H+L) Alexa Fluor 647 Conjugated	IF	Thermo Fisher	Cat#A31573; RRID: AB_2536183
Goat anti-Rabbit Immunoglobulins/HRP	WB	Dako	Cat#P0448; RRID: AB_2617138
Rabbit anti-Goat Immunoglobulins/HRP	WB	Dako	Cat#P0449; RRID: AB_2617143

* Key: IF – immunofluorescence, WB – western blot, co-IP – co-immunoprecipitation,

PLA – proximity ligation assay, ChIP – chromatin immunoprecipitation

Table 3.3 List of gRNAs and PCR primers

Oligo names	Sequences
GATA4_gRNA1_sense	CACCGTGTGGGCACGTAGACTGGCG
GATA4_gRNA1_antisense	AAACCGCCAGTCTACGTGCCCACAC
GATA4_gRNA2_sense	CACCGAGATTGGGGTGTCGGGCGGC
GATA4_gRNA2_antisense	AAACGCCGCCCGACACCCCAATCTC
TBX5_gRNA1_sense	CACCCAAGTCCCCGTCGTCCCCGC
TBX5_gRNA1_antisense	AAACGCGGGGACGACGGGGACTTG
TBX5_gRNA2_sense	CACCCGAAGTGGGCACGGAAATGA
TBX5_gRNA2_antisense	AAACTCATTTCCGTGCCCACTTCG
GATA4_screen1_Forward Primer	GATCTTCGCGACAGTTCCTC
GATA4_screen1_Reverse Primer	GAACAAAGGAGGGATGGACA
GATA4_screen2_Forward Primer	GATCTTCGCGACAGTTCCTC
GATA4_screen2_Reverse Primer	GGTAGGGGCTGGAGTAGGAG
GATA4_screen3_Forward Primer	CTCCTACTCCAGCCCCTACC
GATA4_screen3_Reverse Primer	TGTCCATCCCTCCTTTGTTC
TBX5_screen1_Forward Primer	TTCACCCAGCAGGTAAGGAG
TBX5_screen1_Reverse Primer	CTGATCTTCCGTAGCCTTCG
TBX5_screen2_Forward Primer	TGTTTGATGTGTGGGCATCT
TBX5_screen2_Reverse Primer	TAAAATTCCACGAAGTGGGC
TBX5_screen3_Forward Primer	AGCCTGACGCAAAAGACCT
TBX5_screen3_Reverse Primer	GACGAGGAGAAATTGTGGGA

Table 3.4 List of qChIP primers

Primers	Sequences
WT1_region1_Forward Primer	CCCGGCCCTTATCTTATCA
WT1_region1_Reverse Primer	GACTAAGCCCCACTTGGTCA
TBX18_ Forward Primer	TTTCTCCCGCAGACGTAAAC
TBX18_Reverse Primer	CGGTCAGGGTCACGAAATAA
BNC1_ Forward Primer	CCGCATTTGTGAAAGTTTGG
BNC1_Reverse Primer	GAGTTCCTCGGGATTTGTCA
WNT2B_ Forward Primer	CGTCCCTGCTGAAAGCAT
WNT2B_Reverse Primer	CGCTGCTTGTCTCTGTCTTG
WT1_region2_Forward Primer	GGAGACACTGGGTGCATTCT
WT1_region2_Reverse Primer	ATGGAGAGCAGAGAGGGACA

REFERENCES

1. Menendez, L., et al., Directed differentiation of human pluripotent cells to neural crest stem cells. Nat Protoc, 2013. 8(1): p. 203-12.
2. Ang, Y.S., et al., Disease Model of GATA4 Mutation Reveals Transcription Factor Cooperativity in Human Cardiogenesis. Cell, 2016. 167(7): p. 1734-1749 e22.
3. Luoman Chen, S.D., Multipotent Vascular Progenitor Cells of the Mesothelium Lineage Generated from Human Pluripotent Stem Cells. STAR Protocols, 2020.
4. Colunga, T., et al., Human Pluripotent Stem Cell-Derived Multipotent Vascular Progenitors of the Mesothelium Lineage Have Utility in Tissue Engineering and Repair. Cell Rep, 2019. 26(10): p. 2566-2579 e10.
5. Schneider, C.A., W.S. Rasband, and K.W. Eliceiri, NIH Image to ImageJ: 25 years of image analysis. Nat Methods, 2012. 9(7): p. 671-5.
6. Shimosato, D., M. Shiki, and H. Niwa, Extra-embryonic endoderm cells derived from ES cells induced by GATA factors acquire the character of XEN cells. BMC Dev Biol, 2007. 7: p. 80.
7. Kim, D., B. Langmead, and S.L. Salzberg, HISAT: a fast spliced aligner with low memory requirements. Nat Methods, 2015. 12(4): p. 357-60.
8. Li, H., et al., The Sequence Alignment/Map format and SAMtools. Bioinformatics, 2009. 25(16): p. 2078-9.
9. Anders, S., P.T. Pyl, and W. Huber, HTSeq--a Python framework to work with high-throughput sequencing data. Bioinformatics, 2015. 31(2): p. 166-9.
10. Team, R., RStudio: Integrated Development for R. RStudio, PBC, Boston, MA, 2020.

11. Robinson, M.D., D.J. McCarthy, and G.K. Smyth, edgeR: a Bioconductor package for differential expression analysis of digital gene expression data. Bioinformatics, 2010. 26(1): p. 139-40.
12. Ritchie, M.E., et al., limma powers differential expression analyses for RNA-sequencing and microarray studies. Nucleic Acids Res, 2015. 43(7): p. e47.
13. Gu, Z., R. Eils, and M. Schlesner, Complex heatmaps reveal patterns and correlations in multidimensional genomic data. Bioinformatics, 2016. 32(18): p. 2847-9.
14. Buenrostro, J.D., et al., ATAC-seq: A Method for Assaying Chromatin Accessibility Genome-Wide. Curr Protoc Mol Biol, 2015. 109: p. 21 29 1-21 29 9.
15. Langmead, B. and S.L. Salzberg, Fast gapped-read alignment with Bowtie 2. Nat Methods, 2012. 9(4): p. 357-9.
16. Zhang, Y., et al., Model-based analysis of ChIP-Seq (MACS). Genome Biol, 2008. 9(9): p. R137.
17. Dharmalingam G, B.D., Carroll T, soGGi: Visualise ChIP-seq, MNase-seq and motif occurrence as aggregate plots Summarised Over Grouped Genomic Intervals. R package version 1.20.0., 2020.
18. Liao, Y., G.K. Smyth, and W. Shi, featureCounts: an efficient general purpose program for assigning sequence reads to genomic features. Bioinformatics, 2014. 30(7): p. 923-30.
19. Yu, G., L.G. Wang, and Q.Y. He, ChIPseeker: an R/Bioconductor package for ChIP peak annotation, comparison and visualization. Bioinformatics, 2015. 31(14): p. 2382-3.

20. Heinz, S., et al., Simple combinations of lineage-determining transcription factors prime cis-regulatory elements required for macrophage and B cell identities. Mol Cell, 2010. 38(4): p. 576-89.

21. Quinlan, A.R. and I.M. Hall, BEDTools: a flexible suite of utilities for comparing genomic features. Bioinformatics, 2010. 26(6): p. 841-2.

22. Mi, H., et al., PANTHER version 14: more genomes, a new PANTHER GO-slim and improvements in enrichment analysis tools. Nucleic Acids Res, 2019. 47(D1): p. D419-D426.

23. Ramirez, F., et al., deepTools2: a next generation web server for deep-sequencing data analysis. Nucleic Acids Res, 2016. 44(W1): p. W160-5.

24. Gu, Z., et al., EnrichedHeatmap: an R/Bioconductor package for comprehensive visualization of genomic signal associations. BMC Genomics, 2018. 19(1): p. 234.

CHAPTER 4

DISCUSSION AND CONCLUSIONS

The mesothelium has drawn researchers' attention for its essential roles in organogenesis and its potential clinical applications. Studies have been done to apply its epithelial features and its potential to generate vascular cells for tissue-engineered blood vessel applications. The paracrine effect of mesothelium on cardiomyocytes has also been employed as a promising adjuvant therapy in engineered heart tissue generation [1-6]. However, the molecular mechanisms in mesothelium specification are unclear. An in-depth understanding of mesothelium developmental mechanisms will help us better define the mesothelium *in vivo* and develop more purified mesothelium isolation and differentiation protocols *in vitro* for clinical applications. In this study, we applied RNA-seq and ATAC-seq on an *in vitro* hPSC-based mesothelium developmental model and revealed a transcriptional network within GATA4-TBX5 in human mesothelium specification.

GATA4 is a zinc-finger transcription factor. It consists of two zinc-finger domains; the C-terminal zinc finger domain determines the recognition and binding of DNA and the N-terminal zinc finger domain stabilizes the binding [7]. Along with GATA5 and GATA6, GATA4 belongs to the cardiac group in the GATA family [8]. GATA4 and GATA6 show redundancy in many tissue developments, including cardiac mesoderm and cardiomyocytes [9, 10]. Although they both preferentially bind to a 5-

(A/T)GATA(A/G)-3 motif and share greater than 80% sequences in DNA binding domains, GATA6 cannot fully substitute for GATA4 in heart development [8, 11-15]. Gata4 mutant mice have normal cardiomyocytes differentiation but they showed deficient cardiac maturation and heart tube development [14, 16, 17]. Previously, the friend of GATA2 (FOG2) has been found to be a GATA4 co-factor in the cardiac lineage and regulates the specificity of GATA4 in heart development [12, 13]. In this study, we discovered that TBX5 is a crucial GATA4 co-factor in mesothelium development and GATA4-TBX5 interaction at codon 296 site of human GATA4 is required for mesothelium specification. FOG2 and TBX5 determine the non-redundancy of GATA4 in cardiomyocytes and mesothelium development, respectively. However, when we aligned GATA4 and GATA6 amino acid sequences, we noticed that the binding sites of FOG2 and TBX5 are conserved in GATA4 and GATA6 (data not shown). There are two possible explanations for this. The protein folding of GATA6 may embed its interactive sites and blocks its interaction with TBX5 and FOG2. Even if GATA6 and TBX5 interact in the mesothelium, it is possible that GATA4-TBX5 interaction leads to GATA4 conformational change, which facilitates GATA4 binding to mesothelium chromatin. But GATA6-TBX5 interaction does not have the same effects. Another possibility is that there are additional factors in the GATA4-TBX5 complex for the mesothelium specificity.

It is well-established that GATA4 alone does not directly affect cardiac lineage commitment and differentiation [9, 14, 16-18]. But common heart defects were still observed in various Gata4 mouse mutants, including thinned myocardium walls and cardiac septal defects. GATA4 mutations were identified in patients with cardiac septal

defects [14, 16, 17, 19]. The previous studies on GATA4 and heart defects have only focused on the association between GATA4 and cardiomyocytes. However, cell-autonomous mechanisms of cardiomyocytes cannot exclusively explain the defects seen in Gata4 mutants. The heart is a complex organ, consisting of diverse cell types, and cardiac septation formation also involves cells from different lineages [20-22]. So it is possible that the heart defects from GATA4 mutations are caused by other cell lineage defects, which blocks its downstream effects on cardiomyocytes and inhibits cardiac septation. Epicardium is a critical paracrine center in the heart and positively affects cardiomyocyte proliferation and maturation [23, 24]. Moreover, the epicardium is involved in cardiac septation formation and can generate epicardial derived cells, contributing to atrioventricular junctions [20, 21, 25, 26]. Here, we found the point mutation in GATA4, G296S, which was first identified from congenital heart defects patients and found to disrupt GATA4 and TBX5 interaction, leads to failed mesothelium differentiation. Therefore, defective epicardium/mesothelium formation may be the causative factor of heart defects in GATA4 mutants. Further studies focusing on the cardiac septation formation in epicardium conditional knockout mice will help us get an insight into the mesothelium related cardiac defects and propose a novel mechanism in congenital heart diseases, which eventually lead to therapeutic strategies for heart diseases.

REFERENCES

1. Clarke, J.M., et al., Seeding Dacron arterial prostheses with peritoneal mesothelial cells: a preliminary morphological study. Br J Surg, 1984. 71(7): p. 492-4.

2. Pronk, A., et al., Mesothelial cell adherence to vascular prostheses and their subsequent growth in vitro. Cell Transplant, 1994. 3(1): p. 41-8.

3. Sparks, S.R., et al., Small-caliber mesothelial cell-layered polytetraflouroethylene vascular grafts in New Zealand white rabbits. Ann Vasc Surg, 2002. 16(1): p. 73-6.

4. Campbell, J.H., J.L. Efendy, and G.R. Campbell, Novel vascular graft grown within recipient's own peritoneal cavity. Circ Res, 1999. 85(12): p. 1173-8.

5. Bargehr, J., et al., Epicardial cells derived from human embryonic stem cells augment cardiomyocyte-driven heart regeneration. Nat Biotechnol, 2019. 37(8): p. 895-906.

6. Colunga, T., et al., Human Pluripotent Stem Cell-Derived Multipotent Vascular Progenitors of the Mesothelium Lineage Have Utility in Tissue Engineering and Repair. Cell Rep, 2019. 26(10): p. 2566-2579 e10.

7. Lourenco, D., et al., Loss-of-function mutation in GATA4 causes anomalies of human testicular development. Proc Natl Acad Sci U S A, 2011. 108(4): p. 1597-602.

8. Tremblay, M., O. Sanchez-Ferras, and M. Bouchard, GATA transcription factors in development and disease. Development, 2018. 145(20).

9. Narita, N., M. Bielinska, and D.B. Wilson, Cardiomyocyte differentiation by GATA-4-deficient embryonic stem cells. Development, 1997. 124(19): p. 3755-64.

10. Zhao, R., et al., Loss of both GATA4 and GATA6 blocks cardiac myocyte differentiation and results in acardia in mice. Dev Biol, 2008. 317(2): p. 614-9.

11. Molkentin, J.D., The zinc finger-containing transcription factors GATA-4, -5, and -6. Ubiquitously expressed regulators of tissue-specific gene expression. J Biol Chem, 2000. 275(50): p. 38949-52.

12. Svensson, E.C., et al., Molecular cloning of FOG-2: a modulator of transcription factor GATA-4 in cardiomyocytes. Proc Natl Acad Sci U S A, 1999. 96(3): p. 956-61.

13. Smagulova, F.O., et al., GATA4/FOG2 transcriptional complex regulates Lhx9 gene expression in murine heart development. BMC Dev Biol, 2008. 8: p. 67.

14. Watt, A.J., et al., GATA4 is essential for formation of the proepicardium and regulates cardiogenesis. Proc Natl Acad Sci U S A, 2004. 101(34): p. 12573-8.

15. Borok, M.J., V.E. Papaioannou, and L. Sussel, Unique functions of Gata4 in mouse liver induction and heart development. Dev Biol, 2016. 410(2): p. 213-222.

16. Misra, C., et al., Disruption of myocardial Gata4 and Tbx5 results in defects in cardiomyocyte proliferation and atrioventricular septation. Hum Mol Genet, 2014. 23(19): p. 5025-35.

17. Misra, C., et al., Congenital heart disease-causing Gata4 mutation displays functional deficits in vivo. PLoS Genet, 2012. 8(5): p. e1002690.

18. Ang, Y.S., et al., Disease Model of GATA4 Mutation Reveals Transcription Factor Cooperativity in Human Cardiogenesis. Cell, 2016. 167(7): p. 1734-1749 e22.

19. Srivastava, D., GATA4 mutations cause human congenital heart defects and reveal an interaction with TBX5. Nature, 2003. 424(24): p. 443-447.

20. Poelmann, R.E., et al., The Epicardium in Ventricular Septation During Evolution and Development, in Etiology and Morphogenesis of Congenital Heart Disease: From

Gene Function and Cellular Interaction to Morphology, T. Nakanishi, et al., Editors. 2016: Tokyo. p. 115-123.

21. Nakanishi, T., et al., Erratum to: Etiology and Morphogenesis of Congenital Heart Disease, in Etiology and Morphogenesis of Congenital Heart Disease: From Gene Function and Cellular Interaction to Morphology, T. Nakanishi, et al., Editors. 2016: Tokyo. p. E1-E1.

22. Gittenberger-de Groot, A.C., et al., Basics of cardiac development for the understanding of congenital heart malformations. Pediatr Res, 2005. 57(2): p. 169-76.

23. Weeke-Klimp, A., et al., Epicardium-derived cells enhance proliferation, cellular maturation and alignment of cardiomyocytes. J Mol Cell Cardiol, 2010. 49(4): p. 606-16.

24. Kelder, T.P., et al., The epicardium as modulator of the cardiac autonomic response during early development. J Mol Cell Cardiol, 2015. 89(Pt B): p. 251-9.

25. Lockhart, M.M., et al., Alk3 mediated Bmp signaling controls the contribution of epicardially derived cells to the tissues of the atrioventricular junction. Dev Biol, 2014. 396(1): p. 8-18.

26. Lockhart, M.M., et al., The Epicardium and the Development of the Atrioventricular Junction in the Murine Heart. J Dev Biol, 2014. 2(1): p. 1-17.